

“ MATHEMATICAL MODELLING OF THE
OLKARIA GEOTHERMAL RESERVOIR ”

THIS THESIS HAS BEEN ACCEPTED FOR
THE DEGREE OF... P.H.D. 1997 ...
AND A COPY MAY BE PLACED IN THE
UNIVERSITY LIBRARY.

ALFRED WANYAMA MANYONGE

A thesis submitted in fulfillment for the degree of Doctor of Phi-
losophy in Applied Mathematics at the University of Nairobi.

MAY 1996

UNIVERSITY OF NAIROBI LIBRARY

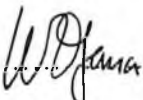
DECLARATION

This thesis is my original work and has not been presented for a degree award in any other university.


Signature..........Date.....16/8/1997 ..

A. W. Manyonge

This thesis has been submitted for examination with our approval as University supervisors.

Signature..........Date.....22/8/97 ..

Prof. W. Ogana

Signature..........Date.....22/8/97 ..

Prof. P.S. Bhogal

ACKNOWLEDGEMENTS

I would like to extend my sincere thanks to my mentor and supervisor Prof. W. Ogana who started supervising me at M.Sc. level. He is the man who introduced me to real research work in numerical solution of partial differential equations. I thank him for his tireless guidance throughout the period of research work for this thesis. I am especially grateful for his diligence and excellent supervision which he showed by sacrificing his valuable time to scrutinize my work. Also I would like to thank my second supervisor Prof. P.S. Bhogal for his excellent help in this work. I wish also to thank the New Zealand Government and the German Academic Exchange Service (DAAD) for providing me with a scholarship and a research grant respectively. The scholarship enabled me to study at the University of Auckland, a study which later proved invaluable to this thesis. The research grant enabled me to carry out the research work successfully. My thanks also go to the staff and management of the Kenya Power Company for their help and for making accessible to me their data for Olkaria. I am also indebted to my wife Pamela Manyonge who gave me moral support throughout the period of research. Finally I thank the management of the University of Nairobi for offering me the Tutorial Fellowship which permitted me to carry out the research.

DEDICATION

This thesis is dedicated to my wife Pamela Abinyi Manyonge and my children.

TABLE OF CONTENTS

TITLE	i
DECLARATION	ii
ACKNOWLEDGEMENTS	iii
DEDICATION	iv
TABLE OF CONTENTS	v
LIST OF SYMBOLS AND NOTATION	viii
GLOSSARY OF TERMS USED	x
ABSTRACT	xiii
CHAPTER ONE: INTRODUCTION	1
1.1 Characteristics of geothermal flows and reservoirs	1
1.2 Role of modelling in geothermal energy exploitation	4
1.3 Characteristics of Olkaria geothermal field	9
1.4 Exploitation of geothermal resources in Kenya	15
1.4.1 Major geothermal resources in Kenya	15
1.4.2 Other geothermal fields in Kenya	22
1.5 Objectives	24
CHAPTER TWO: LITERATURE REVIEW	25
2.1 General Literature Review	25
2.2 Olkaria Literature Review	27

CHAPTER THREE:

DYNAMICS OF FLUID FLOW IN POROUS MEDIA 29

3.1 Structure and properties of porous media 29

3.2 Behaviour of fluids in porous media 32

3.3 Conservation principle 38

3.3.1 Conservation of mass 38

3.4 Darcy's law for anisotropic porous media 41

CHAPTER FOUR: GOVERNING EQUATIONS 44

4.1 Introduction 44

4.2 Basic governing equations 45

4.3 Alternative forms of the mass and energy equations 50

4.4 Initial and Boundary Conditions 51

CHAPTER FIVE: NUMERICAL MODEL 54

5.1 Introduction 54

5.2 Finite difference representation 54

5.3 Development of the solution of the non-linear system 61

5.4 Iterative Techniques 64

CHAPTER SIX:

APPLICATION TO OLKARIA GEOTHERMAL FIELD

6.1 Introduction 69

6.2	Conceptual Model for Olkaria Geothermal System	69
6.3	Numerical modelling of the Olkaria Geothermal System	71
6.4	Natural state Model for Olkaria Geothermal System	73
6.5	Results of production model for Olkaria East field	78
6.6	Results of modelling of future production from Olkaria North East field	84

CHAPTER SEVEN :

DISCUSSION AND CONCLUDING REMARKS	88
APPENDIX A:	90
Finite difference representation of mass and energy equations	90
APPENDIX B:	95
Derivation of the non-linear system of equations for the sample reservoir of 8 blocks	95
LIST OF REFERENCES	104

LIST OF SYMBOLS AND NOTATION

m	: metre
s	: second
N	: Newtons
Pa	: Pascal
J	: Joule
K	: Kelvin
$^{\circ}C$: degree centigrade
l	: length
t	: time
MWe	: Megawatts electric
W	: Watts
A	: Cross-sectional area
c	: specific heat
C	: compressibility
D	: distribution function
h	: enthalpy
k	: permeability
k^l	: k -matrix
K	: thermal conductivity
P	: pressure
q	: flow rate
S	: saturation
u	: internal energy
\vec{v}	: darcy velocity
V	: Volume
ϕ	: porosity

μ	: dynamic viscosity
ρ	: density
Γ	: concentration quantity
Ω	: flux density
Δ	: forward difference operator
$\nabla \cdot$: divergence operator
Φ	: velocity potential
E	: Energy content per unit volume
g	: gravitational acceleration
K_m	: thermal conductivity of a saturated medium
M	: Mass content per unit volume
T	: Temperature
δ	: central difference operator
n	: time level
<i>bar</i>	: 10^5 Pa
<i>ppm</i>	: parts per million
PI	: productivity index
q_e	: energy flowrate per unit volume
q_m	: mass flowrate per unit volume
Q_e	: energy per unit area
Q_m	: mass per unit area
ν	: kinematic viscosity
∇	: gradient operator
m.a.s.l.	: metres above sea level

GLOSSARY OF TERMS

Active margin

Contact lines between two geologic plates.

Basalts

Asthenosphere melts.

Caprock

Nearly impermeable rock covering the top of the reservoir.

Compressible fluids

Fluids with varying density.

Continuity equation

Equation obtained by conserving mass.

Convergent movement

Moving of two geologic plates towards their contact line.

Convergent plate boundary

The boundary of two geologic plates moving towards their contact line.

Enthalpy

Energy per unit mass.

Fumarole

A discharge feature mainly of steam in a geothermal system.

Heat flux

Rate of movement of heat through a porous material.

Incompressible fluids

Fluids with constant density.

Lateral permeability

Permeability in horizontal direction.

Liquid-dominated

A geothermal reservoir with more water than steam in the mixture.

Magma

Molten rock deep in the earth.

Magmatic heat

Heat from magma.

Newton-Raphson method

A numerical method for solving non-linear difference equations.

Permeability zone

Region in the geothermal reservoir with high permeability.

Plate

The earth consists of the lithosphere and the asthenosphere. The lithosphere with continental crust is termed continental plate while lithosphere with oceanic crust is termed oceanic plate.

Plate tectonics

The geology of plates.

Rhyolites

Continental or crustal melts.

Separative movement

Moving away of two geologic plates from their contact lines.

Separative plate boundary

The boundary of two geologic plates moving away from their contact line.

Transform plate boundary

The boundary of two geologic plates with faults moving towards their contact line.

Vapour-dominated

A geothermal reservoir with less water than steam in the mixture.

ABSTRACT

The basic equations which govern the flow of fluids in a geothermal reservoir (often a two-phase mixture of steam and water) are outlined. The governing nonlinear system of partial differential equations that arises is solved by numerical methods which involve replacement of both the spatial and time derivatives by their finite difference equivalents. The equations that result are nonlinear and are linearized using the Newton-Raphson procedure. These equations with their solutions are applied to the Olkaria geothermal reservoir. Two significant variables, namely pressure and enthalpy change are modelled. Both variables are investigated for the present producing reservoir of Olkaria East field and the anticipated extension to the Olkaria North East field which is to have an installed capacity of 64MWe. In order to examine these variables by modelling, two models are set up i.e the natural state model of the field before exploitation and a production model which gives the response of the reservoir to exploitation for electricity generation. The solutions to the models are generated by the MULKOM computer program. The main aim of carrying out this study is to model exploitation of Olkaria East field with a capacity of 45MWe, extension of exploitation to the Olkaria North East field with a capacity of 64MWe, and to assess if Olkaria North East field can sustain the said capacity for a period of 20 years. The natural state model which occupied a surface area of $22km. \times 22km.$ had heat inputs at the base of some of the reservoir blocks. When this model is run over a long period of time, the simulated pressure and temperature, to a reasonable degree of accuracy, matches the observed values at any given location in the field. The actual process of simulation includes inserting heat of a certain magnitude at specific locations at the bottom of the reservoir to represent magmatic bodies. The system is then heated over a long period

of time until the temperature and pressure resemble those we observe in the field by measurements. The production model uses these parameters together with reservoir enthalpy as starting information. Each reservoir block was assigned specific values of pressure, temperature, enthalpy etc. As withdrawal of fluids from the reservoir for electricity generation commences, these parameters change with time. These changes are calculated by the MULKOM program which enables us to find the values of these parameters at any location and time in the reservoir. Production using a 45MWe power station from Olkaria East field was simulated for 14 years of production from 1981 to 1995. The production was then run for another 20 years from 1995 to the year 2015, this time with an extension to Olkaria North East field with a station capacity of 64MWe. The future status of the reservoir in terms of fluid enthalpy and pressure changes were predicted for the period 1995 - 2015. The results of this simulation indicate that a pressure drop of 15 bars is likely to occur over the latter production period. The average production enthalpy is predicted to range from 1350kJ/kg in the year 1995 to 1780kJ/kg in the year 2015. The above enthalpy range shows that the target of 64MWe power generation for 20 years may be met without the enthalpy rising too high(an indication of the increase in vapour-phase in the reservoir). However, a drop of 15 bars in reservoir pressure may call for drilling of extra make-up wells to sustain the 64MWe power generation for 20 years.

CHAPTER ONE

INTRODUCTION

1.1. Characteristics of geothermal flows and reservoirs

The anticipated depletion of natural petroleum oil and gas reservoirs coupled with the spiralling prices of these fuels, has stimulated considerable interest in exploring the potential of alternative sources of energy. One of these alternative sources is the use of geothermal energy to generate electricity and for other processes. Kenya is one of the countries endowed with geothermal resources. Kenya being a developing country with little explored petroleum resources, any effort that may be made towards developing new forms of energy will be a step towards alleviating the problem this country has of depending on oil based fuels.

On the earth's surface there exists, on average, an upward normal conductive heat flux of about 60mW/m which corresponds to a temperature gradient of 30°C/km . However, at certain locations on the surface of the earth anomalously high heat flow occurs particularly in those regions that are associated with active margins, which are the contact lines between two geologic plates. Separative movement of tectonic plate boundaries together with convergent and transform boundaries constitute the active margins. The heat flux in such areas exceeds the average value and thus such areas can have higher temperature gradients. These temperatures sometimes go to the order of 225°C or more. If at the depths where these useful temperatures exist the rock is sufficiently permeable and is accessible by economic drilling, then these areas can be exploited for their energy content.

Geothermal resources can be divided into convective and nonconvective

tive systems (Hochstein 1992). Convective geothermal systems are usually called hydrothermal systems while those without large fluid movement are called geopressured systems. The term convective system is used to describe a heat transfer system in the upper crust of the earth where heat is transferred by fluid movement, i.e. convection, from a heat source to a heat sink, usually at the surface of the earth. The transfer involves the transport of thermal fluid, usually hot water, hot brine, vapour and gases. In each case, fluid particles move under the influence of buoyancy forces and transport heat from a region in the vicinity of a source to the surface, or near surface, discharge area. Thermal fluids can be stored for a certain time in a reservoir between source and sink. Nonconvective geothermal systems are the opposite of the convective systems. These systems are found in large sedimentary basins, where fluid movement is restricted by impermeable layers. For nonconvective geothermal systems, the buoyancy forces are insufficient to induce any fluid movement. There is another type of nonconvective geothermal system called hot dry rock. It is a system with very little or nil fluid content and is both virtually impermeable and imporous. Exploitation is by artificial fracturing and introduction of fluid.

Hydrothermal systems can be further classified as being either liquid dominated or vapour dominated. In this description only geothermal energy from hydrothermal systems is considered. A geothermal reservoir consists of a heat source, a permeable area of porous or fractured rock containing large amounts of water, a layer of caprock and a source of water to replace fluid losses which may occur through fumaroles and other surface discharge features. Heat is then recovered from hot subsurface formations with the help of the water circulating down through fractures, pores and other openings in the rock. The water absorbs the energy and returns to the surface with at an elevated temperature. This circulation can be free

through natural openings e.g. hot springs or partially or totally forced through drilling and artesian or pumped wells. In summary therefore, the basic components of a geothermal system, of which the reservoir is the hot exploitable part, are:

- (a) an aquifer or channel network containing hot fluid,
- (b) a path down which cold water can flow to maintain the fluid flow in the aquifer and
- (c) a source of heat mainly magma intrusions.

Before exploratory drilling takes place, there is generally much uncertainty about four basic characteristics of the reservoir, namely geometry, hydrodynamics, thermal and chemical aspects. The geometry of the reservoir consists of the depth (or thickness), area and porosity which determine the energy content of the reservoir. Hydrodynamics of the reservoir will include natural flow of deep meteoric water which acts as recharge to the reservoir, static pressure, transmissivity and dynamic viscosity of geofluid. The thermal aspect of the reservoir which includes the temperature of water, thermal conductivity and specific heat capacities of water and rocks greatly influence the behaviour and utilization of the geothermal reservoir. For example, in estimating the amount of usable energy in a geothermal reservoir in preliminary studies, a cut-off temperature of 180°C as reference is often used. Finally, the chemical character of the fluid, particularly the salinity, is important as an appreciable amount of chemical species in geothermal fluids completely alters the behaviour of the geothermal reservoir. For instance, a model developed based on the premise that the geothermal fluid is pure aqueous system may have to be changed significantly to be applicable to a geothermal system with dissolved chemical species and high salinity. Knowledge of the above parameters is essential

since these parameters are useful in estimating the available energy, future productivity and possible prediction of the reservoir behaviour under different exploitation schemes.

1.2. Role of modelling in geothermal energy exploitation

A geothermal reservoir as remarked earlier has a surface area and thickness. Overlying the geothermal reservoir may be a cold water zone sealed from the reservoir by a caprock. In the reservoir there may exist a water/steam zone and a hot water zone. The relative magnitudes of these zones are dependent on whether the reservoir is liquid-dominated or vapour-dominated. In a liquid-dominated reservoir, a two-phase region containing a mixture of steam and liquid water overlying a deeper hot liquid layer is present in the natural state. On the other hand a vapour-dominated reservoir also contains an upper two-phase layer. In this case however, the liquid phase is sparse, widely dispersed and immobile. The recharge/discharge areas to the reservoir include recharge inflow, base inflow, natural discharge and well discharge. If a well is drilled in the reservoir, the discharge from the well causes a pressure drop in the entire reservoir. This pressure drop induces a cold recharge from the sides of the reservoir and may change base inflow, steam inflow and natural discharge. Base inflow is a circulatory process. Cold water from recharge surface zones is heated as it travels downwards. This movement is caused by density differences between the cold and the hot water. The base inflow has little significance on the overall behaviour of the reservoir because of the long paths it takes from the base to the top of the reservoir. The recharge inflow will increase with increasing drawdown due to exploitation. This recharge water will have the effect of shifting the cold-hot boundary of the reservoir. The cold water percolates into the reservoir and gets heated by the heat stored in the rock and hot water already resident in the pores.

When exploitation of the field starts, the pressure starts declining thus increasing the pressure difference between the inside and outside of the reservoir. But a very long time may elapse before any effect of recharge is observed due to low permeability zones near the boundary. Natural discharge mainly comes from the cold water zone above the reservoir. If the well discharge is increased sufficiently to decrease the reservoir pressure, the natural discharge may reverse in sign because the pressure difference which maintains the flow becomes reversed. When this happens, a recharge of cold water from above occurs and natural steam flow may stop. The dynamics of the fluids in a geothermal reservoir, whether in its natural state (before exploitation for energy), or under production is a physical phenomenon which can be characterized or represented by a set of mathematical equations describing the physical processes active in the reservoir. These equations are nonlinear partial differential equations that relate the pressure, saturation changes, enthalpy and temperature with time throughout the reservoir. The equations which express the laws of continuum mechanics namely, conservation of mass, momentum and energy in the reservoir, are extremely complex and the presence of specialized boundary conditions such as the ones we find in geothermal reservoirs complicates the formulation even further. The solutions to these equations by analytical means is impossible except for trivial cases and therefore numerical methods are usually the only viable approach. An example of the trivial cases is the idealised situation of isotropic medium, no gravity effects, no sources or sinks, no porosity dependency on pressure, in which case the governing equations will be linear second order partial differential equations whose solutions are easy to find. Mathematical reservoir modelling involves developing a conceptual or descriptive model of the field under investigation, quantifying the model with data obtained

from well test analysis and calibrating it with the history of the field under exploitation. The model should incorporate:

- (i) the source of water,
- (ii) mechanisms for water transport to depth, i.e. conduction and convection,
- (iii) the process of heating in the deeper sections of the system,
- (iv) the subsequent rise of the hot buoyant liquid,
- (v) fluid dispersion into chargeable aquifers,
- (vi) the cooling of aquifer liquids by near surface effects and
- (vii) impervious boundaries that might affect future production.

Circulating ground water attains a maximum temperature under the geothermal area and, due to density differences between the hot and the cold water, the fluid rises under buoyancy force. At some depth below the ground surface, the water reaches saturation pressure and boiling initiates steam bubbles in the water. The rising fluid becomes a mixture of steam and water and the temperature of the mixture follows the the pressure/temperature boiling point curve of water as pressure decreases and the mixture approaches the earth's surface. The upward migration of steam-water mixture is influenced by the relative permeabilities of the rock for each phase but this depends in turn on the relative volumes of each phase in the permeable volume of each rock. At low steam saturation the relative permeability for steam is so low that the steam is practically stagnant or carried with water as small bubbles. As the steam saturation increases at lower pressures, the relative permeability for steam increases and separate movement of the steam bubbles becomes possible. The steam then rises faster than the water and gradually dominates in the largest channels where resistance to flow is lowest. The water lags

behind and the loss of steam with time builds up a concentration gradient of increasing salinity. The impermeable caprock prevents further rising of the steam and the lower pressure head of the reservoir water allows the steam to accumulate under the caprock. Although steam is dominant in this zone, water is also present as condensed pore water and this water flows downwards (Bhogal, 1989).

Modelling in geothermal studies may be divided into two main categories, namely, free convection models which examine the geothermal reservoir behaviour under natural conditions before exploitation and reservoir models which examine exploitation effects. The present study concentrates on reservoir models mentioned above which may be further subdivided into two general types called lumped and distributed parameter models.

Lumped parameter models offer the simplest means of describing the behaviour of a geothermal system under exploitation. In this model the whole geothermal system is regarded as a perfect mixing cell for both mass and energy, so that the space variation in rock and fluid properties is reduced to a single point in space such that instead of considering the internal distribution of mass and energy, focus is restricted to total amounts of mass and energy generated within the system as well as those crossing the boundaries. The system can be characterized mathematically by a set of ordinary differential equations or an equivalent set of algebraic expressions representing total mass and energy. The advantages of lumped parameter models are their simplicity and ease of operation. In addition the models do not need complicated programming and could be solved in a short period of time. Usually the models are used as a first stage in the modelling process and for checking the results of more complicated models. The disadvantages of the lumped parameter method are

that the models do not take into account the spatial variation in reservoir properties and flow within the reservoir.

A model in which the properties of the rock and/or fluid are allowed to vary in space is known as a distributed parameter model. The governing partial differential equations are usually solved numerically.

Developing mathematical equations describing geothermal flow and their solution is important, because it leads to the prediction of the reservoir behaviour particularly with regard to its exploitation for energy. Tied to the above reservoir simulation process is the possibility that estimates of recoverable energy from the system can be made and optimum management techniques of the geothermal resource such as optimum location, spacing and production rates of wells can be determined. Simulation may also aid in refining descriptions of the reservoir geometry, boundary conditions and rock properties. The role of simulation cannot therefore be overemphasised.

There are a number of numerical methods that can be used to solve the mathematical model, namely finite difference, finite element and boundary element methods. The last two methods are efficient at handling complicated boundaries. For instance, the boundary element method presents the governing equations in integral rather than differential form to avoid reference to specific system of coordinates and provides great flexibility in the geometrical description of the flow region. This flexibility is particularly useful when modelling fractured porous media as implemented by Pruess *et al.*(1980) in the computer code named SHAFT 79. However, for nonlinear two-phase flow problems the finite element method requires modifications which lead to lower order approximations. Programming of nonlinear techniques such as the Newton-Raphson method

proves more difficult for the finite element method than the finite difference method. The difference equations that result are fully implicit with Newton-Raphson treatment of nonlinear terms.

1.3. Characteristics of Olkaria geothermal field

Olkaria geothermal field is located in the Great Rift Valley of Kenya(Figure1.3.1). It occupies a surface area of about $50km^2$ (Noble and

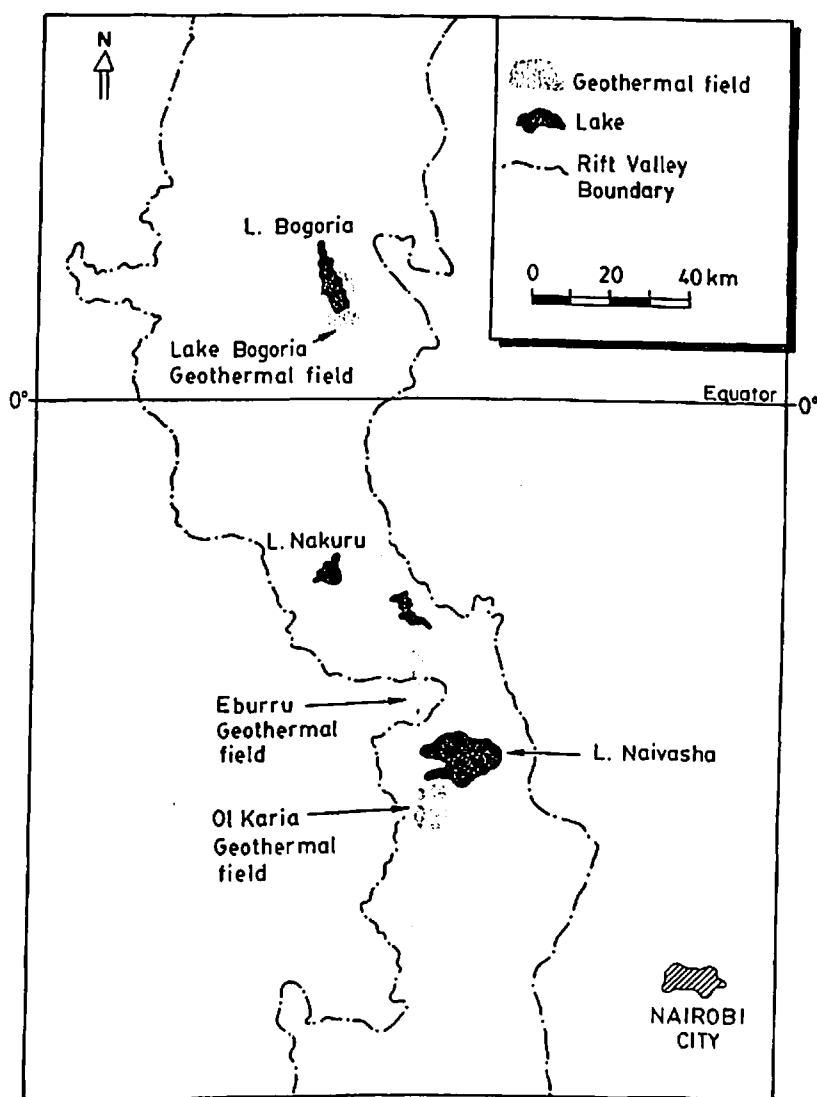


Figure 1.3.1 Location of geothermal resources within the Great Rift Valley of Kenya (adapted from Bodvarsson *et al.* 1987)

Ojiambo 1975). The Olkaria field has three delineated prospect areas: Olkaria West, Olkaria North East and Olkaria East. Olkaria East field, on which the present power station stands, is located in a depression limited to the east by the Ol Njorowa gorge, to the south by the Ololbutot lava and to the north by the high ground forming the Lake Naivasha catchment area.

There are very few surface discharge features to be seen at Olkaria geothermal field apart from fumaroles and steam vents. The fumaroles appear aligned along the Ololbutot fault on the southern boundary of the field. There is only one recorded chloride spring within the area of high heat flow with a sodium-potassium geothermometer temperature of 200°C . (GENZL/KPC 1979/1980).

The Olkaria field is related to the Olkaria volcanic complex located near the western edge of the Rift Valley. The latest volcanic eruption in the area occurred approximately 300 years ago generating the Ololbutot lava (Bodvarsson et al. 1987). The surface geology of the Olkaria area is composed of a surface cover of young quaternary volcanic flow about 300m thick believed to have originated primarily from volcanoes forming mount Longonot and mount Suswa. The surface stratigraphy as given by Naylor (1972) and summarized by KRTA (1984) is described below.

Agglomerates of south Ol Njorowa gorge are exposed in the walls of the Ol Njorowa gorge containing blocks of soda rhyolite lava up to 1m thick. Ol Njorowa pumice tuffs can be seen in the walls of the northern sections of the gorge with thickness up to 125m. Welded agglomerates/tuffs of central Hells Gate can be observed overlying the Ol Njorowa pumice tuffs in the central parts of the gorge. Grey white pumice tuffs and agglomerates of Ol Njorowa overlie the Ol Njorowa pumice tuffs. In

the south-west Olkaria area there are pyroclastics consisting of tuffs, agglomerates and lapilli horizon. The rest of the area is covered by rhyolitic pyroclastics, tuff. cones, lava and obsidian flows and local sedimentary units. The overall stratigraphy (Figure 1.3.2)

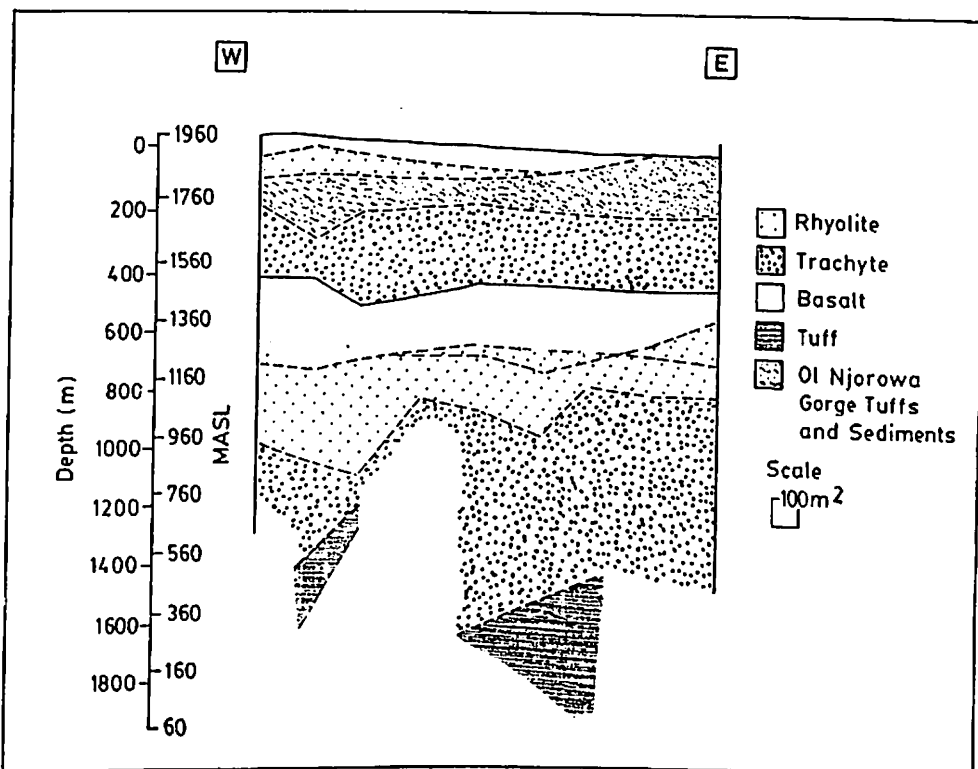


Figure 1.3.2 A section of stratigraphy in Olkaria field
(adapted from Bodvarsson *et. al* 1987)

surface and subsurface consists of composite pile of lavas and pyroclastics of mainly rhyolitic, trachytic and basaltic compositions. This is underlain by a trachyte layer (200-400m). Underlying the trachyte layer is a basalt

unit (400-700m) followed by a rhyolite layer (700-900m). A thick trachyte layer dominates below a depth of 900m. Faults and fractures are prominent in the area, especially in Olkaria West. The faults trend North-South (N-S) and East-West (E-W) with inferred faults striking North-West (N-W), South-East (S-E). The N-S faulting structures are associated with the main trend of rift faulting that provides the major vertical permeability within the Olkaria area and largely controls the movement of thermal fluids at deep levels. Lateral permeability at shallow depths throughout the field is primarily controlled by lithology and may vary quite considerably because of marked variations in thickness and distribution of volcanic units. Hydrothermal alteration present in the cores from deep exploration wells generally show prograde assemblage of alteration mineralogy with increasing depth and temperature. Tuffs and pyroclastics are the most intensely altered lithologies indicating that they have been permeable features during the life of the geothermal system. The lavas generally exhibit lower intensity of alteration except where they have been extensively fractured and brecciated. Areas of altered and warm ground are extensive throughout Olkaria and together with the present surface manifestations show a close association with the prominent N-S structures and the ENE-WSW Olkaria fault zone (GENZL 1986).

Geothermal waters that exist in Olkaria are the cool sodium-bicarbonate type of waters found near the surface of the earth (at a depth of 300-500m) and the hotter sodium-chloride water found deep in the reservoir. Mixing of these waters does occur in many parts of the system with much of it in Olkaria West and above the geothermal reservoir. The sodium-bicarbonate water is believed to be produced from condensation of steam and the gas formed from boiling of deep chloride water and mixing of cooler waters. Reservoir engineering studies indicate that a layer

of bicarbonate water extends over most of the reservoir. Sodium-chloride water appears in all Olkaria East wells without any associated shallow sodium-bicarbonate layer. The sodium-chloride water in the east shows a chloride/silica geothermometer temperature of 300°C . The chloride water in the west is more dilute due to mixing with overlying sodium-bicarbonate water and gives a temperature range of $270 - 290^{\circ}\text{C}$.

The general hydrology of the Olkaria area is the movement of water from the escarpment areas into the Rift Valley and southwards from the Lake Naivasha area. Two major upflow zones, one to the west and the other to the north-east of the field have been identified in the area (Figure 1.3.3). Both of these upflows are related to the Olkaria fault. Boiling

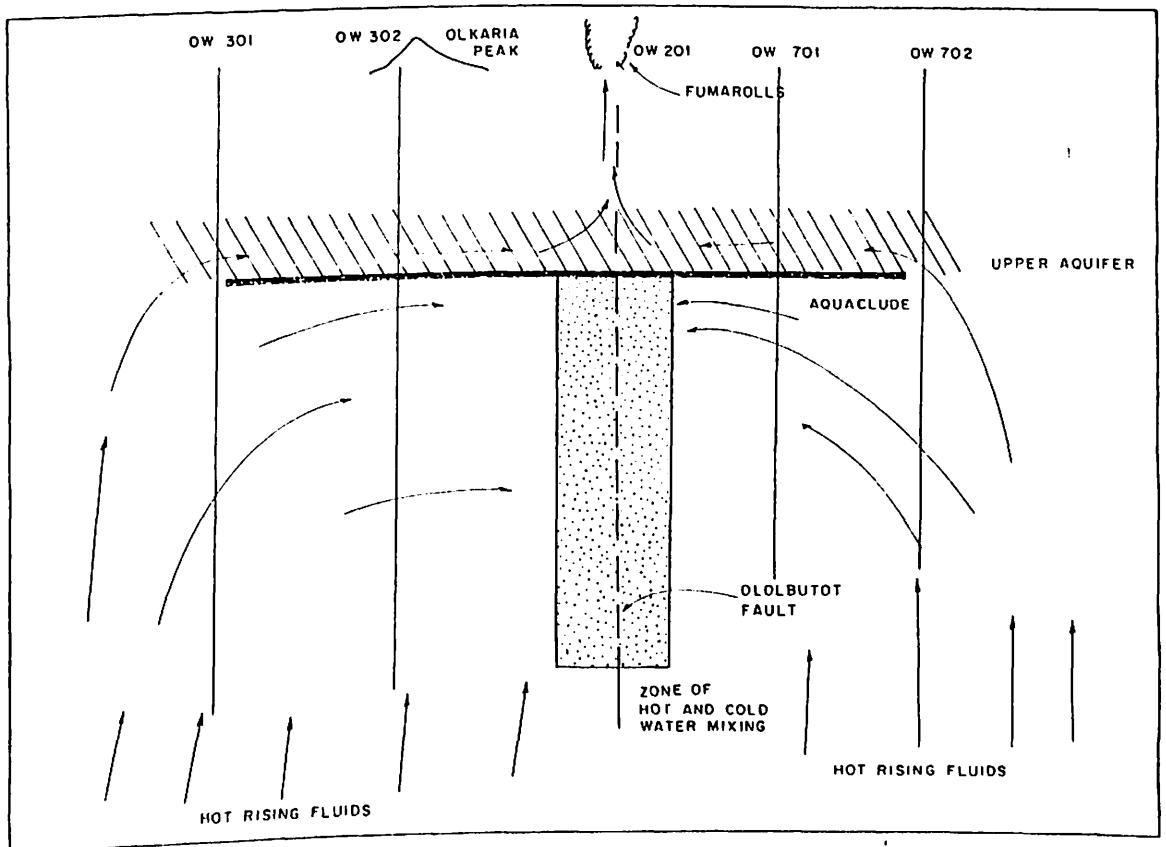


Figure 1.3.3 Upflow zones in Olkaria field (adapted from GENZL, 1986)

fluids from these upflow zones flow laterally along the Olkaria fault and mix with colder water flowing southwards along a central zone bounded by the Ololbutot fracture zone in the east and a parallel fracture zone in the west effectively forming an outflow to the south (KPC 1988).

The Olkaria area has been defined by two separate geophysical anomalies, namely, low rock electrical resistivity and low magnetism both indicators of a deep heat source underlying the area. Resistivity data indicate an area of altered rock of 80km^2 (Hochstein et al. 1981). However, two areas, one in the west and the other in the north-east appear hotter than the rest of the area. Detailed resistivity surveys show that Olkaria West occupies an area of 15km^2 (Mwangi and Bromley 1986). Olkaria north-east area occupies an area of as much as 12km^2 with about 6km^2 proven by drilling.

The locations of permeable zones are as shown in Figure 1.3.4.

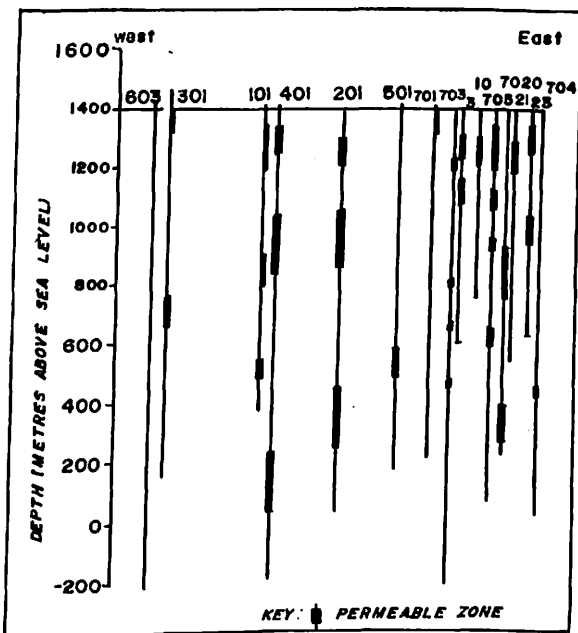


Figure 1.3.4 Permeable zones in Olkaria field

These zones in both production and exploration wells have been inter

puted from completion and discharge tests carried out on the wells. The permeable zones are located within a range from sea level to 1400 m.a.s.l. Permeable zones in Olkaria North East are at 1000 – 900 m.a.s.l. and around 600 m.a.s.l (Figure 1.3.4). Well measurements data show that there is a thin, almost horizontal, aquifer that extends over most of the area at approximately 1300 m.a.s.l. containing high enthalpy mixture of steam and water and a deep liquid dominated reservoir beneath. Permeability of the reservoir is generally low and wells have relatively poor productivity. However, permeability in the North East area appears higher on the average than in the East production field. Wells tapping the high enthalpy reservoir are more productive than those wells extracting fluid from the liquid-dominated reservoir. The reservoir is characterized by randomly distributed permeable zones throughout its thickness.

1.4. Exploitation of geothermal resources in Kenya.

1.4.1. Major geothermal resources in Kenya

There are three extensively explored geothermal fields in Kenya, namely, Olkaria, Eburru and Lake Bogoria (Figure 1.3.1), all located in the Great Rift Valley. Among the three explored fields, only Olkaria has been developed for electrical power generation. Geothermal exploration of the Olkaria geothermal field started in the mid 1950s when two exploration wells code named X-1 and X-2 were drilled (Noble and Ojiambo 1975). The well X-1 was drilled to a depth of 502m and could not discharge any fluid. Steam was encountered at a depth of 370m and a maximum temperature of 120°C was recorded. The well X-2 was drilled to a depth of 1034m and could not discharge any fluid either. A maximum temperature of 235°C was encountered. The two wells were located in a region of high heat flow. The failure of these wells to discharge slowed

any further exploration activity until the early 1970s when systematic exploration of the Olkaria geothermal region resumed (Noble and Ojiambo 1975). The exploration was undertaken by the United Nations Development Program (UNDP) and the Kenya Government when further scientific investigations were embarked on. More work was done on $X - 2$ which this time discharged a two-phase mixture with a maximum temperature of $245^{\circ}C$ recorded at a depth of $940m$. Four more exploration wells were drilled around $X - 2$ with depths ranging from $900m$ to $1350m$ (Grant, *et al.* 1981). Under the UN Program, the first well $OW - 1$ was drilled as the first deep well in Olkaria. It was drilled to the south of Ololbutot lava pile (the youngest lava flow of the field) from 8 *th* October 1973 to 3 *rd* March 1974 to a total depth of $1003m$. The well had a maximum recorded temperature of $126^{\circ}C$. The second deep well, $OW - 2$, was productive and reached temperatures of over $280^{\circ}C$ with flow of up to 40 tonnes/hour of high enthalpy fluid. Subsequent exploration wells were drilled at locations around $X - 2$. By 1982, 21 wells had been drilled with most of them concentrated in the eastern part of the field to be known later as Olkaria East. Most of the wells were good producers with similar conditions. They each produced on average $2MWe$ of electrical equivalent of high enthalpy fluids. To date there are well over 50 wells drilled in the whole of the Olkaria area. Sufficient resource capacity was confirmed in 1980 for power plant planning and the first $15MWe$ turbo-alternator was commissioned in June 1981 using 7 wells. The second and the third units of $15MWe$ each were commissioned in December 1981 and April 1985 respectively bringing the total amount of installed capacity to $45MWe$.

In the early 1980s more exploratory drilling was carried out in two areas, namely, Olkaria North-East and Olkaria West fields (Figure 1.4.1).

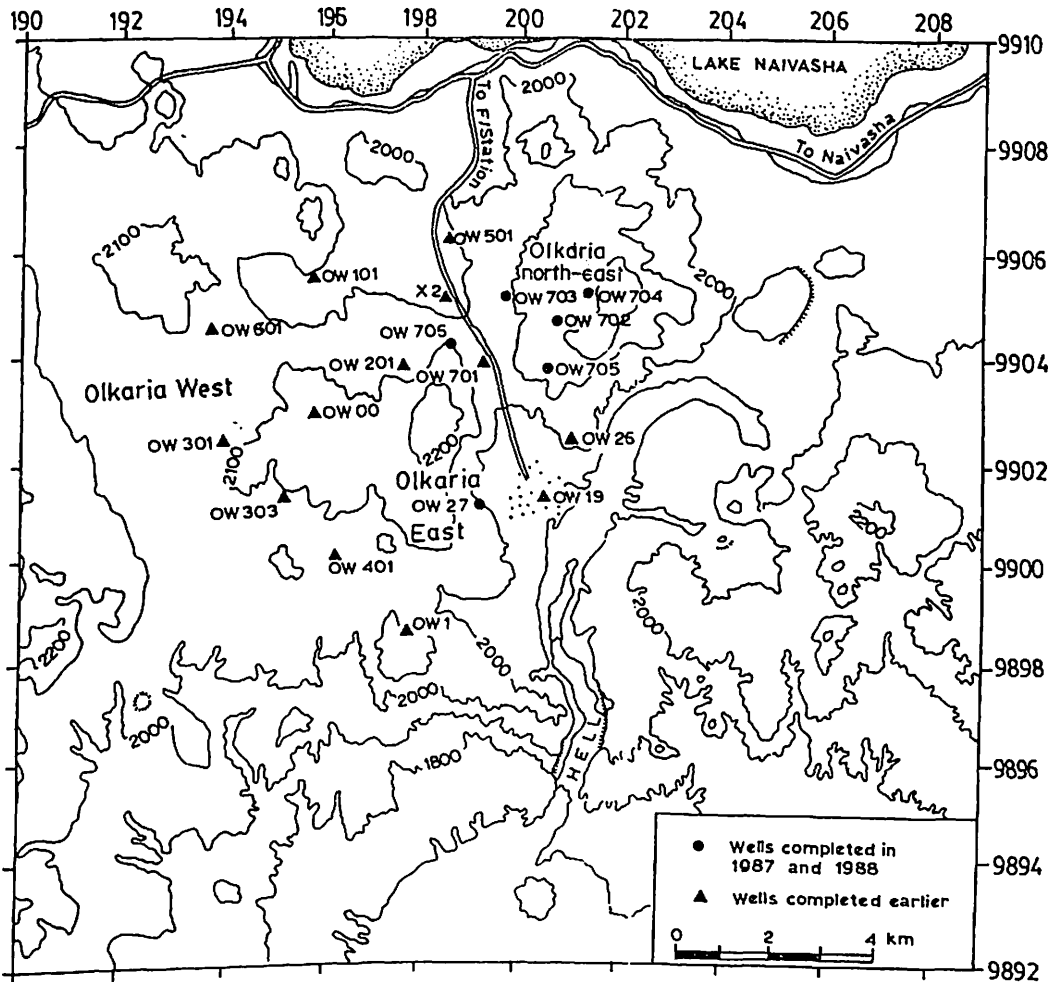


Figure 1.4.1 Well Locations and major structures
(adapted from Mwangi *et. al.* 1986)

These fields are located in areas with low resistivity and surface activities such as fumaroles. The wells in Olkaria North-East field have been drilled and tested and their potential proven for a 64MWe power station (Ambuso and Ouma 1991). Exploratory well drilling in Olkaria North-East field started in 1983 with the first well given the code name

OW – 701. It was drilled to a depth of 1800m. By 1988, five more wells had been drilled and tested in various parts of the Olkaria North-East field. To date, additional wells, to the order of 15 have been drilled and tested in this field. Most wells in this field attain a temperature of 300°C at below the depth of 1800m. The range of electrical production equivalent per well is between 1.6 and 8.0MWe.

Eburru geothermal field is situated within the Great Rift Valley of Kenya (Figure 1.3.1). Geologically the area is covered by pyroclastics which are themselves covered, in some areas, by younger obsidian and rhyolitic flows. In the north, trachytes, phonolites and recent basalts occur. Two major fault systems have been identified in the area, one of which forms the main Rift escarpment. Fumarole activity occurs where these faults intersect the rim of the caldera suggesting major permeability channels. Geophysical surveys, particularly resistivity, indicate the Eburru geothermal resource to have an areal extent of about 5km².

Geophysical mapping of the Eburru geothermal area was first done in the 1960s and early 1970s under the UNDP/Kenya Government geothermal exploration program. Geoscientific surveys were carried out then. Surface manifestations in the area were known and reported during the geological mapping of the area in 1963(see KPC 1990). In 1972 UNDP completed a comprehensive survey (geothermal exploration) of the area and Japan International Co-operation Agency (JICA) made a detailed study of the geothermally active zone on the northern slopes of the Eburru hill. In 1985/86 further extensive study in a much wider area was carried out by KPC scientists (KPC 1990) which culminated in the 1986 scientific review and well siting meeting for Eburru. Motivated by the need to develop geothermal energy for electricity production, exploration drilling started in the late 1980s. Four exploration wells were drilled in the area

between 1988 and 1990. The first well to be drilled in Eburru was code named *EW - 01*. Drilling commenced on 30th December 1988. The well, designed to test the main upflow area, was drilled to a total depth of 2464m and had a measured temperature of up to 285°C. The well was stimulated and discharged brine of high salinity with enthalpy values varying between 1100 – 1200kJ/kg. A report (KPC 1990) on this, noted that Eburru *EW - 1* showed negative enthalpy; that is, the enthalpy of discharge was lower than the enthalpy of the main reservoir, and the average enthalpy lost by water between reservoir and the surface was about 150kJ/kg. The loss in enthalpy relates to the absence of any shallow steam zones feeding the well and possibly the cooling or dilution of the discharge fluid by cooler feed zones. The high salinity in the well suggests a recharge path possibly traversing marine or lacustrine sediments horizons. Reservoir engineering data indicated that reservoir permeability is moderate compared to Olkaria production wells. Calculation of the electrical capacity equivalent give the well a production of 2.5MWe at 6.0 bar pressure. This was equal to the average of the Olkaria production wells.

The second well in Eburru *EW - 02* was located to test the eastern extension of the upflow zone (see Figure 1.4.2 overleaf). It was drilled to a depth of 2780m and could not discharge. A maximum temperature of 140°C was measured in the well. Reservoir engineering tests on the well indicated low permeability. The third well *EW - 03* was located to test the northern extension of the upflow zone. It was drilled to a depth of 2596m and was not able to discharge. The well showed temperature inversions. The bottom hole had a measured temperature of 103°C which was lower than the highest measured temperature of 160°C at 900m. Completed by 24th November 1990, *EW - 04* was located to test the

southern extension of the upflow zone. It was drilled to depth of 2466m and could not discharge on its own. However, after several compressions the well discharged mainly water and almost no steam. On recovery it showed moderate measured temperatures of 180°C

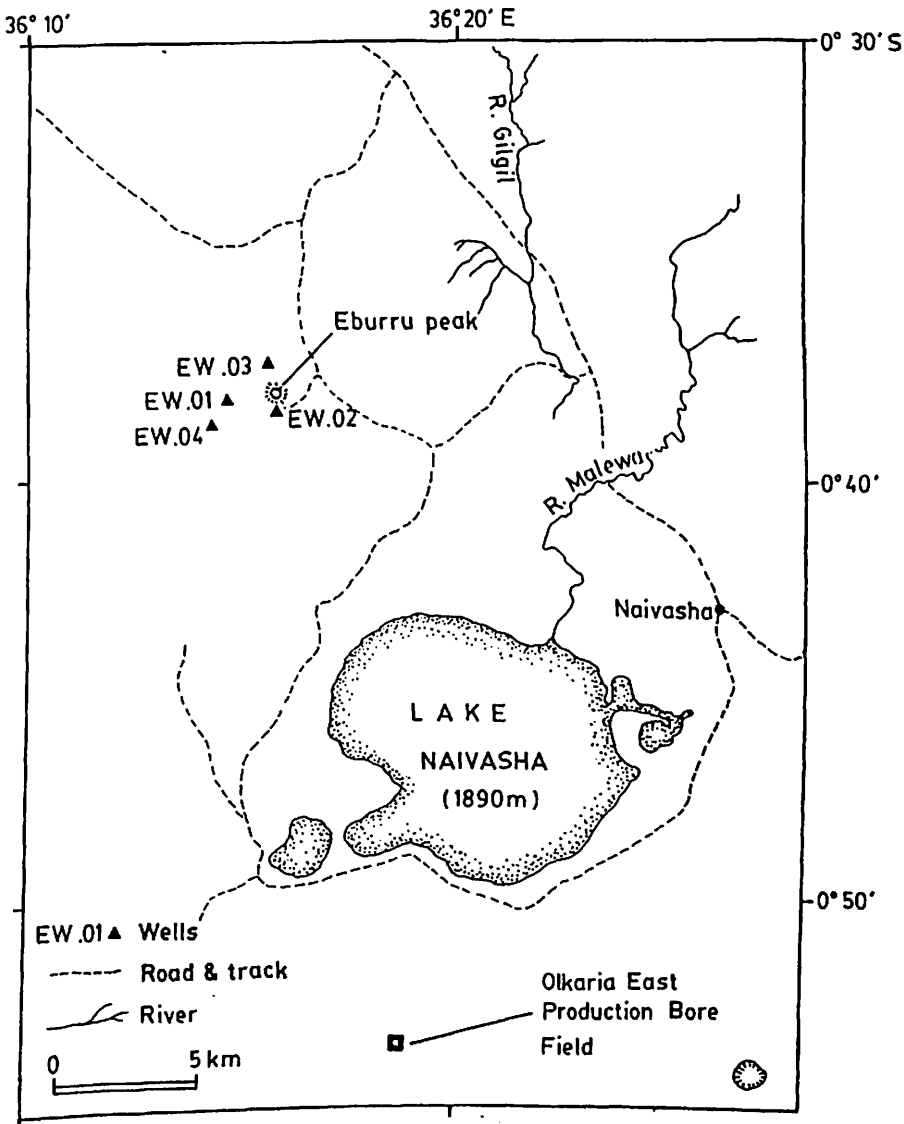


Figure 1.4.2 Eburru field (adapted from KPC 1990)

Eburru EW – 01 confirmed the existence of a high temperature geothermal resource. Wells EW – 02 and EW – 03 are nonproductive due to poor permeability and insufficient temperatures. EW – 04 produces largely water with practically no steam suggesting good reservoir

pressures and possibly moderate permeability but lack of temperature as shown by low enthalpy fluid. Further scientific work is going on at Eburru to enable exploration drilling to continue. In spite of the higher subsurface temperatures at Eburru, Olkaria was the first to be developed for power generation because of its proximity to Nairobi, main power transmission line and the potential at Eburru being much lower than that at Olkaria.

Lake Bogoria geothermal field, the third field of interest, is located on the floor of the Great Rift Valley of Kenya as shown in Figure 1.3.1. It lies between eastings $36^{\circ}4'$ and $36^{\circ}13'$ and northings $1^{\circ}20'$ and $1^{\circ}24'$. Geological mapping and characterization of the area has been done. Resistivity surveys indicate an area of altered rock of about 5km^2 around the lake (Group 7 Incorporated 1972). Geothermal evidence in the area is characterized by widespread occurrence of thermal anomalies such as hot springs and fumaroles. Geochemical studies suggest the probable occurrence of at least two distinct hydrothermal systems. Geochemical sampling of springs and fumaroles give inferred temperatures of $145 - 190^{\circ}\text{C}$. After geological mapping of the area by Geothermica Italiana in 1986, it was concluded that, despite its impressive hot springs, there was no evidence of young magmatic heat sources. Its heat is probably the discharge zone for waters that have circulated deep in the rift fault system. Lake Bogoria geothermal field is therefore considered to be of secondary importance as a prospect for high temperature resource but it may be useful as a low temperature field. There has not been so far any exploration well drilled in the area; this probably explains the low keyed scientific work that has been carried out in this area.

When the UN/Kenya Government recognized the need to develop energy sources that are cheaper than mineral oil or fossil fuel in the face of increasing oil prices, geothermal energy prospecting was mainly targeted

for electricity generation. Therefore the main thrust of scientific work in Kenya in the exploitation of geothermal energy was concentrated in this area of geothermal energy utilization. Development was focused on Olkaria, Eburru and Lake Bogoria fields. However, there are numerous other geothermal fields in the Kenyan Rift Valley, which we examine below.

1.4.2. Other geothermal fields in Kenya

(a) Domes, Suswa and Longonot fields

Reconnaissance exploration has been done in these fields. Geochemical studies of fumarolic and steaming grounds emission has been done in Domes, Suswa and Longonot and some waters from Lake Magadi and Kedong valley. The exploration results showed that steam in Suswa and Longonot areas is derived from two sources namely, meteoric water from rift scarps which is shallow in origin and from water which has been evaporated to some extent or from a mixture of rain water and evaporated water. Gas geothermometry temperatures suggest temperatures in excess of 300°C in both areas (Geothermica Italiana, 1985).

(b) Menengai, Solai fields

Glover (1972) examined geohydrochemical data from surface, thermal and shallow borehole waters and fumarolic emissions from the areas between Lake Elementaita to the south and Lake Bogoria to the north. This report suggests that the hot springs at Lake Elementaita are an outflow of a geothermal reservoir in the area.

(c) North-most fields (Korosi, Paka, Silale, Emuruagogolak, Namuruu and Lake Logipi Barrier)

The British Geothermal Survey has examined the northern part of the Rift Valley covering areas from the southern shores of Lake Baringo to the southern shores of Lake Turkana. They suggest that reservoirs in these

northern prospects have chloride concentration of about 500ppm and that reservoir temperatures are estimated as 200°C for Korosi and more than 225°C for Silale and Paka (Geothermica Italiana, 1985).

Although the immediate aim of research in geothermal energy in Kenya is to provide the country with electricity, the geothermal fields outlined above can be used in many other ways. For example the low enthalpy fluids may be used in the drying of pyrethrum and other crops at Eburru.

A number of scientists, both local and from overseas have contributed immensely to the existing body of knowledge about geothermal exploration in Kenya. Glover (1972) analyzed the chemical characteristics of water and steam discharges in the Rift Valley of Kenya, with two major aims: to determine the location of areas of highest subsurface temperature and suggest the most favourable areas for a future drilling programme and to give a survey of the heat flow. Three favourable areas in Olkaria were identified, namely, Olkaria East, Olkaria West and Olkaria North East. He concluded that the heat flow in the Rift Valley increased in amount from Bogoria through Eburru and Olkaria respectively. McCann (1974) gave a hydrologic investigation of the Rift Valley catchments. He concluded that substantial annual precipitation recharges ground water reservoirs. Electrical resistivity prospecting in the Rift Valley of Kenya has been done, for example Bhogal (1978) outlines methods of exploration and their application at Lake Bogoria, Eburru and Olkaria geothermal prospects. Contributions by various other scientists in this field in Kenya, particularly on modelling, are outlined in the literature survey given in chapter two of the present study.

Although individual scientists and consulting companies have been

carrying out research in geothermal energy in Kenya, they have done so as consultants to either the Kenya Power Company or the Ministry of Energy. Among the disciplines of geothermal energy research that are costly in terms of consultancy fees is reservoir modelling. Furthermore not all information regarding the model will be available to the Kenya Power Company or Ministry of Energy from the consultants as they prefer to give model results only. There is therefore need and justification to develop local expertise in this discipline. This way the local companies such as the Kenya Power Company and the Ministry of Energy will cut down on the costs of modelling and retain much original information.

1.5 Objectives

The objectives of the present study are:

- (i) To develop a reservoir model for Olkaria which examines the response to exploitation of the Olkaria East reservoir when it has a capacity of $45MWe$ from the time the wells went on line to present time(1995),
- (ii) To model the extension to the Olkaria North East field with a proposed installation of a $64MWe$ power station,
- (iii) To examine how the overall reservoir pressure and enthalpy are changing over the model production period and
- (iv) To assess if this area can sustain the above capacity and for how long.

CHAPTER TWO

LITERATURE REVIEW

2.1. General Literature Review

This literature survey examines the efforts that have been made over time to solve the geothermal flow equations. The first reservoir model applied to a geothermal field problem was a lumped parameter model developed by Whiting and Ramey (1969). This model allowed fluid influx from an adjacent aquifer and was used to simulate the two-phase steam-water behavior of the Wairakei geothermal field in New Zealand. Faust and Mercer (1979) reported that other workers applied lumped parameter models to geothermal reservoirs with varying reservoir properties such as liquid and gas phases distributed throughout the reservoir and also assuming that the reservoir is closed i.e. nothing enters or leaves the reservoir. Harlow and Pracht (1972) considered the problem of extracting heat from dry rock using a distributed parameter model which simulated rock fracturing and single-phase liquid or vapour flow. The first application of a distributed parameter model to a geothermal field problem was made by Mercer and Faust (1975). The equations were solved by a numerical method that used Galerkin finite elements. The model which solved for temperature and pressure was areal (i.e. vertical component of flow assumed negligible) and was restricted to liquid-dominated reservoirs only. Faust and Mercer (1979) also pointed out in their paper that two-phase two dimensional reservoir models that incorporated well bore models were developed. The models which were restricted to the saturation vapour pressure curve, solved for pressure and saturation and used a finite difference technique that involved Newton-Raphson iteration.

At this stage in the reservoir modelling process, the reservoir mod-

els that existed were either for compressed water or for conditions on the saturated vapour curve. An evolution in the modelling process occurred in 1975 at the United Nations symposium on the development and use of geothermal resources, held in San Francisco. Three independent groups presented distributed parameter models capable of simulating both liquid and vapour-dominated geothermal reservoirs. Faust and Mercer (1975) applied both Galerkin finite element and finite difference techniques to approximate a pressure-enthalpy formulation of the multi-phase flow equations in two horizontal dimensions. Garg *et al.* (1975) and Lasseter *et al.* (1975) formulated multi-phase flow equations in terms of fluid flow internal energy and density. Garg *et al.* (1975) used finite difference techniques to approximate their equations whereas Lasseter *et al.* (1975) used an integrated finite difference technique. Both of these models were capable of treating three dimensional problems.

Later, Schroeder (1980) developed a computer program code named SHAFT 79 (Simultaneous Heat And Fluid Transport). SHAFT is an integrated finite difference program for computing two-phase non-isothermal flow in porous media and is designed for geothermal reservoir simulation. In the numerical method used, space discretization of the governing equations is achieved with the integrated finite difference method. This method allows a very flexible geometric description because it does not distinguish between one-, two-, or three dimensional regular or irregular geometries. Time is discretized fully implicitly as a first order finite difference. This process yields non-linear difference equations which are solved using the Newton-Raphson method. The set of linear equations arising at each iteration step is solved by a matrix solver. Two examples of matrix solvers are, MULKOM computer code, a new version of SHAFT 79 developed in 1983 at the Lawrence Berkeley Laboratory, and TOUGH (Transport of Unsatu-

rated Ground Water and Heat) developed due to Pruess(1987). TOUGH is a multi-dimensional numerical model for simulating the coupled transport of water, vapour, air and heat in porous and fractured media. The program was initially developed to study high-level nuclear waste isolation in partially saturated geological media. The numerical methods used are similar to those used in SHAFT 79.

TOUGH2 which is a more general version of TOUGH is closely related in methodology to TOUGH. TOUGH2 was developed by K. Pruess in 1991. It is a numerical simulation program for multi-dimensional coupled fluid and heat flows of multi-phase multi component fluid mixtures in porous and fractured media. It is designed for a variety of uses e.g. geothermal reservoir engineering, nuclear waste disposal and unsaturated zone hydrology.

2.2 Olkaria Literature Review

We now turn to literature survey concerning modelling work related to the Olkaria geothermal field. Several computer models to simulate the performance of the Olkaria geothermal field have been developed. Simulation studies were done in 1980 and 1981 to test the reservoir behaviour under exploitation. The first study by Bodvarsson (1980) addressed the question of the effects of the vertical permeability on the production capacity of the field and subsequently on what would happen to the production capacity of the field if production was from the steam zone or water zone or both, using a simple vertical 1-D model with reservoir area of 12 km and a thickness of 1250m. The results showed that excessive production from the steam zone would lead to localized boiling and pressure decline and this would then limit the productive life of the reservoir. On the other hand considerable production from the liquid zone leads to counter flow of

both steam and water resulting in optimal depletion of the reservoir. The second model, Bodvarsson and Pruess (1981), considered the effects of both horizontal and vertical permeabilities on the production capacity of the field. The results obtained indicated that a power production 45MWe for 30 years was feasible at Olkaria.

A three dimensional model for Olkaria East field was developed by Bodvarsson *et al.* (1987). The 3-D model allowed calibration using data from individual wells and hence had the capability to predict the performance of each well. It was a three layer model with 54 elements modelling the steam zone, upper and lower liquid zones, with a total reservoir model area of 9 km and a thickness of 850m. The model had boundary conditions of zero mass flow through the top and bottom with open recharge through the sides. The model was calibrated against 6.5 years of production history from July 1977 to December 1983. The model matched well the flow rate, enthalpy and pressure decline data. Bodvarsson *et al.* (1987) considered three exploitation schemes with different scenarios, namely the effect of well spacing on well deliverabilities, power production of 45 MWe and 105 MWe and the effect of injection on well performance and reservoir depletion. These modellers concluded, among other things, that the present well density in Olkaria East field is too high and that injection could help sustain steam flow rates from wells thus reducing the need for new replacement wells. The parameters in the model such as pressure, enthalpy were determined by the Lawrence Berkeley Laboratory's general purpose simulator MULKOM.

CHAPTER THREE

DYNAMICS OF FLUID FLOW IN POROUS MEDIA

3.1 Structure and properties of porous media

Fluid flow in porous media is described by a number of basic concepts which will first be explored before we can adequately consider the formulation of basic equations which govern flow in porous media. A porous material is any solid containing pores or holes or voids either in a regular or random manner, provided such holes occur relatively frequently within the solid (Collins, 1961). We now identify some of the important governing parameters required in the formulation of the geothermal reservoir equations.

3.1.1 Porosity

Porosity denoted by the symbol ϕ , is defined as the fraction of the bulk volume of the material occupied by voids. If V_p denotes the volume of the pores and V_B the bulk volume of the material then

$$\phi = \frac{V_p}{V_B} \quad (3.1.1)$$

The portion of the bulk volume not occupied by pores is termed the matrix of the material. Thus if V_s denotes the volume of the solid matrix, then:

$$\frac{V_s}{V_B} + \frac{V_p}{V_B} = 1 \quad (3.1.2)$$

This means that

$$1 - \phi = \frac{V_s}{V_B} \quad (3.1.3)$$

Two classes of porosity occur in nature, namely absolute or total porosity and effective porosity. Absolute or total porosity is the fractional void space with respect to the bulk volume regardless pore connections.

Effective porosity is the fraction of the bulk volume constituted by inter-connecting pores. Effective porosity is an indication of permeability (see below).

Porosity depends on the distribution of grain size of the porous materials. Compaction; which is a process of volume reduction due to an externally applied pressure; has the effect of changing the porosity. Chemical leaching and physical erosion due to the flow of ground water through the porous rocks enlarge the pores and thus has a direct effect on the porosity. On a microscopic scale, porosity may vary greatly throughout a system. In fractured rock for example, ϕ may vary from little more than 0 in the rock itself to unity in the fractures (Freestone, 1992). On a large scale, however, an average porosity is defined and it is this value which is used in the analysis of a reservoir.

3.1.2 Permeability

Permeability, denoted by k , is defined as that property of the porous material which characterizes the ease with which a fluid may be made to flow through the material due to a pressure gradient. Permeability may be directional, i.e. different from one direction to another. A system with directionally varying permeability is said to be anisotropic. A system in which permeability is the same in all directions is said to be isotropic. Geothermal systems frequently have anisotropic permeability (Freestone, 1992). Permeability is expressed in the units of area, namely, m^2 .

3.1.3 Thermal conductivity

The thermal conductivity, K , of a material is a measure of its ability to transfer heat energy by conduction alone, when stressed by a thermal gradient. The units are Watt/mK. Typical values for rock are in the range of 2- 2.5W/mK.

3.1.4 Compressibility of rocks

Mechanical properties of porous materials are not usually important in problems of fluid flow through porous media. However, in the particular case of deeply buried sedimentary rocks, these properties may have some bearing on the flow of geothermal fluids in porous media. Compressibility of rocks denoted C_r is defined as the ratio of change in total volume of the rock to the product of total volume and change in pressure. In symbols, it is defined as:

$$C_r = \frac{-1}{V_B} \frac{\partial V_B}{\partial P} \quad (3.1.4)$$

Where ∂P denotes externally applied pressure. Thus if ρ_r is the density of the rock and m its mass then, since $m = \rho_r V_B$ it can readily be shown that

$$C_r = \frac{1}{\rho_r} \frac{\partial \rho_r}{\partial P} \quad (3.1.5)$$

3.1.5 Other parameters

The relative permeability, denoted by k_r , is defined as the the permeability of the porous material at a given fluid saturation to the permeability of the same porous material when it is 100% saturated with the same fluid. It is a dimensionless quantity.

The specific heat capacity of a material, denoted c_r is defined as a measure of the amount of heat energy which must be supplied to raise a unit mass of the material by $1^\circ K$. Hence it is given in terms of energy per mass per degree K . A typical value for rock is $1000 J/kgK$, where J is the energy in Joules (Freestone, 1992).

The density ρ_r of the rock is defined as a measure of the ratio of mass to volume averaged over the material.

Thermal conductivity of a water saturated rock depends on both the conductivity of the rock itself and that of the fluid, i.e. it is a mixture of

rock and fluid properties:

$$K = (1 - \phi)K_r + \phi K_f \quad (3.1.6)$$

where K_r and K_f denote the thermal conductivities of the rock and fluid respectively. Since ϕ is usually small, the value of K depends mainly on K_r .

3.2 Behaviour of fluids in porous media

The ability to predict the behaviour of geothermal reservoirs is closely related to the ability to predict the flow characteristics of the fluid in the reservoir. Darcy performed an experiment from which he deduced what is called Darcy's law of flow through porous media, see for example (Collins, 1961). A fluid was passed in a horizontal column filled with a porous material (Figure 3.2.1).

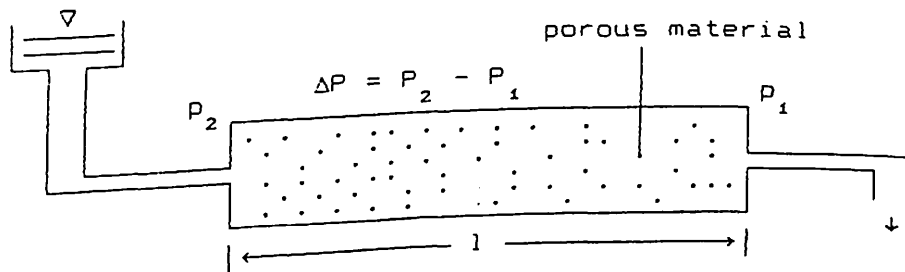


Figure 3.2.1 Darcy's Experiment

If l denotes the length of the porous material, A , the cross-sectional area of the column, q the flow rate and ΔP the pressure difference at the ends of the column, Darcy deduced that

$$q = -k' \frac{A \Delta P}{l}, \quad (3.2.1)$$

where k' is the permeability and depends on the properties of both the porous medium and the fluid. In fact $k' = k/\mu$ where k is the permeability of the porous medium and μ is the shear viscosity of the fluid.

Therefore

$$q = -\frac{kA\Delta P}{\mu\ell} \quad (3.2.2)$$

Thus, rate of flow of a homogeneous fluid through a porous medium is proportional to the pressure gradient and the cross-sectional area normal to the direction of flow and inversely proportional to the dynamic viscosity of the fluid. This is the statement of Darcy's law. The flux or Darcy velocity \bar{v} , is the average volume flux or flow rate per unit cross-sectional area of the porous medium.

Dimensional analysis of Equation (3.2.1) shows that k has the dimensions of length squared. Hence k is roughly a measure of the mean square pore diameter in the porous medium.

One special unit often used is the Darcy which is approximately equal to $10^{-12}m^2$ or millidarcy which is approximately equal to $10^{-15}m^2$. Saturation of a porous medium with respect to a particular fluid say 1 denoted by S_1 , is defined as:

$$S_1 = \frac{\text{Volume of fluid in the medium}}{\text{Total volume of voids in the medium}}$$

Thus for two fluids 1 and 2 jointly filling the pore space,

$$S_1 + S_2 = 1 \quad (3.2.3)$$

Saturation is a dimensionless quantity.

Below we summarize some fundamental thermodynamic and transport properties of water. As pressure increases, so does the saturation temperature, namely the temperature at which water boils.

Saturated water and steam densities denoted by ρ_w and ρ_s respectively are defined as the ratios of mass to volume of water or steam. The

units are usually kg/m . At saturation temperature and pressure, i.e. on the saturation line, the density of each phase (water/steam) is different.

Internal energy denoted by u is a measure of the total amount of heat stored in a material. The specific internal energies i.e. energy stored per unit mass due to liquid water and steam are denoted by u_w and u_s respectively. The enthalpy of the fluid denoted by h is a measure of the sum of the internal energy and an amount due to work stored by the action of pressures. Specific enthalpies i.e. enthalpy of fluid per unit mass due to water and steam are denoted by h_w and h_s . The two types of energy measure are related by

$$h_w = u_w + \frac{p}{\rho_w}$$

$$h_s = u_s + \frac{p}{\rho_s}$$

where p is the pressure. Both quantities are measured in units of energy/mass.

The dynamic viscosities of water and steam denoted μ_w and μ_s , respectively, depend mainly on temperature and vary only slightly with pressure. Units often used are Pascal second (kg/ms), and Nm^{-2} . The kinematic viscosities ν_s, ν_w are the quotient of dynamic viscosity divided by density ($\nu = \frac{\mu}{\rho}$).

A two phase flow system exists when two fluids exist within the same pore space. The fluids are separated by boundaries called interfaces, across which discontinuities in density and pressure exist. An interface is made possible by the existence of forces called inter-facial forces that act only at boundaries between separate phases and are tangential to the boundaries. When boundaries are curved; as they usually are in porous media, (e.g. Collins, 1961), the tangential inter-facial force produces pressure discontinuities at the interfaces. The pressure difference denoted by P_c is called

the capillary pressure. When two or more fluid phases occupy a porous medium, one of the fluids is adsorbed on the solid surface more strongly than the other (e.g. Collins, 1961). The fluid which is strongly adsorbed and which displaces the other fluid from the adsorbed film is called the wetting fluid phase. The displaced film is the non-wetting fluid phase. In most cases, liquids are adsorbed more strongly than gases and as a consequence, in a two-phase system involving a liquid and a gas, the liquid will usually be the wetting phase. One effect of inter-facial forces is the tendency to compress the non-wetting phase relative to the wetting phase. Thus the non-wetting phase has a higher pressure than the wetting phase.

Capillary pressure is a function of saturation; thus if P_1 and P_2 denote the pressure of the non-wetting fluid and the wetting fluid respectively then the capillary pressure, P_c , in the porous medium, is given by

$$P_c(S_1) = P_1 - P_2 \quad (3.2.4)$$

In experimental methods for determining capillary pressure curves, the sample is initially saturated with either a wetting or a non-wetting fluid. The capillary pressure-saturation curves obtained for the two initial states are not the same. This phenomenon is termed capillary hysteresis. The curve obtained (Figure 3.2.2) beginning with the sample saturated with the wetting fluid is termed the drainage curve, and that beginning with the sample

UNIVERSITY OF NAIROBI LIBRARY

saturated with the non-wetting fluid is called the imbibition curve.

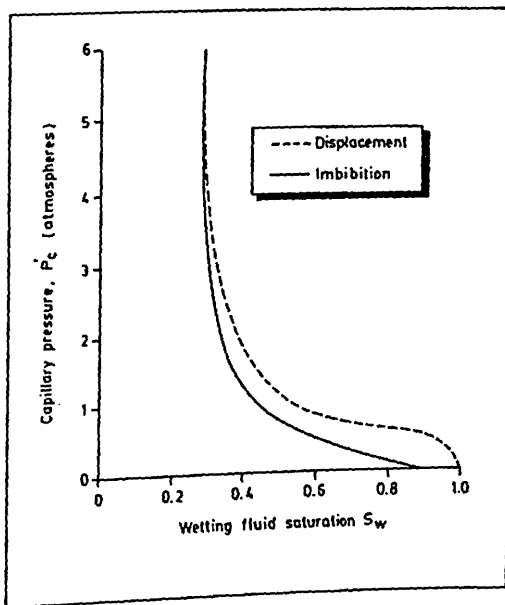


Figure 3.2.2 Capillary hysteresis

Capillary pressure-saturation curves have been employed to infer what is termed as the pore size distribution of porous materials. If a porous material is viewed as composed of a collection of pores having some distribution radii, then there exist equations which relate this distribution function to the capillary pressure distribution function. For example for a cylindrical tube of radius r_i

$$P_c(r_i) = \frac{2\gamma_{12} \cos \theta}{r_i}, \quad (3.2.5)$$

where γ_{12} , with subscripts 1 and 2 referring to non-wetting and wetting fluid respectively, is the surface tension in both non-wetting and wetting fluid and the distribution function, $D(r_i)$ is related to P_c as follows (Collins, 1961):

$$D(r_i) = \frac{P_c \phi}{r_i} \times \frac{dS_2}{dP_c} \quad (3.2.6)$$

The expression $\frac{dS_2}{dP_c}$ can be determined from a capillary pressure saturation-curve. The complexity of naturally porous structures defies all attempts to define pore size. Even so, simple definitions such as those

employed above do have some utility and contribute to our understanding of the part played by pore-size distribution in determining the characteristics of flow through porous materials.

Common reservoir fluids encountered may be classified into three groups depending on their compressibility, namely, incompressible, slightly compressible and compressible. Incompressible fluids have a constant density, slightly compressible fluids have a measurable change of density with pressure and compressible fluids have a significant density change with pressure. Isothermal compressibility C of a fluid is defined as

$$C = \frac{-1}{V} \frac{\partial V}{\partial P} \quad (3.2.7)$$

where V is the volume and P is the pressure of the fluid. It can be shown that

$$C = \frac{1}{\rho} \frac{\partial \rho}{\partial P}, \quad (3.2.8)$$

where ρ is the density of the fluid and P is the pressure. Integrating this equation we have:

$$\rho = \rho_0 e^{C(p-p_0)} \quad (3.2.9)$$

where ρ_0 and p_0 are reference density and pressure respectively. For incompressible fluids, $C = 0$. For slightly incompressible fluids, $C \approx 0$ and hence the density is given by

$$\rho = \rho_0 e^{C(p-p_0)} = \rho_0 \left[(1 + C(p-p_0) + \frac{C^2(p-p_0)^2}{2!} + \dots) \right] \quad (3.2.10)$$

which is obtained by using Taylor series expansion of the exponent in Equation (3.2.9). Since $C \approx 0$, neglecting second or higher order terms in Equation (3.2.10) yields:

$$\rho = \rho_0 (1 + C(p-p_0)) \quad (3.2.11)$$

Reservoir waters are among fluids that are slightly incompressible. For compressible fluids e.g. gases, the truncation of the series expansion of the exponential is not valid. The complete series must be taken.

In fluid saturated porous media, there can be as many as three fluid phases present. In rocks saturated with more than one fluid, the ability of each fluid to move under an applied pressure gradient is a function of the relative permeability of that phase. Thus

$$k_{r1} = \frac{k_1}{k} \quad (3.2.12)$$

where subscript 1 denotes fluid 1 and k denotes the permeability of the medium.

3.3 Conservation principle

3.3.1 Conservation of mass

In fluid flow, one of the most useful mathematical tools is that obtained from the principle of the conservation of mass, momentum or energy. From the conservation of mass we can derive the continuity equation.

Consider, in the field of flow, an element of volume in the form of a rectangular parallelepiped having sides $\Delta x_1, \Delta x_2$, and Δx_3 in a field of flow as in Figure 3.3.1

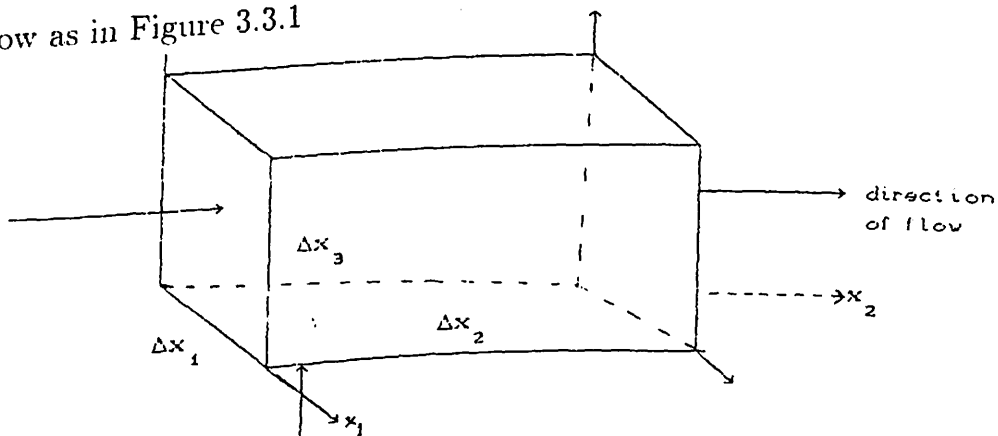


Figure 3.3.1 Volume element in the region of flow

Let the concentration of the quantity be G , expressed in units per unit volume, the flux density of the quantity be denoted by $\vec{\Omega}$ expressed in units transported per unit time per unit area and the physical quantity in question be released within the field of flow at a rate of G units per unit time per unit volume. The quantities Γ, G and $\vec{\Omega}$ are variables.

The conservation of the physical quantity can be mathematically formulated using the average flux density across each face of the volume element. Let $\bar{\Omega}_1(x_1, x_2, x_3, t)$ be the average value of Ω_1 over the face with sides Δx_2 and Δx_3 located at x_1 and $\bar{\Omega}_1(x_1 + \Delta x_1, x_2, x_3, t)$ the average value of Ω_1 over the corresponding face located at $x_1 + \Delta x_1$. Similar definitions can be made for the other faces. The amount of the physical quantity entering the volume element during the time interval t to $t + \Delta t$ is

$$[\bar{\Omega}_1(x_1, x_2, x_3, t)\Delta x_2\Delta x_3 + \bar{\Omega}_2(x_1, x_2, x_3, t)\Delta x_1\Delta x_3 + \bar{\Omega}_3(x_1, x_2, x_3, t)\Delta x_1\Delta x_2]\Delta t.$$

Similarly the amount leaving the volume element during this time is:

$$[\bar{\Omega}_1(x_1 + \Delta x_1, x_2, x_3, t)\Delta x_2\Delta x_3 + \bar{\Omega}_2(x_1, x_2 + \Delta x_2, x_3, t)\Delta x_1\Delta x_3 + \bar{\Omega}_3(x_1, x_2, x_3 + \Delta x_3, t)\Delta x_1\Delta x_2]\Delta t$$

Also during this time, an amount

$$G(x_1, x_2, x_3, t)\Delta x_1\Delta x_2\Delta x_3\Delta t$$

is released within the volume element. As a result of the possible excess of inflow over outflow and the release of the material within the element of volume, the amount of the physical quantity within the element changes, during the time Δt , by an amount:

$$[\Gamma(x_1, x_2, x_3, t + \Delta t) - \Gamma(x_1, x_2, x_3, t)]\Delta x_1\Delta x_2\Delta x_3$$

Since the physical quantity in question must be conserved, it follows that:

$$\left(\begin{array}{c} \text{Amount} \\ \text{in} \end{array} \right) - \left(\begin{array}{c} \text{Amount} \\ \text{out} \end{array} \right) + (\text{Amount generated}) = \text{Increase in content} \quad (3.3.1)$$

Substituting in Equation (3.3.1) the expressions given above, and dividing through by $\Delta x_1, \Delta x_2, \Delta x_3$ and Δt and taking limits as $\Delta x_1, \Delta x_2, \Delta x_3$ and Δt are each allowed to approach zero, there results the equation:

$$-\left(\frac{\partial \Omega_1}{\partial x_1} + \frac{\partial \Omega_2}{\partial x_2} + \frac{\partial \Omega_3}{\partial x_3} \right) + G = \frac{\partial \Gamma}{\partial t} \quad (3.3.2)$$

which in vector notation becomes

$$-\nabla \cdot \vec{\Omega} + G = \frac{\partial \Gamma}{\partial t} \quad (3.3.3)$$

This is the continuity equation for fluid flow and can be applied to situations as described below.

(a) Single-phase incompressible flow

For incompressible fluids the volume of an element of fluid is not altered by changes in pressure. Hence fluid volume is conserved and in Equation (3.3.3), $\vec{\Omega}$ becomes the volumetric fluid density i.e. velocity \vec{V} . Also the concentration Γ becomes the concentration of fluid volume which is the porosity ϕ . Thus Equation (3.3.3) becomes:

$$-\nabla \cdot \vec{V} + G = \frac{\partial \phi}{\partial t} \quad (3.3.4)$$

This is the equation which governs a single-phase incompressible flow.

(b) Single-phase compressible flow

In the flow of compressible fluid through a porous medium, the volume of an element of the fluid may change due to changes in pressure.

Therefore, fluid volume is not conserved. However, the mass of an element of fluid remains unchanged. It can readily be shown for this case of single-phase compressible flow that

$$\rho \vec{v} = \vec{\Omega}$$

and

$$\Gamma = \phi \rho.$$

Hence substituting these expressions in Equation (3.3.3) we find

$$-\nabla \cdot (\rho \vec{v}) + G = \frac{\partial(\phi \rho)}{\partial t} \quad (3.3.5)$$

Equation (3.3.5) describes the flow of an incompressible fluid in a porous medium.

(c) Multi-phase flow of two immiscible fluids

For the simultaneous flow of immiscible fluids, two independent conservation principles must be invoked. If we denote the fluids by subscripts 1 and 2 for wetting and for non-wetting fluids, respectively, then Equation (3.3.5) becomes

$$-\nabla \cdot (\rho_1 \vec{v}) + G = \frac{\partial(\rho_1 \phi S_1)}{\partial t} \quad (3.3.6)$$

Similarly

$$-\nabla \cdot (\rho_2 \vec{v}) + G = \frac{\partial(\rho_2 \phi S_2)}{\partial t} \quad (3.3.7)$$

Equations (3.3.6) and (3.3.7) describe multi-phase flow of two immiscible fluids in a porous medium.

3.4 Darcy's law for anisotropic porous medium

In the discussion of Darcy's law of flow through porous media, it is assumed that the permeability and relative permeability are independent of the direction of fluid flow within the medium. This is not generally true

of all the porous media. For some porous materials such as sedimentary rocks, the fluid transmissibility is not the same in all directions. To take this characteristic of the porous media into account requires a further generalization of the laws of flow. The correctness of such extensions can be established only by appeal to experiments for confirmation of predictions based on such extensions. The most general linear relationship between the components of velocity V_i and the components $\partial\Phi/\partial x_j$ that can be postulated takes the form:

$$V_i = -\frac{\rho}{\mu} k_{ij} \frac{\partial\Phi}{\partial x_j} \quad (i, j = 1, 2, 3) \quad (3.4.1)$$

In which Φ is the velocity potential. Here the nine quantities k_{ij} ($i = 1, 2, 3, j = 1, 2, 3$) form the elements of a tensor. The nine elements form what is called the k -matrix. If a rotation of the coordinate axis is considered, the manner in which the k -matrix transforms under such a rotation can be investigated. Such an investigation shows that, if the k -matrix is symmetric, then the rotation of the axes to a particular orientation produces a diagonal matrix. Thus if $k_{ij} = k_{ji}$, $i = 1, 2, 3, j = 1, 2, 3$ for a particular set of rectangular axes x'_i , $i = 1, 2, 3$ (i.e. particular orientation of the coordinate system), the k -matrix takes the form (denoted as the k^1 -matrix).

$$k^1 = \begin{pmatrix} k_1 & 0 & 0 \\ 0 & k_2 & 0 \\ 0 & 0 & k_3 \end{pmatrix} \quad (3.4.2)$$

The directions of the particular set of coordinate axis to which the k -matrix corresponds are called the principal axes of the porous medium. Thus for the coordinate axis oriented parallel to the principal axis of the porous medium having orthogonal principal axes, the postulated form of Darcy's law becomes:

$$v_i = \frac{-k_i}{\mu} \rho \frac{\partial\Phi}{\partial x_i} \quad i = 1, 2, 3 \quad (3.4.3)$$

This rotation of axes also requires a change in the form of porosity, ϕ . Thus since in general not one of the primed coordinates is parallel to the vertical (direction of the gravitational force) ϕ must be written as:

$$\phi = \sum_{i=1}^3 x_i' \cos \alpha_i \int_0^p \frac{dp}{\rho} \quad (3.4.5)$$

(Collins, 1961)

Here the α_i , $i = 1, 2, 3$ are the angles between the respective primed axes, x_i' , $i = 1, 2, 3$ and x_3 which was assumed vertical. The basic concepts of fluid flow in porous media having been explored in this chapter, we are now in a position to consider the formulation of equations which govern flow in porous media in the next chapter.

CHAPTER FOUR

GOVERNING EQUATIONS

4.1 Introduction

Scientists studying physical phenomenon are faced with the problem of finding solution to some physical processes that occur in nature. Nature itself being complex, the solutions to these processes are usually approximations. Nevertheless, these approximate solutions advance our understanding of the behaviour of the physical process in question. Modelling of the physical processes has for long been recognized. The modelling process involves the use of models to obtain some insight into the behaviour of some physical processes. In a very general sense, there are two types of models, namely, physical and mathematical models. Physical models are the scaled down reproductions of the original. Mathematical models on the other hand are systems of mathematical equations that describe the physical behaviour of the process under investigation. In geothermal reservoir work, these equations are complex, non-linear partial differential equations and, because of the complexity of these models, a computer is required to solve the resultant system of equations. Mathematical modelling can be a repetitive process in the sense that when the modeller inputs data related to the parameters in the model, the model simulates and produces results. When the produced results are analyzed by the modeller, there may be need to improve or modify these findings i.e. the process of data input is repeated until the upgraded results are reasonable. In this way the modeller can develop an efficient and a fairly reasonable predictive tool for the process under study.

4.2 . Basic governing equations

The mathematical model for geothermal systems describes the three dimensional flow of water, steam or both and transport of heat in porous media. These equations which express the laws of conservation of mass, momentum and energy in a geothermal reservoir are non-linear parabolic partial differential equations. Derivation of these equations has been done by a number of authors. For example Faust and Mercer (1979) give a detailed derivation of the equations and state the major assumptions used while Grant et al. (1982) give a more general derivation. The balance equations discussed in this section are based on the following simplifying assumptions which are assumed to hold:

1. Capillary pressure effects are negligible
2. Thermal equilibrium exist among the steam, water and rock
3. Relative permeability is a function of liquid saturation
4. The reservoir is single-component water consisting either of one or two phases
5. Viscosities are considered functions of temperature
6. Porosity is a linear function of pressure
7. Rock density and permeability are functions of space
8. Rock enthalpy is a linear function of temperature.

Some of these assumptions are discussed as we develop the equations. The basic governing equations may be expressed in terms of pairs of basic unknown thermodynamic quantities as independent variables, for instance, fluid enthalpy and pressure, or density and internal energy, or pressure and temperature or pressure and saturation. These models how-

ever, have their inherent restrictions. The pressure-temperature model is for example restricted in its use to hot water geothermal systems only while the pressure-saturation model works only in two-phase reservoirs on the saturation vapour line. Faust and Mercer (1975) point out that fluid pressure-enthalpy formulation is preferred because these parameters uniquely define the thermodynamic state of the system in single-phase hot water or superheated steam flow and two-phase flow consisting of both water and steam, conditions that are commonly obtained in geothermal field situations. In addition, this formulation offers the advantage of avoiding the necessity of using three unknown parameters which is the case when the pressure-temperature-saturation formulation is used. The basic field equations which express the laws of continuum mechanics are given below.

(a) conservation of mass

Conservation of mass is governed by the following equation, as derived in section 3.3:

$$\frac{\partial M}{\partial t} + \nabla \cdot \vec{Q}_m = q_m, \quad (4.2.1)$$

where M is the mass content per unit volume and is given by

$$M = \phi(\rho_s S_s + \rho_w S_w) \quad (4.2.2)$$

in which ϕ is the medium porosity, ρ_w and ρ_s are the densities of water and steam respectively. The quantities S_w and S_s are the water and steam saturations respectively and satisfy Equation(3.2.3) of chapter three. The average fluid density ρ of the steam-water is defined by

$$\rho = \rho_w S_w + \rho_s S_s \quad (4.2.3)$$

The symbol q_m is the mass contribution from sources and sinks. The mass flux, \vec{Q}_m is given by

$$\vec{Q}_m = \vec{Q}_{mw} + \vec{Q}_{ms}. \quad (4.2.4)$$

where the water and steam fractions are \bar{Q}_{mw} and \bar{Q}_{ms} respectively and are given by a modified form of Darcy's law:

$$\bar{Q}_{mw} = -\frac{kk_{rw}\rho_w}{\mu_w}(\nabla P - \rho_w\vec{g}) \quad (4.2.5a)$$

$$\bar{Q}_{ms} = -\frac{kk_{rs}\rho_s}{\mu_s}(\nabla P - \rho_s\vec{g}) \quad (4.2.5b)$$

(b) Conservation of energy

Conservation of energy is governed by the following equation, as derived in section 3.3 (except that the quantity to be conserved is the energy rather than the mass):

$$\frac{\partial E}{\partial t} + \nabla \cdot \bar{Q}_e = q_e \quad (4.2.6)$$

in which E , the energy content per unit volume which is a contribution of energy from the rock and the fluid is given by

$$E = (1 - \phi)\rho_r h_r + \phi(\rho_w S_w h_w + \rho_s S_s h_s) \quad (4.2.7)$$

where h_r , ρ_r are the rock specific enthalpy and rock density respectively, h_w , and h_s are the specific enthalpies for water and steam phases respectively. The symbol q_e is the energy from sources and sinks. The total enthalpy of the water-steam mixture is defined by

$$h = \frac{\rho_w h_w S_w + \rho_s h_s S_s}{\rho} \quad (4.2.8)$$

The energy flux \bar{Q}_e is given by

$$\bar{Q}_e = h_w \bar{Q}_{ew} + h_s \bar{Q}_{es} - K_m \nabla T, \quad (4.2.9)$$

see for instance (Freestone, 1992). The vector quantities in \bar{Q}_{ew} and \bar{Q}_{es} are as given in Equation(4.2.5). The last term in Equation (4.2.9) represents the energy movement resulting from conduction. Here T represents

the temperature of the reservoir while K_m is the thermal conductivity of the saturated porous medium and is a sum of the thermal dispersion and conduction terms for the rock, steam and water. This combination is reasonable and is based on the assumption that local thermal equilibrium among the phases is achieved in an instant since the movement of steam and water through porous media is sufficiently slow and the surface areas of all the phases are sufficiently large.

Since pressure and enthalpy are two basic thermodynamic variables, the temperature T in Equation (4.2.9) is a function of pressure P and enthalpy h . Thus the gradient vector ∇T can be expressed as follows:

$$\nabla T = \left(\frac{\partial T}{\partial P} \right) |_h \nabla p + \left(\frac{\partial T}{\partial h} \right) |_p \nabla h \quad (4.2.10)$$

where $\left(\frac{\partial T}{\partial P} \right) |_h$ and $\left(\frac{\partial T}{\partial h} \right) |_p$ are partial derivatives evaluated at constant enthalpy and pressure respectively.

Relative permeabilities for steam and water phases, which are functions of water saturation, express the fact that the presence of one phase impedes the flow of the other. These relative permeabilities are therefore normally less than unity if both phases are present. They approach unity as the saturation of the other phase approaches zero. Each relative permeability may approach zero even though the saturation for that phase is not zero. The fluid phase concerned is immobile and the saturation of the fluid phase at which this occurs is termed the residual saturation. These ideas are illustrated in Figure 4.2.1.

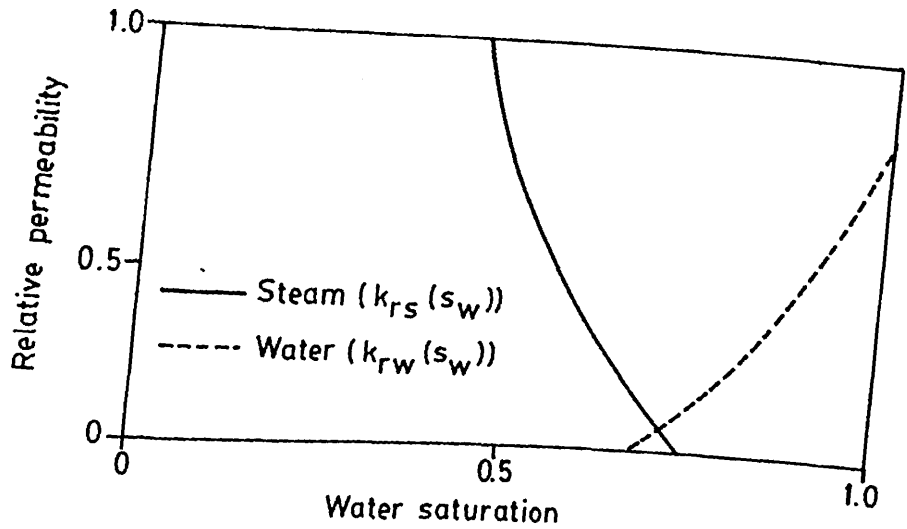


Figure 4.2.1 Relative permeabilities to steam and water of sandstone (adapted from Grant *et. al* 1982)

The exact functional forms of $k_{rw}(s_w)$ and $k_{rs}(s_w)$ are poorly known. Relative permeability functions are a property of the reservoir rock and they depend on pore structure and the geometry of fractures. The commonly used relative permeabilities for homogeneous media are those suggested by Corey (1972), namely,

$$k_{rw} = S_w^{*4}, \quad (4.2.11)$$

$$k_{rs} = (1 - S_w^{*2})(1 - S_w^*)^2, \quad (4.2.12)$$

where

$$S_w^* = \frac{(S_w - S_{wr})}{(1 - S_{wr} - S_{sr})}$$

in which S_{wr} and S_{sr} are the residual saturations at which the water and steam phases, respectively, become immobile. For Olkaria reservoir, water relative permeability k_{rw} is assumed to be a linear function of saturation S_w . This leads to the equation

$$k_{rw} = \frac{S_w - 0.3}{0.6} \quad (4.2.13)$$

in which the water residual saturation S_{wr} is assumed to be 0.3. This choice of s_{wr} made a satisfactory match to the observed enthalpies in Chapter six. Equation (4.2.13) is derived by assuming a linear function through saturation points (0.3, 0) and (0.9, 1), see Figure 4.2.1.

4.3 Alternative forms of the mass and energy equations

Inserting Equation (4.2.4) into Equations (4.2.1) and (4.2.6) yields equations of the form:

$$\frac{\partial M}{\partial t} - \nabla \cdot \left[\frac{k k_{rw} \rho_w}{\mu_w} (\nabla P - \rho_w \vec{g}) + \frac{k k_{rs} \rho_s}{\mu_s} (\nabla P - \rho_s \vec{g}) \right] - q_m = 0 \quad (4.3.1a)$$

$$\begin{aligned} \frac{\partial E}{\partial t} - \nabla \cdot \left[\frac{k k_{rw} \rho_w}{\mu_w} (\nabla P - \rho_w \vec{g}) + \frac{k k_{rs} \rho_s}{\mu_s} (\nabla P - \rho_s \vec{g}) + \frac{k k_{rs} \rho_s h_s}{\mu_s} (\nabla P - \rho_s \vec{g}) \right] \\ - \nabla \cdot \left[K_m \left(\frac{\partial T}{\partial p} \right) \Big|_p \nabla h \right] - q_c = 0 \end{aligned} \quad (4.3.1b)$$

Define the following symbols:

$$T_s = \frac{k A k_{rs} \rho_s}{\mu_s} \quad T_w = \frac{k A k_{rw} \rho_w}{\mu_w} \quad (4.3.2a)$$

$$T_h = T_w h_w + T_s h_s + K_m A \left(\frac{\partial T}{\partial p} \right) \Big|_h \quad T_c = K_m A \left(\frac{\partial T}{\partial h} \right) \Big|_p \quad (4.3.2b)$$

called the transmissibility terms, where A is the cross-sectional area perpendicular to the flow direction in a grid block. Substituting the above quantities in Equation (4.3.2) into Equation (4.3.1) yields Equations (4.3.3a) and (4.3.3b) for conservation of mass and energy respectively.

$$\frac{\partial M}{\partial t} - \nabla \cdot \left[(T_s + T_w) \nabla p \right] + \nabla \cdot (T_s \rho_s \vec{g} + T_w \rho_w \vec{g}) \quad (4.3.3a)$$

$$\frac{\partial E}{\partial t} - \nabla \cdot \left[(T_h \nabla P + T_c \nabla h) \right] + \nabla \cdot (T_s h_s \rho_s \vec{g} + T_w h_w \rho_w \vec{g}) - q_c = 0 \quad (4.3.3b)$$

The mass and energy contributions q_m and q_c , from sources or sinks are termed source/sink terms. They represent the amount of mass and heat

lost (gained) to sources or sinks. For two-phase, the flow mass rate loss to a source/sink is defined as

$$q_m = q_s + q_w \quad (4.3.4)$$

and the heat rate loss to a source/sink is

$$q_c = h_s q_s + h_w q_w, \quad (4.3.5)$$

where a negative rate loss would indicate a loss from the reservoir. The quantities q_s and q_w represent mass source terms for the steam and water phases respectively. Equations (4.3.3a) and (4.3.3b) are the final three-dimensional equations describing two-phase flow of heat in a steam-water-rock system. They will be the subject of study in subsequent chapters.

4.4 . Initial and Boundary Conditions

Fluid movement, and consequently energy movements in a geothermal reservoir may be viewed as a phenomenon which occurs in space (x -, y - and z - dimensions) and in time (t). If we consider the reservoir as a system confined by a boundary, it is possible to state two facts related to it. Firstly, any fluid that enters or leaves this system must cross this boundary. Secondly, at some initial time the system can be described by a given set of conditions. The two statements describe the boundary and initial conditions of the system respectively. If some parameter of the reservoir, for instance pressure or enthalpy, is considered, three possibilities arise:

- (i) within some section of the boundary, no observed flux of the parameter crosses the boundary implying a zero gradient.
- (ii) in some section of the boundary there may be a known flux of the parameter entering the reservoir.

(iii) there may be a section in the boundary which is defined by a fixed value of the parameter.

Parabolic partial differential equations describing geothermal flow are either initial value problems or initial boundary value problems. The boundary conditions can be one of the following three types.

Dirichlet boundary condition: The solution here is prescribed along the boundary. If the solution takes on a zero value along the boundary, the condition is termed homogeneous Dirichlet condition.

Neumann boundary condition: Here the derivative of the solution is specified along the boundary. We may also have homogeneous or inhomogeneous Neumann boundary conditions.

Mixed boundary conditions: In this case the solution and its derivatives are prescribed along the boundary. We may also have homogeneous or inhomogeneous mixed boundary conditions.

The most common boundary condition in geothermal reservoir modelling is the specification of the fluxes. Usually the flux is specified as zero, indicating a no flow boundary condition. When mass flux is specified, the following equation which is derived from Equation(4.2.5) gives mass flux for steam and water, must be specified:

$$\bar{q}_m^* = -\left(\frac{k k_{rs} \rho_s}{\mu_s} + \frac{k k_{rw} \rho_w}{\mu_w}\right) \frac{\partial(P - \rho \bar{q})}{\partial \hat{n}}, \quad (4.4.1)$$

where \bar{q}_m^* is the specified mass flux at the boundary and $\partial/\partial \hat{n}$ is the outward normal derivative. Corresponding to the specified mass flux, a convective energy flux must also be specified according to an equation similar to Equation (4.3.5):

$$q_h^* = q_s^* h_s^* + q_w^* h_w^*, \quad (4.4.2)$$

where h_s^* and h_w^* are the saturated steam and water enthalpies, respectively, and q_s^* and q_w^* are the fractional steam and water fluxes, respectively, at the boundary. Since the total energy flux consists of the convective and conductive heat fluxes, a conductive heat flux at the boundary can be determined by

$$q_h^{**} = -K_m \partial T / \partial \hat{n} |_{\text{boundary}} \quad (4.4.3)$$

The derivations of Equations (4.4.1) to (4.4.3) may be found in Faust and Mercer (1979). A constant pressure condition can also be encountered. This means a mass flux at the boundary has to be calculated from Equation (4.4.1) and used in Equation (4.4.3) to determine the convective energy flux. Initial distributions of the principal parameters such as pressure, enthalpy, temperature and water saturation in the reservoir need to be specified. For example the reservoir may have initial water saturation as one. The specific initial and boundary conditions that were applied to the Olkaria reservoir are outlined in Chapter Six (Section 6.2). The model equations developed in this chapter are used as the basic model for obtaining the numerical solution in Chapter Five and its applications to the Olkaria reservoir in Chapter Six.

CHAPTER FIVE

NUMERICAL MODEL

5.1 Introduction

The reliability of predictions of geothermal reservoir behaviour depends on how well the geothermal model approximates the field situation. Simplifying assumptions must always be made in order to construct a model because the field situations are too complicated to simulate exactly. Usually the assumptions necessary to solve the mathematical model analytically are fairly restrictive, for example, an analytic solution would require that the medium be homogeneous and isotopic. To deal with the situation more realistically, however, makes the geothermal equations extremely complex and a numerical solution is therefore the only way that a solution to this system of equations can be obtained. The numerical model in this chapter presents the finite difference method for obtaining the solution to the model by using a computer.

5.2. Finite difference representation

The finite difference method entails two basic ideas, namely, that the domain of the solution of the partial differential equation is subdivided by a net with a finite number of mesh points and that the derivative of the function at each point is replaced by a finite difference approximation. The finite difference equations are derived by making a Taylor series expansion of the function at a given point and then solving for the required derivative. In order to solve the partial differential equations by finite differences, the region of interest, in this case the geothermal reservoir, is divided into grid blocks, usually rectangular in shape. Suppose each reservoir block has a volume V and is connected to an adjacent block by an area A termed the interface area, such that the flow is perpendicular to the area A .

The basic Equations(4.2.1) and (4.2.6) can be rewritten using Equations(4.2.4) and (4.2.5) by first defining the forms below:

$$T_m = T_{mw} + T_{ms} \quad (5.2.1)$$

where T_{mw} and T_{ms} are defined in Equation(4.3.2a) and

$$T_e = h_w T_{mw} + h_s T_{ms} + K_m \left(\frac{\partial T}{\partial P} \right)_h \quad (5.2.2)$$

$$T_h = K_m \left(\frac{\partial T}{\partial h} \right)_p, \quad (5.2.3)$$

where the subscripts m, h and e refer to mass enthalpy and energy respectively. The quantities are substituted into Equations (4.2.1) and (4.2.6) to yield:

$$V \frac{\partial M}{\partial t} = \nabla \cdot (T_m \nabla P) - \nabla \cdot (T_{mw} \rho_w \vec{g} + T_{ms} \rho_s \vec{g}) + q_m V \quad (5.2.4a)$$

$$V \frac{\partial E}{\partial t} = \nabla \cdot (T_e \nabla P) + \nabla \cdot (T_h \nabla h) - \nabla \cdot (h_w T_{mw} \rho_w \vec{g} + h_s T_{ms} \rho_s \vec{g}) + q_e V \quad (5.2.4b)$$

From a thermodynamic point of view, in a two-phase geothermal reservoir, temperature is strictly a function of pressure alone. Zyvoloski *et al.* (1979) noted that the conduction term can be dropped since its effect is negligible in two-phase reservoirs. Thus Equation (5.2.4b) may be written as

$$V \frac{\partial E}{\partial t} = \nabla \cdot (T_e \nabla P) - \nabla \cdot (T_{mw} \rho_w h_w \vec{g} + T_{ms} \rho_s h_s \vec{g}) + q_e V \quad (5.2.5)$$

The term T_m in Equation(5.2.1) with T_s and T_w as defined in Equation(4.3.2a) is sometimes referred to as transmissibility term. Since it contains permeability which is directional, it depends on space coordinates x , y and z . Similarly for T_e as defined in Equation(5.2.2). T_m and T_e with a space subscript indicates transmissibility in that space direction. For example T_{mx} , T_{my} and T_{mz} are the transmissibilities in the x -, y -

and z -directions, respectively, and are related to the total transmissibility T_m by

$$\vec{T}_m = T_{mx}\hat{i} + T_{my}\hat{j} + T_{mz}\hat{k} \quad (5.2.6)$$

In order to show clearly the derivatives involved, Equations (5.2.4a) and (5.2.5), written in cartesian space coordinates yield:

$$\begin{aligned} V \frac{\partial M}{\partial t} &= \frac{\partial}{\partial x} (T_{mx} \frac{\partial P}{\partial x}) + \frac{\partial}{\partial y} (T_{my} \frac{\partial P}{\partial y}) + \frac{\partial}{\partial z} (T_{mz} \frac{\partial P}{\partial z}) \\ &\quad - \frac{\partial}{\partial z} (T_{ms}\rho_s g + T_{ms}\rho g) + V q_m \end{aligned} \quad (5.2.7a)$$

$$\begin{aligned} V \frac{\partial E}{\partial t} &= \frac{\partial}{\partial x} (T_{ex} \frac{\partial P}{\partial x}) + \frac{\partial}{\partial y} (T_{ey} \frac{\partial P}{\partial y}) + \frac{\partial}{\partial z} (T_{ez} \frac{\partial P}{\partial z}) \\ &\quad - \frac{\partial}{\partial z} (h_w T_{mw} \rho_w g + h_s T_{ms} \rho_s g) + V q_e \end{aligned} \quad (5.2.7b)$$

A more elaborate presentation of the governing Equations (5.2.4a) and (5.2.4b) which will be useful in latter sections, are derived in Appendix A. The solution to the flow equations described above involves determination of pressure and enthalpy in space and time. To obtain this solution at discrete points in space and time, the spatial domain is broken into cells, grids or blocks (Figure 5.2.1). The time domain is also discretized into a number of time steps, during each of which the problem is solved to obtain new values of pressure or enthalpy.

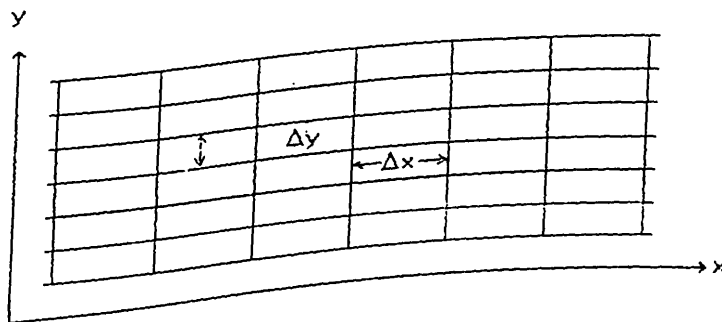


Figure 5.2.1(a): grid system for a 2-D problem

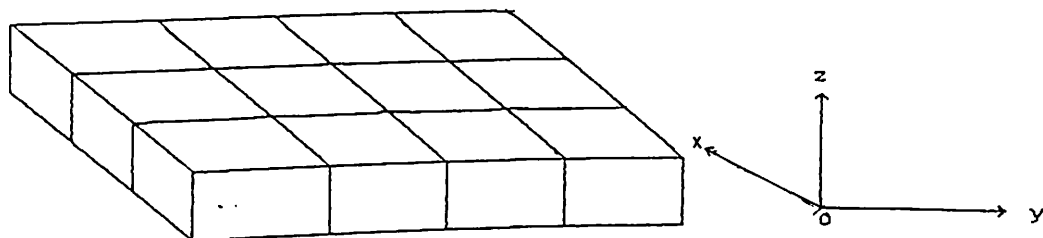


Figure 5.2.1(b) :grid system for a 3-D problem

Now pressure p , and enthalpy h and any other dependent variables are functions of the space variables x , y and z and the time variable t . Suppose, we subdivide the reservoir area into rectangular blocks of sides Δx , Δy and Δz at a given time interval Δt . In addition suppose that i , j , k and n are the cell locations on the grid, then the x , y and z coordinates will be given by $x = i\Delta x$, $y = j\Delta y$ and $z = k\Delta z$ while the time component will be given by $t = n\Delta t$ where i , j , k and n are counters in the x , y , z and t directions, respectively. Using this notation the pressure at a point (x, y, z, t) , for example, may be represented by

$$p(x, y, z, t) \equiv p(i\Delta x, j\Delta y, k\Delta z, n\Delta t) \equiv p_{i,j,k}^n \quad i, j, k, n = 1, 2, \dots$$

Let n be the old time level, then $(n+1)$ will be the new time level. If the value of the dependent variable at the new time level is computed entirely in terms of the values at the old time level, the problem formulation is said to be explicit. We illustrate the concept of explicit formulation through the following example:

EXAMPLE 1.

Consider the following partial differential equation:

$$\frac{\partial^2 P}{\partial x^2} + \frac{\partial^2 P}{\partial y^2} = \frac{\partial P}{\partial t} \quad (5.2.8)$$

Replacing the partial derivatives in space coordinates with the central finite differences and the time derivative with the forward finite difference, we find:

$$\begin{aligned} \frac{p_{i+1,j}^n - 2P_{i,j}^n + p_{i-1,j}^n}{\Delta x^2} + \frac{p_{i,j+1}^n - 2P_{i,j}^n + p_{i,j-1}^n}{\Delta y^2} \\ = \frac{p_{i,j}^{n+1} - p_{i,j}^n}{\Delta t} \end{aligned} \quad (5.2.9)$$

Equation (5.2.9) has only one unknown value, the new pressure at time $(n + 1)$. This equation can be rearranged to obtain the new pressures at the previous time level, namely,

$$p_{i,j}^{n+1} = p_{i,j}^n + \Delta t \left(\frac{p_{i+1,j}^n - 2P_{i,j}^n + p_{i-1,j}^n}{\Delta x^2} + \frac{p_{i,j+1}^n - 2P_{i,j}^n + p_{i,j-1}^n}{\Delta y^2} \right) \quad (5.2.10)$$

This is the explicit finite difference equivalent of Equation (5.2.8). On the other hand if all the unknown pressures or enthalpies at grid blocks are solved for simultaneously at the new time level, the formulation is termed implicit. The concept of implicit formulation can be illustrated by again considering Equation(5.2.8) and its finite difference equivalent Equation(5.2.9). This equation, namely, Equation(5.2.9) has only one unknown, $P_{i,j}^{n+1}$; however, we can set up Equation(5.2.9) to solve for all the three $P_{i,j}$ values in the equation as follows:

$$\begin{aligned} \frac{p_{i+1,j}^{n+1} - 2P_{i,j}^{n+1} + p_{i-1,j}^{n+1}}{\Delta x^2} + \frac{p_{i,j+1}^{n+1} - 2P_{i,j}^{n+1} + p_{i,j-1}^{n+1}}{\Delta y^2} \\ = \frac{p_{i,j}^{n+1} - P_{i,j}^n}{\Delta t} \end{aligned} \quad (5.2.11)$$

Simplifying Equation(5.2.11) gives an equation with all the unknown pressures at the new time level

$$\begin{aligned} p_{i+1,j}^{n+1} - 2P_{i,j}^{n+1} + p_{i-1,j}^{n+1} + p_{i,j+1}^{n+1} - 2P_{i,j}^{n+1} + p_{i,j-1}^{n+1} \\ = \frac{\Delta x^2}{\Delta t} (p_{i,j}^{n+1} - P_{i,j}^n) \end{aligned} \quad (5.2.12)$$

in which we have assumed that the grid spacing in both x and y directions are equal. We solve the unknown pressures implicitly. The implicit finite differencing is a concept introduced largely to help widen the range of stability of the solution to the partial differential equation.

Implicit formulation applied to Equations(5.2.7a) and (5.2.7b) yields:

$$\begin{aligned} V \left(\frac{M^{n+1} - M^n}{\Delta t} \right) &= \frac{1}{\Delta x^2} \left[\delta_x (T_{mx} \delta_x P^{n+1}) \right] + \frac{1}{\Delta y^2} \left[\delta_y (T_{my} \delta_y P^{n+1}) \right] \\ &+ \frac{1}{\Delta z^2} \left[\delta_z (T_{mz} \delta_z P^{n+1}) \right] - \frac{1}{\Delta z} \delta_z (T_{mw} \rho_w g + T_{ms} \rho_s g) \\ &+ V q_m \end{aligned} \quad (5.2.13a)$$

$$\begin{aligned} V \left(\frac{E^{n+1} - E^n}{\Delta t} \right) &= \frac{1}{\Delta x^2} \left[\delta_x (T_{ex} \delta_x P^{n+1}) \right] + \frac{1}{\Delta y^2} \left[\delta_y (T_{ey} \delta_y P^{n+1}) \right] \\ &+ \frac{1}{\Delta z^2} \left[\delta_z (T_{ez} \delta_z P^{n+1}) \right] - \frac{1}{\Delta z} \delta_z (h_w \rho_w g + h_s T_{ms} \rho_s g) \\ &+ V q_e \end{aligned} \quad (5.2.13b)$$

The difference operator, δ , acts as follows:

$$\begin{aligned} \delta_x (T_{mx} \delta_x P^{n+1}) &= T_{mxi+1/2,j,k} (P_{i+1,j,k}^{n+1} - P_{i,j,k}^{n+1}) \\ &- T_{mxi-1/2,j,k} (P_{i,j,k}^{n+1} - P_{i-1,j,k}^{n+1}) \end{aligned} \quad (5.2.14a)$$

$$\begin{aligned} \delta_y (T_{my} \delta_y P^{n+1}) &= T_{myi,j+1/2,k} (P_{i,j+1,k}^{n+1} - P_{i,j,k}^{n+1}) \\ &- T_{myi,j-1/2,k} (P_{i,j,k}^{n+1} - P_{i,j-1,k}^{n+1}) \end{aligned} \quad (5.2.14b)$$

$$\begin{aligned} \delta_z (T_{mz} \delta_z P^{n+1}) &= T_{mzi,k+1/2,k} (P_{i,j,k+1}^{n+1} - P_{i,j,k}^{n+1}) \\ &- T_{mzi,k-1/2,k} (P_{i,j,k}^{n+1} - P_{i,j,k-1}^{n+1}) \end{aligned} \quad (5.2.14c)$$

The inter block transmissibilities i.e. those evaluated at positions $i \pm 1/2$, $j \pm 1/2$, and $k \pm 1/2$ (Fig.5.2.2) are weighted e.g. Equation(A-11) of Appendix A. Density and viscosity are evaluated as arithmetic averages of the values in the adjacent blocks. If say the i -th block is connected to

the j -th block, then as an example, density is evaluated as follows:

$$\rho_{wi,j} = \frac{1}{2}(\rho_{wi} + \rho_{wj})$$

$$\rho_{si,j} = \frac{1}{2}(\rho_{si} + \rho_{sj}),$$

where $\rho_{wi,j}$ or $\rho_{si,j}$ refers to water or steam density for both blocks i and j . Relative permeability values are assigned the upstream value i.e. the value at the rid block having higher fluid potential. This procedure ensures to some extent the stability of the solution. The absolute permeabilities are calculated using harmonic means, i.e. total permeability k is given by

$$\frac{1}{k} = \left(\frac{d_1}{k_1} + \frac{d_2}{k_2}\right)/d,$$

where k_1 and k_2 (Figure 5.2.2) are the absolute relative permeabilities in two adjacent blocks 1 and 2. The letters d_1 and d_2 are the distances between the interface and nodes in blocks 1 and 2 respectively.

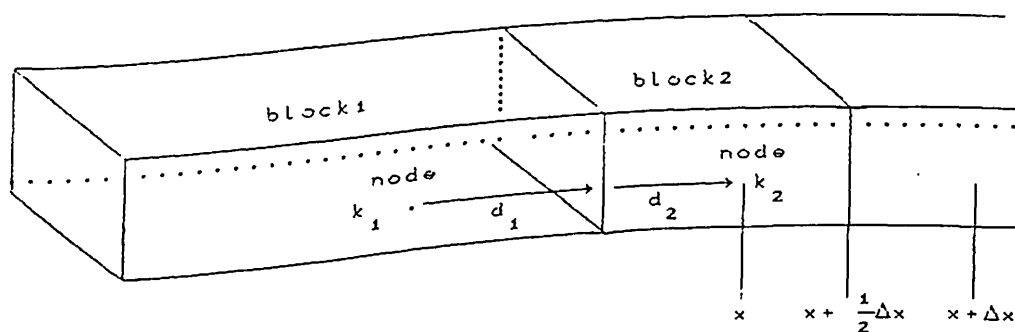


Figure 5.2.2: Adjacent Grid blocks

The non-linearities inherent in the formulation of the difference Equations (5.2.13a) and (5.2.13b) are the transmissibilities, T_m and T_e , the source/sink terms q_m and q_e and the accumulation terms $(M^{n+1} - M^n)$ and $(E^{n+1} - E^n)$, all of which are functions of pressure and enthalpy. Due to this nonlinear nature of the difference equations, the Newton-Raphson technique that is used to linearize them is introduced in the next section.

5.3 Development of the Solution of the non-linear system

Numerical methods are generally required to solve the complex geothermal flow equations. Most of the solution procedures or schemes that are used to solve these equations differ in three aspects. These aspects are space approximations, nonlinear techniques and matrix solution method. In spatial approximations, we can either use the finite difference method or the finite element method. The basic difference between these two methods is in the numerical approximation of the gradient operator ∇ and space discretization of the flow region. For nonlinear techniques we use the fully implicit Newton-Raphson iteration. Finally for matrix solution methods, both Gaussian elimination and relaxation methods are used. The accuracy and efficiency of a model depend on the numerical approximation for evaluating the spatial gradient ∇ and the time derivative $\partial/\partial t$ and on the solution scheme of the algebraic equations. Grid blocks are laid over each other in a reservoir area. The number of blocks depends on the reservoir area to be modelled, depth of deepest feed zones as indicated by drilled wells and on the degree of accuracy of the computed parameters. Obviously more blocks of smaller sizes will be needed to increase the definition in regions where better control is required. The value of the dependent parameter can either be calculated at the centre of the block or at the intersection of the interfaces for two adjacent blocks. The choice really depends on the boundary conditions specified or prescribed in the problem. The block centered grid is generally used with the Neumann type boundary condition. The latter type of grid configuration is generally suited to a Dirichlet type boundary condition. In the block centred grid which we shall adopt in this study, the value of the independent variable at a given node represents the average of the values within the block enclosed by the surrounding interfaces on which the fluxes are evaluated.

Writing Equation(A-10) of Appendix A for each grid block, we find:

$$\begin{aligned}
 & a_i P_{i-1,j,k} - \{b_i + c_j + \alpha_k\} P_{i,j,k} + C_i P_{i+1,j,k} \\
 & + d_j P_{i,j-1,k} + f_j P_{i,j+1,k} + g_k P_{i,j,k_1} + l_k P_{i,j,k+1} \\
 & - m_i h_{i,j,k} - r_k \rho_w g - s_k \rho_s g + \frac{(B_{i,j,k} P_{i,j,k}^n + C_{i,j,k} h_{i,j,k}^n)}{\Delta t} \\
 & + q_{mi,j,k} = 0
 \end{aligned} \tag{5.3.1a}$$

$$\begin{aligned}
 & a'_i P_{i-1,j,k} - \{b'_i + c'_j + \alpha'_k\} P_{i,j,k} + C'_i P_{i+1,j,k} \\
 & + d'_j P_{i,j-1,k} + f'_j P_{i,j+1,k} + g'_k P_{i,j,k_1} + l'_k P_{i,j,k+1} \\
 & - m'_i h_{i,j,k} - \{r'_i + u'_j + \beta'_k\} h_{i,j,k} + s'_i h_{i+1,j,k} \\
 & + \beta'_j h_{i,j-1,k} + v'_j h_{i,j+1,k} + w'_k h_{i,j,k-1} + u'_k h_{i,j,k+1} \\
 & - v'_k \rho_w g h_w - l'_k h_s g + \frac{(D_{i,j,k} P_{i,j,k} + E_{i,j,k} h_{i,j,k})}{\Delta t} + q_{ei,j,k} = 0
 \end{aligned} \tag{5.3.1b}$$

In our three dimensional problem, each grid block is connected to at most six adjacent blocks. The number of nonlinear equations is $2N$ where N is the number of grid blocks. Since there are two unknowns p and h appearing simultaneously, each nonlinear equation has a maximum of seven unknown grid block values for both pressure and enthalpy i.e. 14 unknowns per equation.

EXAMPLE 2: Development of the solution of the non-linear system for a sample reservoir with 8 blocks.

As an illustration of the above explanation, suppose we have a reservoir which is divided into 64 rectangular blocks numbered 1 through 64 as shown in Figure 5.3.1. We shall denote our sample reservoir of 8 blocks with blocks numbered 1 through 8 (see Figure 5.3.1(a)). Suppose that each of the 8 reservoir block's three exposed surfaces are in contact with the boundary blocks numbered 9 through 64 as shown in Figures 5.3.1(a), 5.3.1(b), 5.3.1(c), and 5.3.1(d). A system of cartesian coordinates is superimposed on the reservoir domain with the origin at

an appropriate location. Each block, for both reservoir and boundary is allocated a position in terms of i , j and k directions with respect to this origin. For this case $N = 8$ and thus we have 16 non-linear equations as developed in Appendix B by varying i , j and k appropriately for grid blocks 1 through 8. For grid block 1, Equation(5.3.1) yields Equation(B-2).

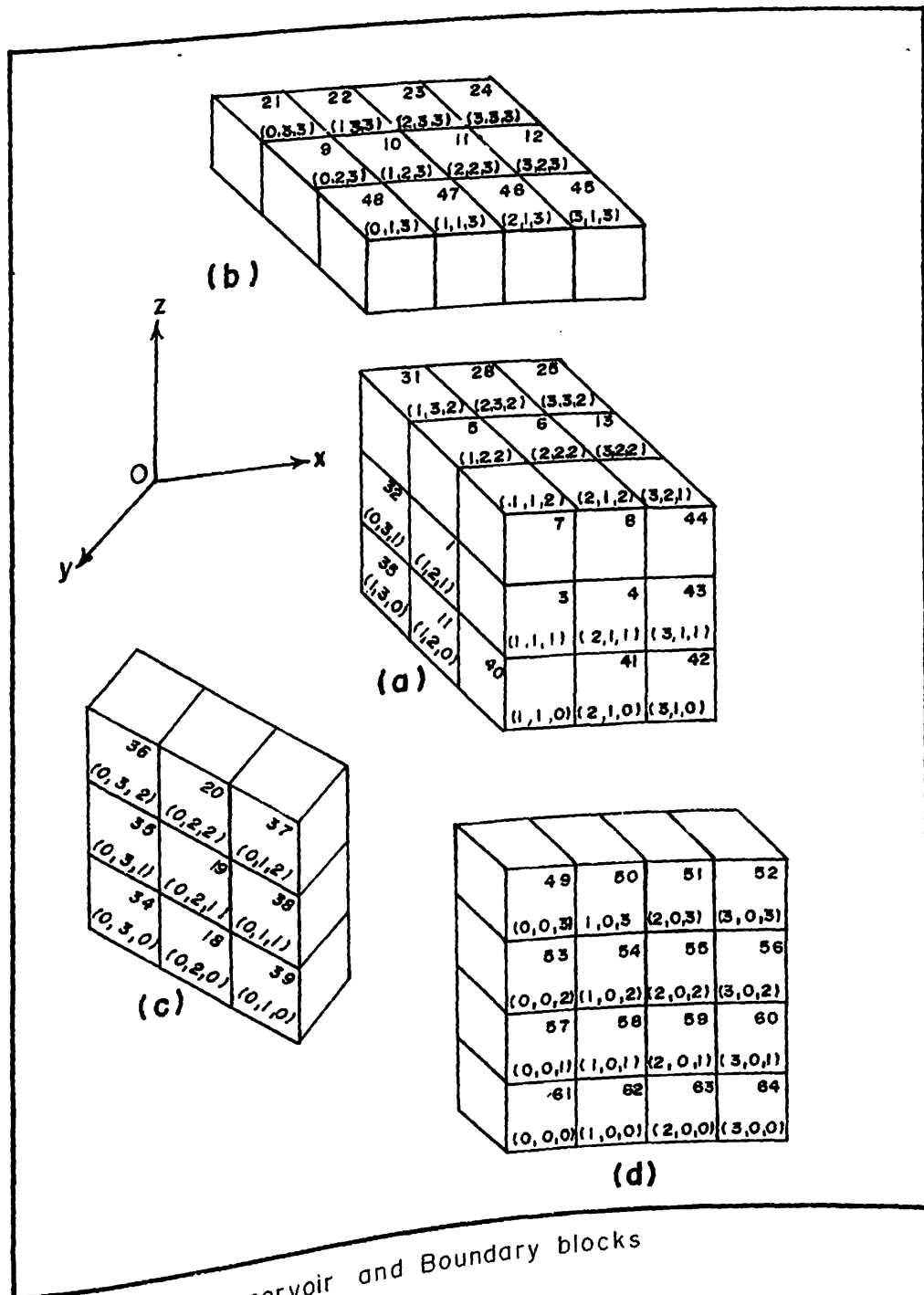


Figure 5.3.3: Reservoir and Boundary blocks

A similar procedure is continued for grid blocks 2 through 8 to yield the system of non-linear system equations

$$\vec{f}(\vec{x}) = 0 \quad (5.3.2)$$

in which the vectors \vec{x} and \vec{f} are defined in Appendix B. For nonlinear difference equations the coefficients of the unknowns are functions of the solution. The equations are usually solved iteratively after being linearized in some way (Smith (1987)). Taylor's expansion provides a standard way of doing this and the method is usually referred to as Newton's method. Making a Taylor series expansion about an assumed solution of Equation(5.3.2), we can write the linearized set of equations as:

$$\vec{f}(\vec{x}) + \sum_i \left[\frac{\partial \vec{f}(\vec{x})}{\partial x_i} \right]^k (x_i^{k+1} - x_i^k) = 0, \quad (5.3.3)$$

where i sums over the number of unknown variables at each grid block. This number is 14 and comes from the fact that there are two variables P and h and each grid block is connected to atmost six adjacent blocks creating seven unknown pressures and seven unknown enthalpy values at each grid block. This number 14 would apply to a general case of grid blocks or to our sample grid blocks.

5.4 Iterative Techniques

Let k denote the iteration level as indicated in Equation(5.3.3).Equation(5.3.3) may be written in the form:

$$J^{(k)}(\Delta\vec{x}) = -\vec{f}(\vec{x}^{(k)}), \quad (5.4.1)$$

where J is a $2N \times 2N$ Jacobian matrix of derivative terms evaluated using the values of the variables at the old k -th iterations. $\Delta\vec{x}$ is a column vector of $2N$ unknowns given by

$$\Delta\vec{x}^{(k)} = \vec{x}^{(k+1)} - \vec{x}^{(k)}, \quad (5.4.2)$$

and is determined by Equation(5.4.1). A new approximation to the solution is given by

$$\vec{x}^{(k+1)} = \vec{x}^{(k)} + \Delta\vec{x}^{(k)} \quad (5.4.3)$$

and $\vec{f}(\vec{x}^{(k)})$ is a column vector of $2N$ right hand side values from the previous iteration level. The process is initiated by values from the time step zero. For example,

$$P_{i,j,k}^{1,0} = P_{i,j,k}^{0,0} \quad (5.4.4)$$

We therefore iteratively adjust the values of $P_{i,j,k}^{n+1}, h_{i,j,k}^{n+1}$ using the formulas:

$$P_{i,j,k}^{n+1,k+1} = P_{i,j,k}^{n+1,k} + \Delta P_{i,j,k}^k \quad (5.4.5)$$

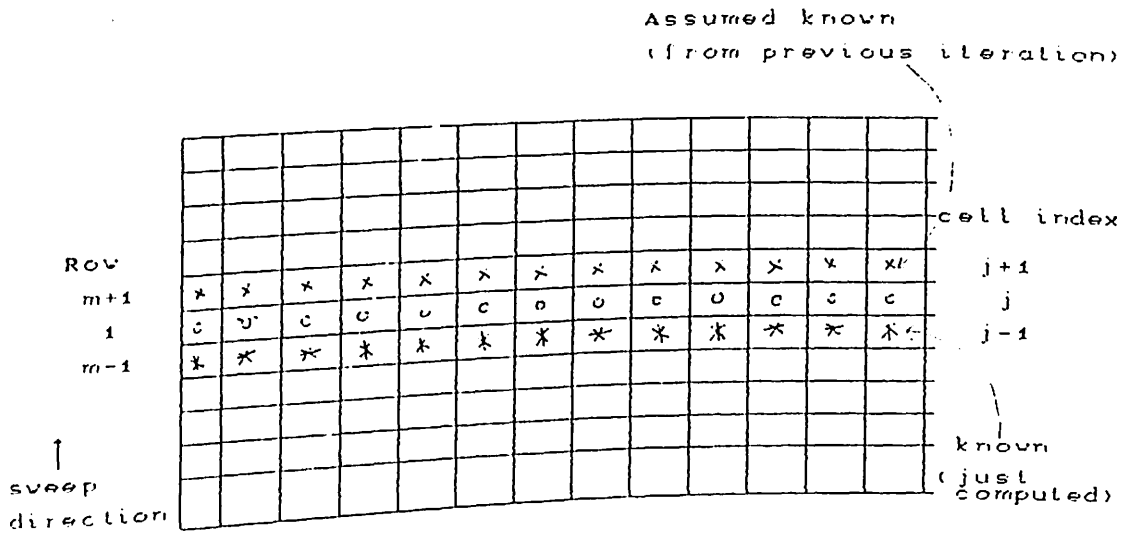
obtained from Equation(5.4.3) where $\Delta P_{i,j,k}^k$ and $\Delta h_{i,j,k}^k$ are the changes in the variables $\vec{\Delta x} = (x_i^{k+1} - x_i^k)$ which are given by the solution of the linearized Equation(5.4.1). Each nodal value of the variables is successively updated until the maximum absolute changes of pressure or enthalpy over all grid blocks are less than the desired convergence criteria.

The actual number of blocks used in the modelling of Olkaria geothermal reservoir in chapter six is 392 (from 8 layers with 49 blocks in each layer). Out of these there are $24 \times 8 = 192$ boundary blocks leaving 200 as reservoir blocks. This model therefore has 400 equations in 400 unknown pressures and enthalpies. The equations derived for the sample reservoir blocks can be extended to this number of reservoir blocks which will be used in chapter six.

The efficiency of the numerical model depends on how well the algorithm for solving pressure or enthalpy works. Solving the matrix equation is the most time consuming part of the simulation process. It is therefore imperative that this operation be performed as efficiently as possible.

Equation(5.4.1) represents a system of simultaneous linear algebraic equations. The size of the matrix depends on the number of nodes and the number of variables. For example in a region of N nodes, solving simultaneously for the two thermodynamic variables p and h , the matrix is $2N \times 2N$ in size as we noted in our sample reservoir. The solution of the $2N$ unknown nodal values in $\bar{\Delta}r$ of Equation(5.4.1) can be obtained through either direct elimination or iterative method. The method to use for any given problem, whether direct or iterative, depends on a number of factors, one of which is: computational speed, namely the number of machine operations required to solve the system. Computational speed is an important element to consider when choosing the type of matrix solution process to use in the problem at hand. Accuracy and stability i.e. a measure the correctness of the solution are obviously significant in the solution process. Another equally important item to consider is programming ease, which is a measure of the time and therefore money required to develop a model under a given formulation.

Line Relaxation: The successive Overrelaxation(SSOR) can be applied to a group of grid cells at a time, say to a group along a line that is column or row. This method will relax one line at a time and is referred to as Line Successive Overrelaxation(LSOR). As an illustration we consider the fully implicit finite difference formulation(Equation(5.2.9)) of Equation(5.2.8). To implement LSOR, the pressure values on a line are solved simultaneously. We can obtain some insight into how this method works by examining Figure 5.4.1 below.



LSOR: Line Successive Overrelaxation

Assuming that those values of the pressure on the previous lines, that is line $j-1$, are known (they are known since they have just been computed) and that the values at $j+1$ are approximated by the old iteration values, the system is swept row by row say from bottom to top. Then the $P_{i,j}^{n+1,k+1}$ (k -iteration level) values are solved for simultaneously on a line. After each line computation, the next approximation to $P_{i,j}^{n+1,k+1}$ values are obtained by overrelaxation as follows:

$$P_{i,j}^{n+1,k+1} = P_{i,j}^{n,k} + \omega(P_{i,j}^{n+1,k+1} - P_{i,j}^{n,k}) \quad (5.4.6)$$

where ω is the relaxation parameter. The iterative procedure is continued until a convergence criterion is satisfied. For instance, until the relative error

$$\max_{i,j} \frac{|P_{i,j}^{n+1,k+1} - P_{i,j}^{n+1,k}|}{|P_{i,j}^{n+1,k+1}|} \leq \epsilon \quad \forall \quad i,j \quad (5.4.7)$$

where ϵ is some prescribed error tolerance.

We have dwelt at length on LSOR method for one good reason. The Slice Successive Overrelaxation(SSOR) used in the model in chapter six is similar to LSOR in two dimensions, except rather than solve each row(line) implicitly, each vertical cross-section(3-dimensions) in the grid is solved implicitly. The SSOR method relaxes one slice at a time. Since pressure and enthalpy are solved for simultaneously, there are 14 unknowns per equation. Each unknown pressure and enthalpy are coupled to six other unknowns in three dimensions. SSOR assumes that the values of pressure or enthalpy on the previous row in a slice are known and that the values in the next row are approximated by the old iterate values.

The advantages of both direct and iterative techniques can be combined in the block iterative techniques. In the block iterative methods, the coefficient matrix is partitioned into blocks and all the elements of a block are operated on during an iterative step.

CHAPTER SIX

APPLICATION TO OLKARIA GEOTHERMAL FIELD

6.1. Introduction

The mathematical model for Olkaria geothermal reservoir in this study covers an area of 24km^2 and encompasses the present production field of Olkaria North East field. This model has 8 layers and a thickness of 1550m running from 1600 to 50m.a.s.l. This model thus examines the region above the steam zone and the deepest feed zones in the wells. A natural state model of the Olkaria system covering an area of 22km^2 square is set up to provide initial conditions for the production model. Production simulations for the Olkaria East field were carried out for a period of 14 years from 1981 to 1995 to coincide with the theoretical commissioning of the proposed 64MWe power station for Olkaria North East field. Large scale production from both fields was simulated for an a period of 20 years.

6.2 Conceptual Model for Olkaria Geothermal System

A reservoir model is a mathematical representation of the physical behaviour of the reservoir. To develop a reservoir model, one needs first to develop a conceptual model of the same reservoir based on its physical behaviour. To set up a conceptual model of the reservoir requires the following data base:

- (1) Geological data which gives a three dimensional picture of the geological structure of the field. Stratigraphy, lithology, faults and other features enable us to locate regions of high and low permeability.
- (2) Geochemical data which includes geochemistry of surface manifestations, such as hot springs, and drilled wells can be used to infer fluid

movement and location of heat inputs. Chemical geothermometers help to infer deep reservoir temperatures.

(3) Geophysical data consisting of resistivity surveys can delineate the extent and boundary of the reservoir.

A conceptual model of the Olkaria geothermal system constructed from geoscientific data assumes the existence of a principal producing reservoir overlain by a layer of trachytic rocks. The aquifer consists mainly of the more permeable basalts and rhyolites. Trachyte rocks act as caprock to the system. Most wells intersect two distinct reservoirs. The upper reservoir which is capped and contains high enthalpy mixture of steam and water has a temperature of 240°C and a pressure of 35 bars. It occurs at approximately 1350 m.a.s.l. and is around 100m thick. The lower reservoir which underlies the steam zone is liquid dominated, much thicker and extends from 1200 m.a.s.l. to sea level. Its temperature is assumed to follow the boiling point with depth curve (Bodvarsson *et.al.* 1987). Boiling of deep ascending chloride water forms steam which condenses in the water present in the upper reservoir forming sodium-bicarbonate water. This conceptual picture of the Olkaria system is represented in Figure 6.2.1 overleaf. Deep hot fluid rises vertically and flows along the Olkaria fault into a central zone and then along the Ololbutot fault. Lateral flow causes phase separation which leads to the formation of a steam zone over a liquid layer. Some of the fluid discharges to surface springs in the Hell's Gate gorge to the south and some steam is lost to fumaroles along the Ololbutot fault.

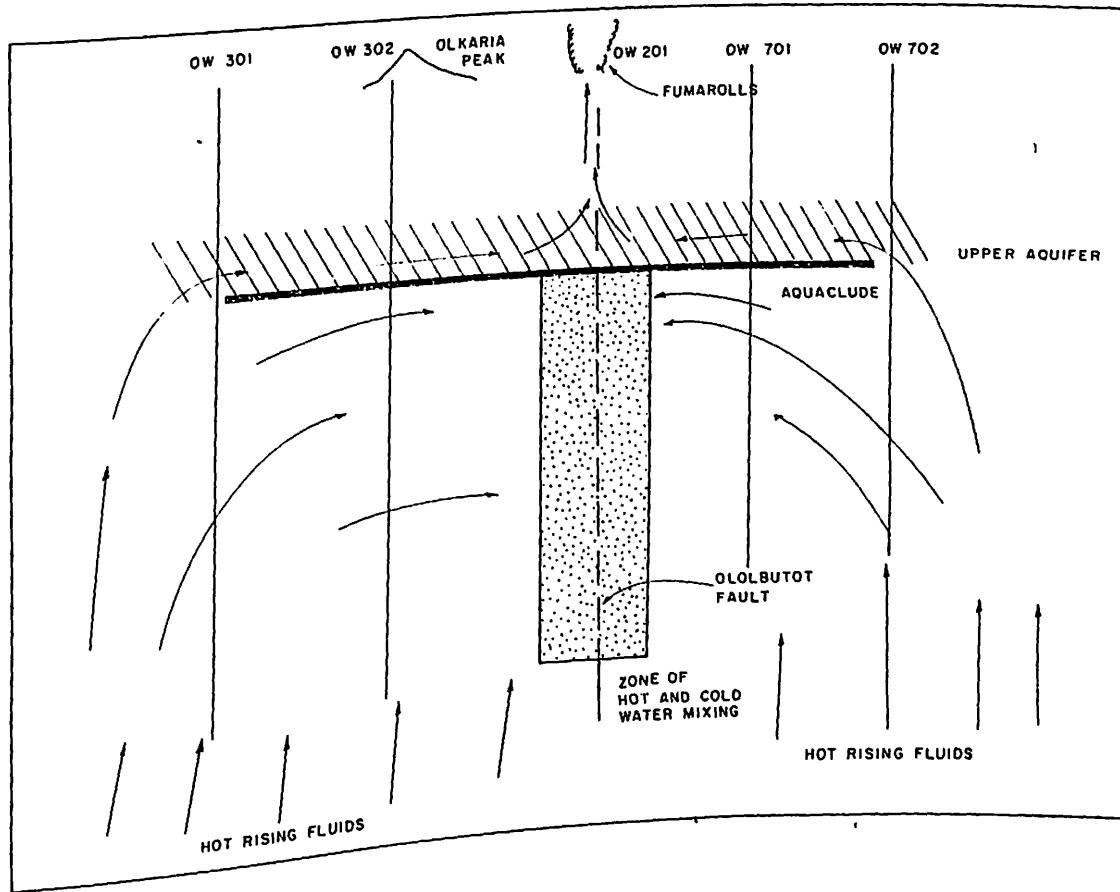


Figure 6.2.1 Conceptual cross- sectional model of the Olkaria field along the Olkaria fault (Adapted from GENZL, 1986)

6.3 . Numerical Modelling of the Olkaria Geothermal System

Numerical modelling of a geothermal reservoir is a process that simulates the performance of the reservoir in either its natural state or under a variety of exploitation strategies. The actual reservoir condition is simulated by a computer model having a number of interconnected blocks. The properties of the reservoir such as permeabilities, temperatures, pressures, rock

and fluid properties, heat flow, mass flow etc. are assigned to each block based on the geology, geochemistry, geophysics and data obtained from well measurements. Fluid dynamics in the reservoir is represented by the mathematical model in chapter four in the form of governing equations and boundary conditions. The models in chapters four and five are applicable to any geothermal system i.e. it is a general model. It is important to recognize that no two geothermal systems can be the same, although they could have similar behaviour like Olkaria and Krafla in Iceland. The parameters, for instance, porosity, permeability, relative permeability specific heat capacity of rock, thermal conductivity, etc., pertaining to Olkaria field used in this chapter, together with the initial and boundary conditions, were analysed and input in Equation (A-8a) and (A-8b) of appendix A and the solutions in the form of reservoir pressures, enthalpy, saturation were generated by the computer program MULKOM. The program is based on some of the assumptions listed in section 4.2 and the further assumption that the rock is porous and is saturated with the geothermal fluid in liquid and vapour forms. The assumptions are valid for Olkaria reservoir. For example the second assumption stated in section 4.2 is valid for Olkaria reservoir as the rock matrix at Olkaria is sufficiently permeable to allow convective heat transfer to occur entirely in the matrix. The fourth assumption is an adequate approximation of the Olkaria conditions as the reservoir fluids are of the sodium-chloride type with about 200–500 ppm of chloride (Munn, 1982); this is low salinity. The sixth assumption about porosity is also valid for Olkaria since we are assuming a porous medium model rather than a fractured medium model for it is difficult to handle the modelling of a fractured reservoir due to the more computational work necessary. However, the results based on the porous medium model are found to be reasonable.

6.4 Natural State Model for Olkaria Geothermal System

A plan view of the mesh used in the computer model is as shown in Figure 6.4.1. The surface of the field was divided into rectangles and squares, large enough to include all the features in the conceptual model.

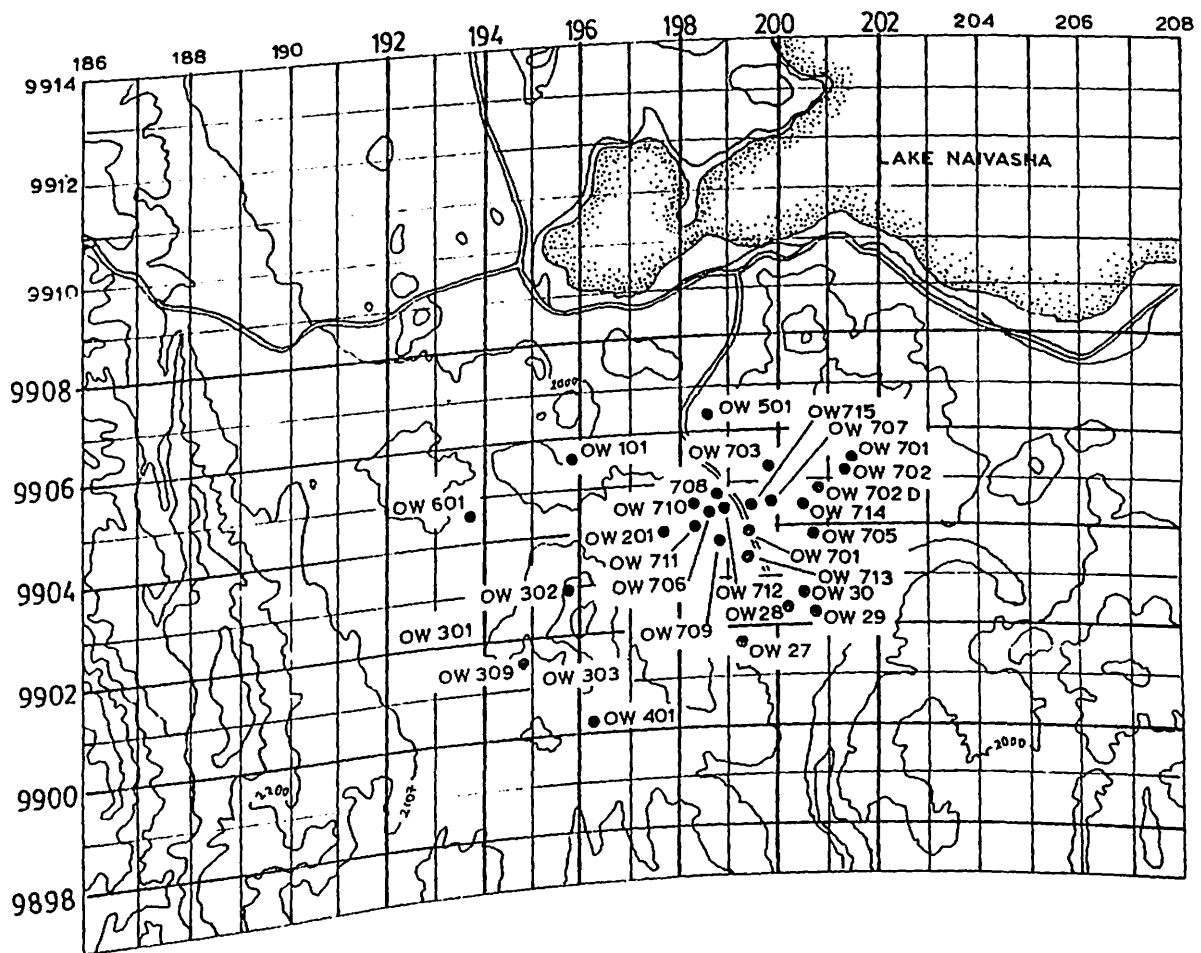


Figure 6.4.1 Olkaria Geothermal field and layout of the grid for the computer model

The mesh which consists of 8 layers with 43 blocks in each layer covers an area of 22km. square and includes all production and exploration wells. The large mesh size is chosen so as to encompass the whole of the convective system that is believed to exist and to model the natural state conditions of the system before it was exploited. The blocks are of different sizes as shown in Figure 6.4.2. The $2\text{km.} \times 2\text{km.}$ grids squares were chosen for the blocks named 2-6, 9-13, 16-20, 23-27 and 30-34. The $6\text{km.} \times 6\text{km.}$ square grids were chosen for blocks 36, 42, 43 and 49. The rest of the blocks are $2\text{km.} \times 6\text{km.}$ rectangle grids. The smaller block sizes i.e. $2\text{km.} \times 2\text{km.}$ in the reservoir compared to the bigger block sizes e.g. $6\text{km.} \times 6\text{km.}$ are used to increase the definition needed in the reservoir for better control of the parameters in the reservoir as stated in section 5.3. The model is three dimensional in space to model the deepest feed zones as found in the wells (Figure 6.4.3)

43	44	45	46	47	48	49
1	2	3	4	5	6	7
8	9	10	11	12	13	14
15	16	17	18	19	20	21
22	23	24	25	26	27	28
29	30	31	32	33	34	35
36	37	38	39	40	41	42

Figure 6.4.2 Sizes of grid blocks

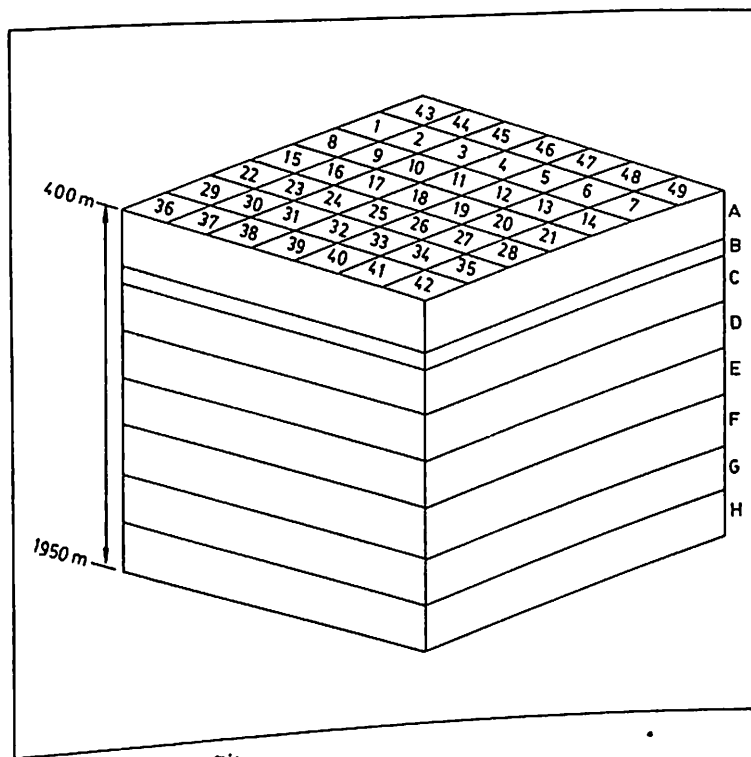


Figure 6.4.3 3-D model structure for Olkaria geothermal field

The reservoir which is taken to have a thickness of 1550m starts from 1600 to 50m.a.s.l. and the thickness of each layer is summarized in in Table 6.4.1.

Table 6.4.1: Layer thickness

Layer	Number of elements	Thickness (m)
A	49	250
B	49	100
C	49	200
D	49	200
E	49	200
F	49	200
G	49	200
H	49	200

The natural state model simulates the natural reservoir conditions before exploitation. A match is obtained with the actual natural state data obtained before the reservoir was exploited. The natural state model is the used as a framework on which a numerical exploitation model is developed

to simulate the actual exploitation behaviour of the reservoir. After a match is obtained with actual data observed or measured in the field, this model is then used to estimate, with some degree of accuracy, the future performance of the reservoir under exploitation. The natural state model was set up using the permeability structure and rock properties shown in Table 6.4.2 with heat inputs of varying magnitudes at some elements in the bottom layer. The rock properties shown in Table 6.4.2 are the average for the rock formations in Olkaria and are taken from the geology and reservoir engineering data at Olkaria. The different layers represent different rocks of variable permeabilities. Horizontal permeabilities range from 1–20 darcy metres. The permeabilities in the layers B, C, D and G, which are later regarded as producing layers, were assigned values based upon those determined by the model for Olkaria East field (Bodvarsson *et. al.* 1987) rather than those inferred from well tests because of the uncertainty in the well test analysis.

Table 6.4.2 Material properties for the reservoir layers

Layer	Density (kg/m ³)	Heat cap (J/kgK)	Thermal cond. (W/mK)	Porosity
A	2500	20	2.5	0.1
B	2500	20	2.5	0.1
C	2500	20	2.5	0.1
D	2500	20	2.5	0.1
E	2500	20	2.5	0.1
F	2500	20	2.5	0.1
G	2500	20	2.5	0.1
H	2500	20	2.5	0.1

Permeability ($\times 10^{-15}$) $\begin{matrix} x- \\ 1-20 \end{matrix}$ $\begin{matrix} y- \\ 1-20 \end{matrix}$ $\begin{matrix} z- \\ 0.1-2.0 \end{matrix}$

Both horizontal permeabilities (x - and y - directions) were adjusted to values between $1 \times 10^{-15} - 20 \times 10^{-15} m^2$, or $1 - 20 mDarcy$, as these gave a reasonable match to the observed temperatures in the field. Porosity, density, thermal conductivity and heat capacity of the various reservoir rock units (layers) were held constant with the values as shown in Table 6.4.2. Simulations were run over a period of 3000 years, equivalent to the development of the geothermal system over geological time. The numerical model that best reproduced the observed data before exploitation is the natural state model of the Olkaria system. Comparisons between observed and calculated temperature profiles for typical wells in Olkaria are as shown in Figure 6.4.4. The observed data for wells was obtained from the GD Manager (Geothermal Development Data gathered and stored) available at GENZL and KPC in Olkaria. The graph shows good agreement at most of the depths. Initial and Boundary conditions

The final run conditions for the natural state model provided initial conditions for the production model. These initial conditions for the producing layers obtained from the natural state model are as shown in Table 6.4.3.

Table 6.4.3: Initial conditions for the production model

Layer	Fluid state	Temp. ($^{\circ}C$)	Pressure (bars)	Vapour Saturation
B	two-phase	241	33.9	0.49
C	single-phase	256	43.6	0.00
D	single-phase	271	59.1	0.00
E	single-phase	276	74.4	0.00
G	single-phase	295	104.5	0.00

The boundary conditions the model used were: (a) Open recharge (mass

and heat flux) from all directions and (b) zero mass flow through the top and the bottom.

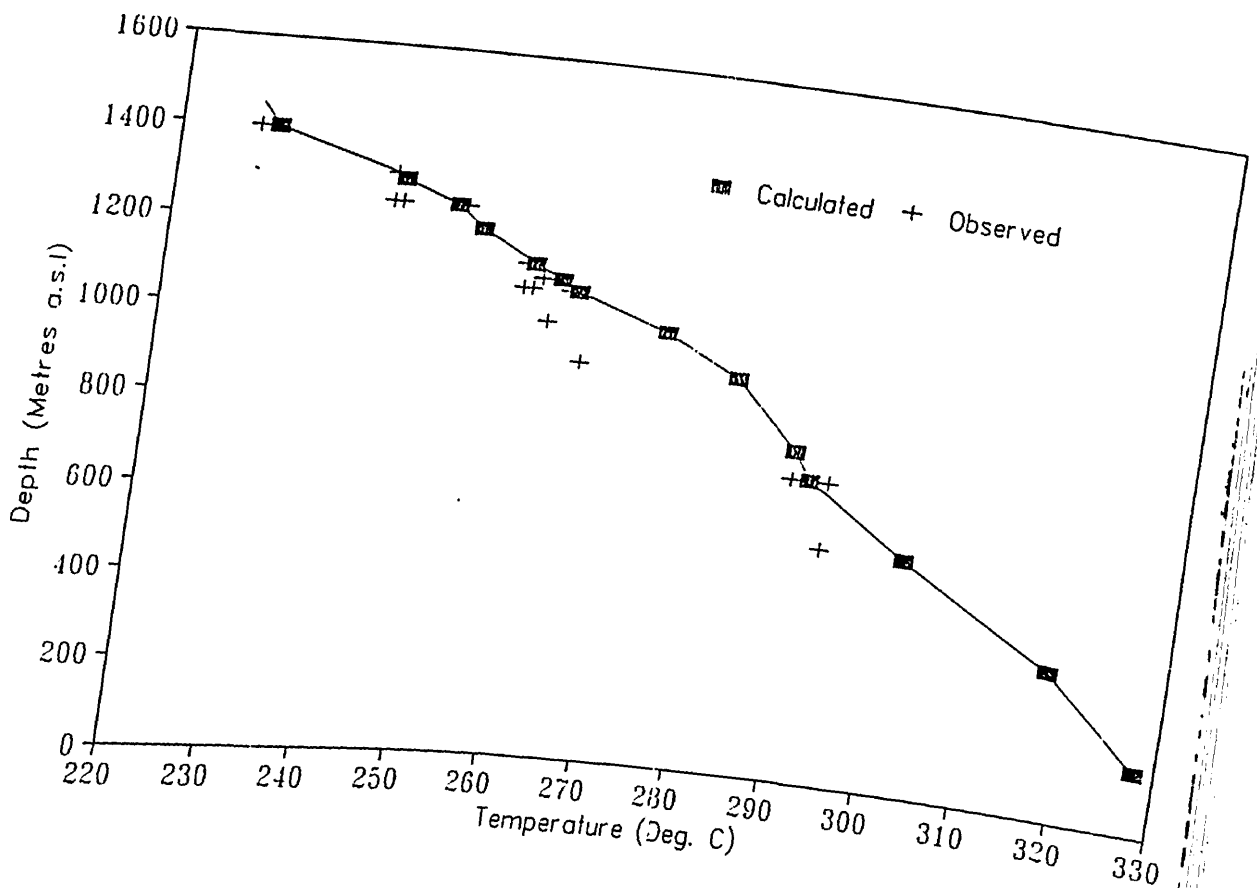


Figure 6.4.4 Temperature Profile For Natural State of Olkaria Geothermal System

6.5 . Results of production model for Olkaria East field

Grid blocks numbered 12, 13, 19, 20, 26, and 27 (see Figure 6.4.2) of the natural state model were subdivided into 1km by 1km grid squares of area 24km to provide a finer mesh as shown in Figure 6.5.1. All the production wells in Olkaria East field were assumed to be in block 69 and produce as one "big" well. Based on the location of feed zones in Olkaria East field, production was mainly from layers B, C, D, E with only well OW - 19

with a deeper feed zone in layer G. Based on the data of cumulative mass withdrawal of steam and water from June 1981 when production started to June 1995, an average mass withdrawal of 90kg/s per year was calculated. an estimated contribution from each layer is as shown in Table 6.5.1.

Table 6.5.1 percentage contribution from each production layer in Olkaria East field

Layer	Production
B	65%
C	11%
D	9%
E	9%
G	6%

The Production was run for 14 years form 1981 to 1995.

1	2	3	4	5	6	7		
				50	51	52	53	14
8	9	10	11	54	55	56	57	
				58	59	60	61	21
15	1	17	18	62	63	64	65	
				66	67	68	69	28
22	2	24	25	70	71	72	73	
29	3	31	32	33	34			35

Figure 6.5.1 Smaller mesh size model of the Olkaria geothermal field

Calculated mass extraction rate and enthalpies were compared to yearly values of observed mass flow and enthalpies for the field and the results are as shown in Figures 6.5.2 and 6.5.3. The model agrees fairly well with enthalpy and mass variation with time for observed data up to the year 1995. In Figure 6.5.2 below, the total mass withdrawn, consisting of steam and water drops steadily from about mid-1986 to a minimum low in 1994 before it starts to increase again. One reason for this is that the power station has not been on full load (45 MWe) all the time.

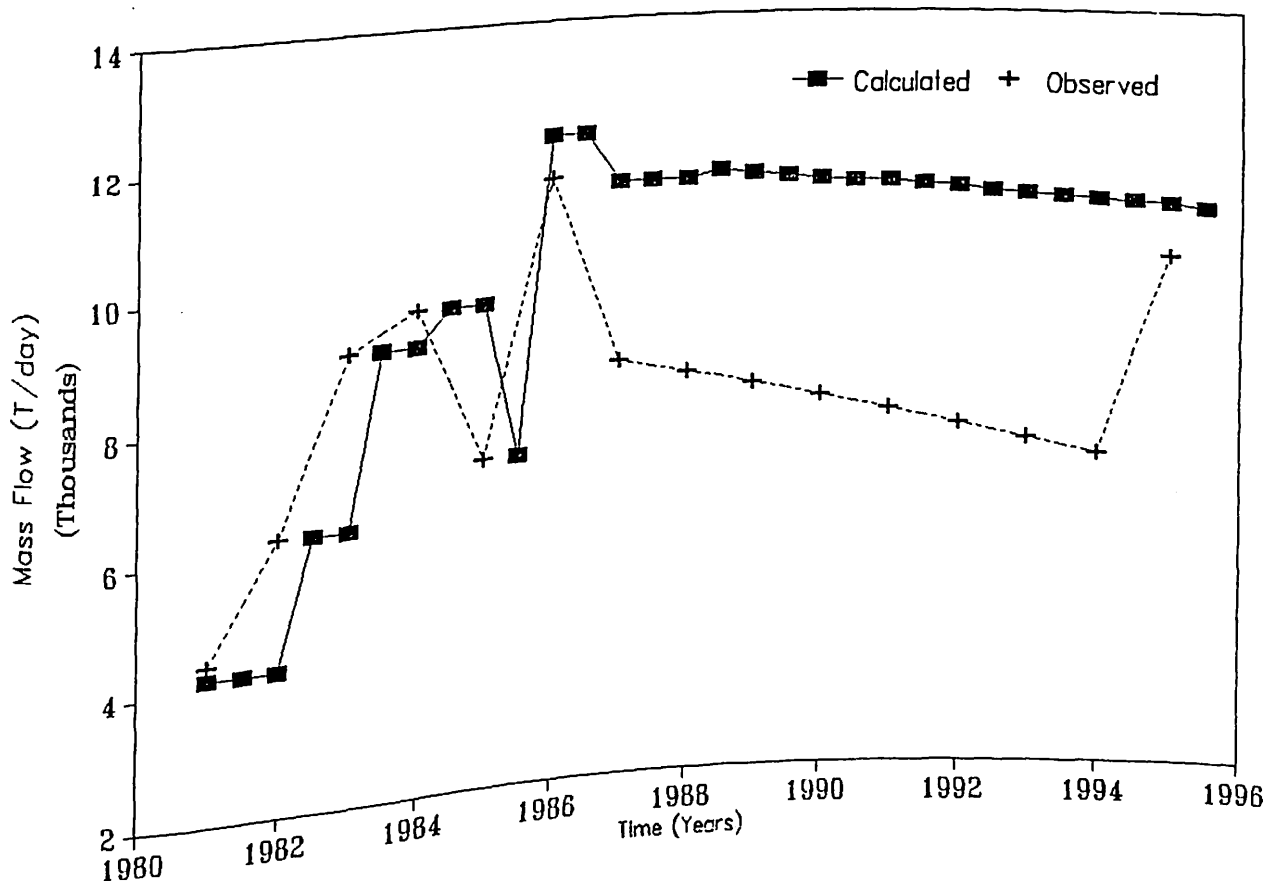


Figure 6.5.2 Comparison Between Observed and Simulated Mass Flow For Production History

In fact in 1994 only 31 MWe were being generated (Table 6.5.2).

Table 6.5.2 Yearly average power Load

Year	Average Load (MWe)
1981	15
1982	15
1983	30
1984	30
1985	45
1986	45
1987	38
1988	37
1989	36
1990	35
1991	34
1992	33
1993	32
1994	31
1995	45

The results of the model differ with the picture in Table 6.5.2 considerably because the model assumes a constant load of 45 MWe throughout the simulation period. Reducing the amount of fluid withdrawn is important since it allows the reservoir pressure to recover after a substantial drop. This is done by shutting in some of the wells. Figure 6.5.3 shows there is a small rise in the total field enthalpy, especially towards 1994. This is an indication of boiling in the reservoir. The average field enthalpy ranges between 2250- 2450J/kg. The difference between the values of the enthalpy calculated by the model and those observed from the field agree to within measurements error.

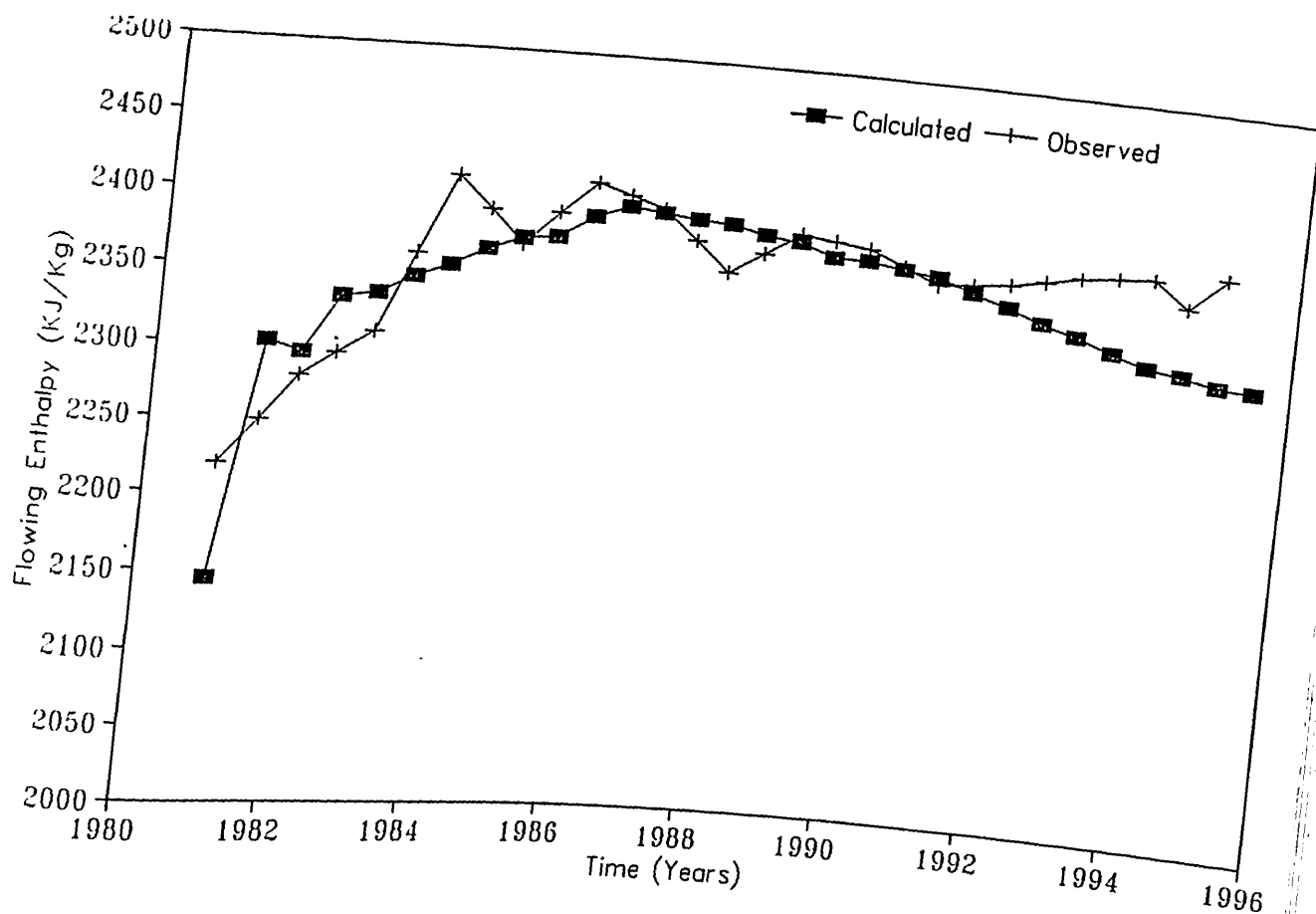


Figure 6.5.3 Comparison Between Observed and Simulated Enthalpy for Production History

In simulating the first 14 years of production from Olkaria East field, a problem of severe pressure drop was experienced in layer *B*, up to 10 bars, at the 10th year of production, which causes induced flow of fluid of lower enthalpy into layer *B* effectively lowering the overall production enthalpy. This situation is attributed to continued overproduction from this layer. To overcome this problem, a pressure dependent mass flow relation for layer *B* was prescribed. This relation which is sometimes referred to as deliverability option (O'Sullivan, 1992) is of the form:

$$q_m = \left\{ \begin{array}{l} PI(P_{res} - P_0) \\ q_{max} \end{array} \right\} \quad (6.5.1)$$

where q_m is the rate of mass flow into the block, q_{max} is the maximum flow

into the block. PI is the productivity index of the block which depends on the properties of the well and the feedzone. Initial values for the PI for each block are obtained from well test analysis data. P_{res} is the block pressure while P_0 is a down hole well pressure below which no flow will occur from the well. If the calculated block pressure is greater than P_0 , flow will occur into the block otherwise flow is taken as q_{max} . This pressure dependent mass flow is important as the wells are expected to decline in flow with reservoir pressure decline. By fixing the maximum steam flow from layer B and keeping the bottom hole pressure to a fixed value, the productivity index was varied till a reasonable enthalpy trend was achieved. The pressure decline in producing layers for the period 1981 to 1995 were plotted against time to give Figure 6.5.4.

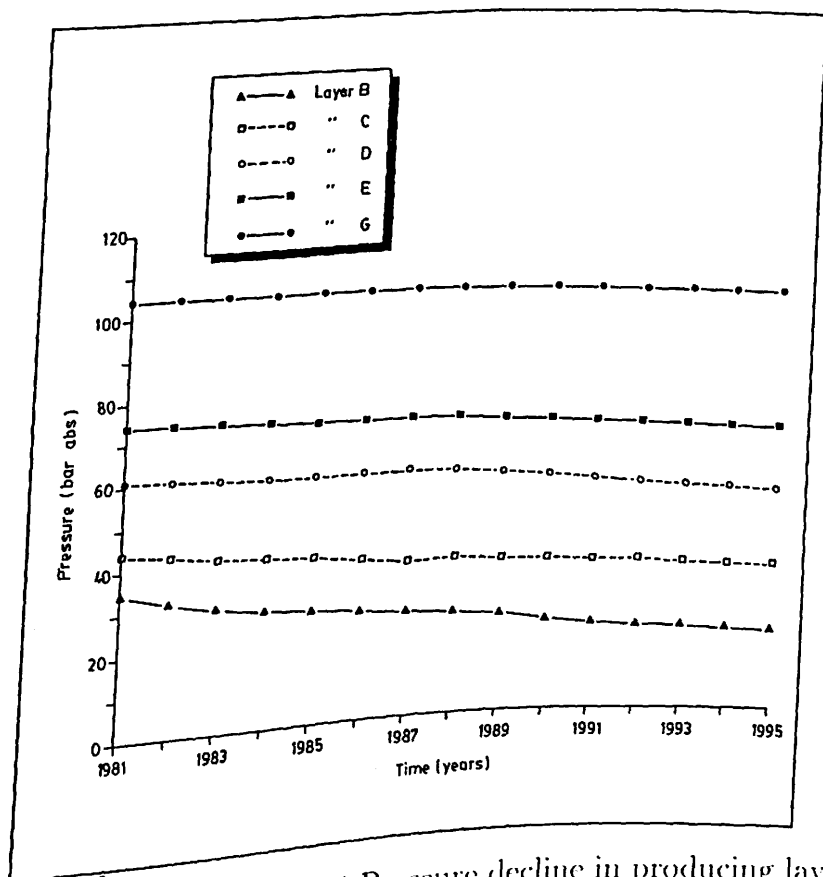


Figure 6.5.4 Pressure decline in producing layers

A pressure decline of 3 to 15 bars has occurred with the largest decline in layer B and negligible decline in layer G. The respective pressure declines are attributed to the amount of production from these layers. When the fluid extraction rate to maintain a power generation of 45MWe goes down, new wells have to be "turned on" to maintain the power production at 45MWe. This requires either drilling more wells or carrying out reinjection of the fluid into the wells, to maintain same flow rate. Therefore the overall pressure decline in the reservoir will lead to drilling of make-up wells or addressing the question of reinjection.

6.6. Results of Modelling of future production from Olkaria North East field

To model the future production of the reservoir with extension to the Olkaria North East field, production exploitation was assigned to grid block elements 55B, 60C, 65D, 56E, and 57G (Under this notation, the number refers to the location of grid and the letter refers to the layer, see Figures 6.4.3 and 6.5.1 to represent production from wells located in these areas. The total amount of fluid production required to sustain 64MWe from the Olkaria North East field was calculated using the proportions from each layer required to maintain 45MWe from Olkaria East field. The fluid extraction rates from the Olkaria North East field was put on the same schedule as in Olkaria East field, i.e. layer B was put on deliverability option while the rest of the layers extracted fluid at a constant rate. This approach is justified since Olkaria North East field is similar in properties to the Olkaria East field. The relatively smaller rates of extraction are expected to give moderate pressure drops hence maximizing the production life of the reservoir. Fluid extraction was limited to an area of 5km^2 an area proven by drilling (Mwangi *et. al.*, 1986).

The calculated percentage contribution from each layer is as shown in Table 6.6.1.

Table 6.6.1 Percentage contribution from each production layer in Olkaria North East field

Layer	Production
B	35%
C	20%
D	20%
E	20%
G	5%

Conditions at 14 years of production were used to start the simulations for a period of 20 years. The simulated production in terms of pressure drop and enthalpy variation with time is shown in Figures 6.6.1 to 6.6.3. Starting with Figure 6.6.1, the pressure drops off fairly uniformly in layers *B* and *C* up to the year 2009 with very little drop thereafter in layer *C*. Figure 6.6.2 shows pressure variation in layers *D* and *G*. Layer *G* shows minimal pressure drops during the period of production. Pressure drops of 0.3 – 15 bars are expected to occur in the reservoir with the highest drop occurring within the *B* layer and the lowest within the *G* layer.

Figure 6.6.3 shows the variation of average enthalpy with time during the production period. The average enthalpy rises initially and falls with no major fall after the year 2009. The initial rise in enthalpy is attributed to localized boiling around the producing wells. The fall in field average enthalpy could be linked to induced recharge into the reservoir as a result of pressure drop or due to natural recharge of cold fluids into the reser-

voir. When individual block enthalpies of producing elements are plotted against time, element 57B shows greater decline in enthalpy with time. Because of the proximity of this block 57 to block 54 which contains well OW - 704 with an observed inversion at depth, it is possible that cooler fluids from the north are causing the above enthalpy observation.

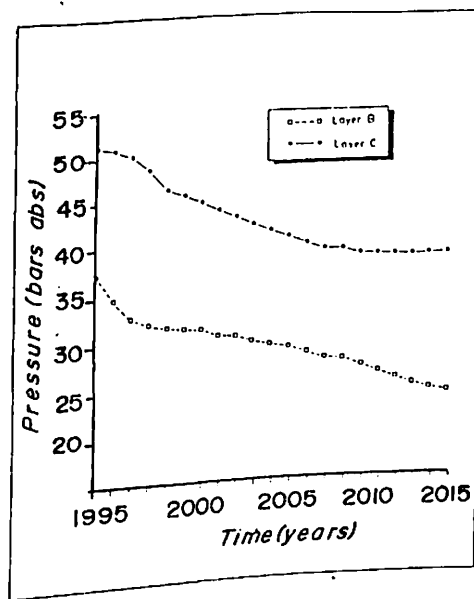


Figure 6.6.1 Simulated pressure variations for layers *B* and *C*

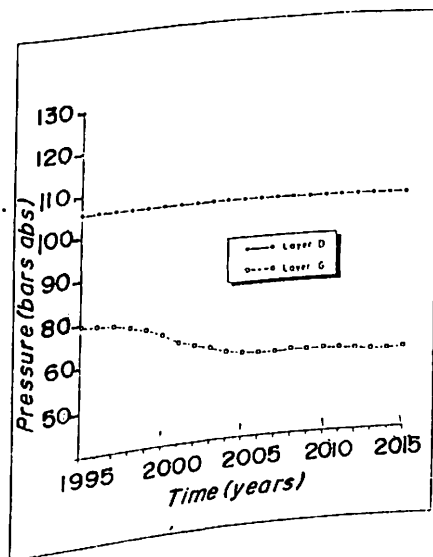


Figure 6.6.2 Simulated pressure variations for layers *D* and *G*

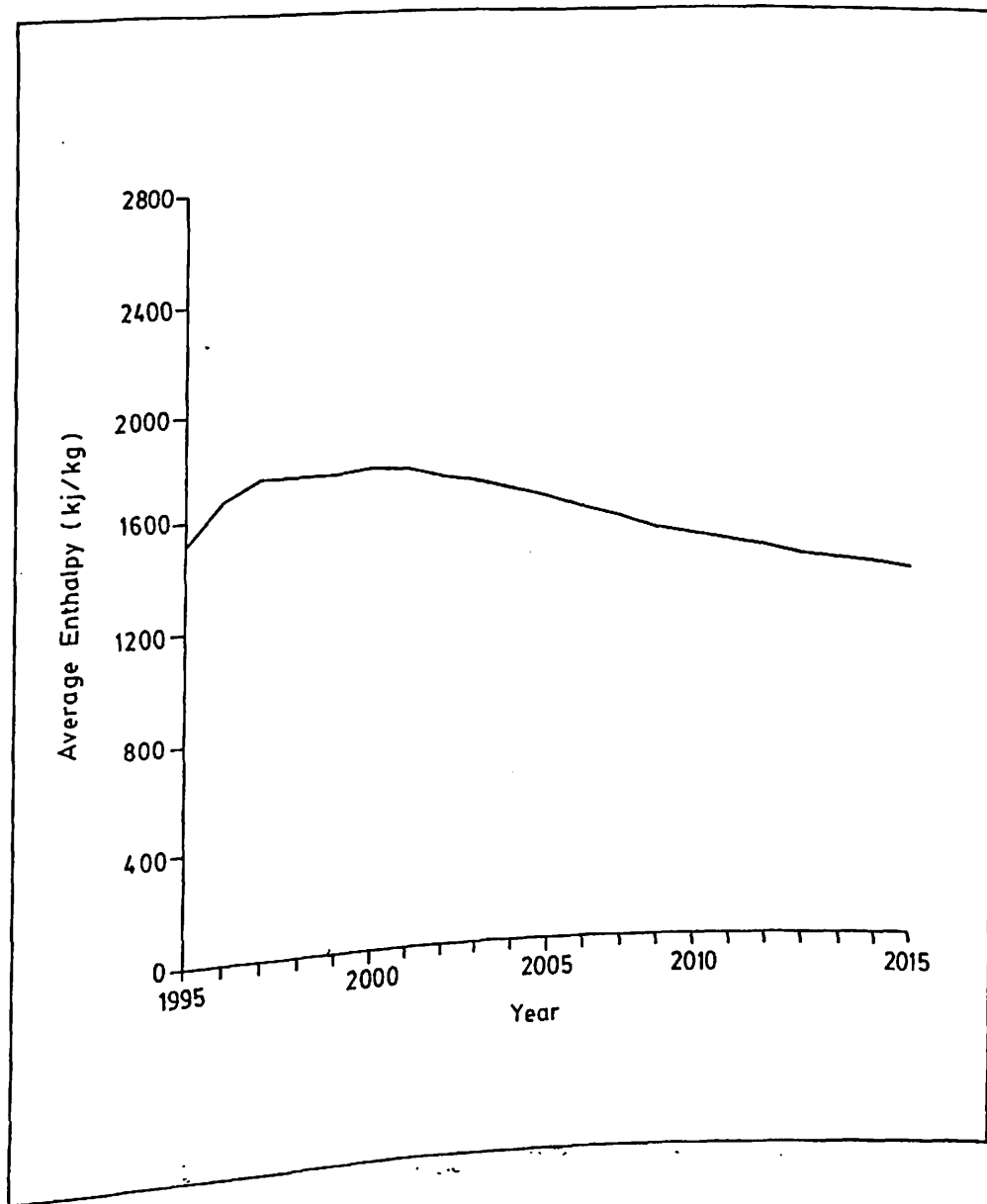


Figure 6.6.3 Simulated enthalpy variation for Olkaria North East field

CHAPTER SEVEN

DISCUSSION AND CONCLUDING REMARKS

Considering the total simulation period for the Olkaria North East field, the pressure draws down to a range of 0.3 – 15.0 bars in all producing layers. The pressure drop is more evident in layer *B* attaining a value of 15 bars at the end of the simulation period. Layer *G* exhibits the lowest pressure drop of 0.3 bars during the same period of simulation. The pressure in layers in *B, C, D* and *E* drop substantially because these are layers where most production is taken. The pressure declines uniformly, attaining an almost constant value from the year 2009 up to the end of the simulation period (the year 2015). The production enthalpy averages within 1350-1780kJ/kg after about 6 years of production and falls off uniformly to attain a minimum value at the end of the simulation period. Compare this with the average field enthalpy for Olkaria East field which ranges between 2250-2450kJ/kg. The target of 64MWe generation for 20 years is met without enthalpies rising too high. This is explained by the low extraction rates from the reservoir which reflect the low permeability at Olkaria. Drilling-make up wells would mean that the well field area in Olkaria North East field has to be extended to provide sufficient steam to supply the proposed 64MWe power station. Although this is a coarse model whose predictions may be less accurate, it does reinforce the current mood of optimism that Olkaria North East field can sustain a power generation of 64MWe. The long term medium-scale production simulation based on the natural state model shows that the development of the Olkaria North East field would not encounter major problems in terms of supporting a simulated 64MWe development. The results also show that recharge from the north may be significant. A finer grid probably well

by well incorporating all production wells in individual grids, would definitely increase the accuracy of the predictions made by the present model and would highlight the individual variations in enthalpy of the producing wells.

Appendix A
Finite difference representation of the mass and energy equations

Consider the accumulation terms:

$$M = \phi\rho \tag{A-1}$$

$$E = \phi\rho h + (1 - \phi)\rho_r h_r \tag{A-2}$$

from which we have

$$\frac{\partial M}{\partial t} = \frac{\partial(\phi\rho)}{\partial t} \tag{A-3a}$$

$$\frac{\partial E}{\partial t} = \frac{\partial}{\partial t} \{ \phi\rho h + (1 - \phi)\rho_r h_r \} \tag{A-3b}$$

Expanding the right hand side of Equation (A-3) yields:

$$\frac{\partial M}{\partial t} = \left\{ \rho \frac{d\phi}{dp} + \phi \left(\frac{\partial \rho}{\partial p} \right)_h \right\} \frac{\partial p}{\partial t} + \phi \left(\frac{\partial \rho}{\partial h} \right)_p \frac{\partial h}{\partial t} \tag{A-4a}$$

$$\begin{aligned} \frac{\partial E}{\partial t} = & \left\{ (h\rho - \rho_r h_r) \frac{d\phi}{dp} + \phi h \left(\frac{\partial \rho}{\partial p} \right)_h + (1 - \phi) \rho_r c_r \left(\frac{\partial T}{\partial p} \right)_h \right\} \frac{\partial p}{\partial t} \\ & + \left\{ \phi h \left(\frac{\partial \rho}{\partial h} \right)_p + (1 - \phi) \rho_r c_r \left(\frac{\partial T}{\partial h} \right) + \phi \rho \right\} \frac{\partial h}{\partial t} \end{aligned} \tag{A-4b}$$

in which we have assumed that

$$h_r = c_r T \tag{A-5}$$

where c_r denotes the specific heat capacity of the rock and T the temperature respectively. This shows that the rock enthalpy as defined above, is a function of the reservoir temperature.

Define the coefficients B, C, D and E thus:

$$B = \rho \frac{d\phi}{dp} + \phi \left(\frac{\partial \rho}{\partial p} \right)_h, \quad C = \phi \left(\frac{\partial \rho}{\partial h} \right)_p \tag{A-6a}$$

$$D = (h\rho - \rho_r h_r) \frac{d\phi}{dp} + \phi h \left(\frac{\partial \rho}{\partial p} \right)_h + (1 - \phi) \rho_r c_r \left(\frac{\partial T}{\partial p} \right)_h \tag{A-6b}$$

$$E = \phi h \left(\frac{\partial \rho}{\partial h} \right)_p + (1 - \phi) \rho_r c_r \left(\frac{\partial T}{\partial h} \right)_p + \phi \rho \quad (A-6c)$$

Substitution of Equation (A-6) into Equation (5.2.4) yields:

$$B \frac{\partial P}{\partial t} + C \frac{\partial h}{\partial t} = \frac{1}{V} [\nabla \cdot \{T_m \nabla P - (T_{mw} \rho_w \vec{g} + T_{ms} \rho_s \vec{g})\}] + q_m \quad (A-7a)$$

$$D \frac{\partial P}{\partial t} + E \frac{\partial h}{\partial t} = \frac{1}{V} [\nabla \cdot \{T_e \nabla P - (h_w T_{mw} \rho_w \vec{g} + h_s T_{ms} \rho_s \vec{g}) + T_h \nabla h\}] + q_c \quad (A-7b)$$

Equations (A-7a) and (A-7b) can be written in cartesian coordinates as follows:

$$B \frac{\partial P}{\partial t} + C \frac{\partial h}{\partial t} = \frac{1}{V} \left[\frac{\partial}{\partial x} (T_{mx} \frac{\partial P}{\partial x}) + \frac{\partial}{\partial y} (T_{my} \frac{\partial P}{\partial y}) + \frac{\partial}{\partial z} (T_{mz} \frac{\partial P}{\partial z}) - \frac{\partial}{\partial z} (T_{mwz} \rho_w g + T_{msz} \rho_s g) \right] + q_m \quad (A-8a)$$

$$D \frac{\partial P}{\partial t} + E \frac{\partial h}{\partial t} = \frac{1}{V} \left[\frac{\partial}{\partial x} (T_{ex} \frac{\partial P}{\partial x}) + \frac{\partial}{\partial y} (T_{ey} \frac{\partial P}{\partial y}) + \frac{\partial}{\partial z} (T_{ez} \frac{\partial P}{\partial z}) + \frac{\partial}{\partial x} (T_{hx} \frac{\partial h}{\partial x}) + \frac{\partial}{\partial y} (T_{hy} \frac{\partial h}{\partial y}) + \frac{\partial}{\partial z} (T_{hz} \frac{\partial h}{\partial z}) - \frac{\partial}{\partial z} (h_w T_{mwz} \rho_w g + h_s T_{msz} \rho_s g) \right] + q_c \quad (A-8b)$$

Fitting finite difference equivalents to the spatial and time derivatives in Equations (A-8a) and (A-8b) using fully implicit formulation for pressure and enthalpy in grid block gives the following equations:

$$\begin{aligned} & \frac{B_{i,j,k}^{n+1} (P_{i,j,k}^{n+1} - P_{i,j,k}^n)}{\Delta t} + \frac{C_{i,j,k}^{n+1} (h_{i,j,k}^{n+1} - h_{i,j,k}^n)}{\Delta t} \\ &= \frac{1}{V} \left[\frac{T_{mi+1/2,j,k} (P_{i+1,j,k}^{n+1} - P_{i,j,k}^{n+1})}{\Delta x^2} - \frac{T_{mi-1/2,j,k} (P_{i,j,k}^{n+1} - P_{i-1,j,k}^{n+1})}{\Delta x^2} \right. \\ &+ \frac{T_{mi,j+1/2,k} (P_{i,j+1,k}^{n+1} - P_{i,j,k}^{n+1})}{\Delta y^2} - \frac{T_{mi,j-1/2,k} (P_{i,j,k}^{n+1} - P_{i,j-1,k}^{n+1})}{\Delta y^2} \\ &+ \frac{T_{mi,j,k+1/2} (P_{i,j,k+1}^{n+1} - P_{i,j,k}^{n+1})}{\Delta z^2} - \frac{T_{mi,j,k-1/2} (P_{i,j,k}^{n+1} - P_{i,j,k-1}^{n+1})}{\Delta z^2} \\ &\left. - \left(\frac{(T_{mwi,j,k+1/2}^{n+1} - T_{mwi,j,k-1/2}^{n+1})}{\Delta z} \rho_w g + \frac{(T_{msi,j,k+1/2}^{n+1} - T_{msi,j,k-1/2}^{n+1})}{\Delta z} \rho_s g \right) \right] + q_{m,i,j,k}^{n+1} \quad (A-9a) \end{aligned}$$

$$\begin{aligned}
& \frac{D_{i,j,k}^{n+1}(P_{i,j,k}^{n+1} - P_{i,j,k}^n)}{\Delta t} + \frac{E_{i,j,k}^{n+1}(h_{i,j,k}^{n+1} - h_{i,j,k}^n)}{\Delta t} \\
&= \frac{1}{V} \left[\frac{T_{ei+1/2,j,k}(P_{i+1,j,k}^{n+1} - P_{i,j,k}^{n+1})}{\Delta x^2} - \frac{T_{ei-1/2,j,k}(P_{i,j,k}^{n+1} - P_{i-1,j,k}^{n+1})}{\Delta x^2} \right. \\
&+ \frac{T_{ci,j+1/2,k}(P_{i,j+1,k}^{n+1} - P_{i,j,k}^{n+1})}{\Delta y^2} - \frac{T_{ci,j-1/2,k}(P_{i,j,k}^{n+1} - P_{i,j-1,k}^{n+1})}{\Delta y^2} \\
&+ \frac{T_{ci,j,k+1/2}(P_{i,j,k+1}^{n+1} - P_{i,j,k}^{n+1})}{\Delta z^2} - \frac{T_{ci,j,k-1/2}(P_{i,j,k}^{n+1} - P_{i,j,k-1}^{n+1})}{\Delta z^2} \\
&+ \frac{T_{hi+1/2,j,k}(h_{i+1,j,k}^{n+1} - h_{i,j,k}^{n+1})}{\Delta x^2} - \frac{T_{hi-1/2,j,k}(h_{i,j,k}^{n+1} - h_{i-1,j,k}^{n+1})}{\Delta x^2} \\
&+ \frac{T_{hi,j+1/2,k}(h_{i,j+1,k}^{n+1} - h_{i,j,k}^{n+1})}{\Delta y^2} - \frac{T_{hi,j-1/2,k}(h_{i,j,k}^{n+1} - h_{i,j-1,k}^{n+1})}{\Delta y^2} \\
&+ \left. \frac{T_{hi,j,k+1/2}(h_{i,j,k+1}^{n+1} - h_{i,j,k}^{n+1})}{\Delta z^2} - \frac{T_{hi,j,k-1/2}(h_{i,j,k}^{n+1} - h_{i,j,k-1}^{n+1})}{\Delta z^2} \right] \\
&- \left(\frac{(T_{mwi,j,k+1/2}^{n+1} - T_{mwi,j,k-1/2}^{n+1})}{\Delta z} \rho_w g + \frac{(T_{msi,j,k+1/2}^{n+1} - T_{msi,j,k-1/2}^{n+1})}{\Delta z} \rho_s g \right) + q_{ei,j,k}^{n+1} \quad (A-9b)
\end{aligned}$$

Equation (A-9a) and (A-9b) can be re-arranged and written as follows:

$$\begin{aligned}
& \frac{T_{mi-1/2,j,k}^{n+1} P_{i-1,j,k}^{n+1}}{\Delta x^2 V} - \left\{ \frac{B_{i,j,k}^{n+1}}{\Delta t} + \frac{1}{\Delta x^2 V} (T_{mi+1/2,j,k}^{n+1} + T_{mi-1/2,j,k}^{n+1}) \right\} P_{i,j,k}^{n+1} \\
&+ \frac{T_{mi+1/2,j,k}^{n+1} P_{i+1,j,k}^{n+1}}{\Delta x^2 V} + \frac{T_{mi,j-1/2,k}^{n+1} P_{i,j-1,k}^{n+1}}{\Delta y^2 V} - \left\{ \frac{1}{\Delta y^2 V} (T_{mi,j+1/2,k}^{n+1} \right. \\
&+ \left. T_{mi,j-1/2,k}^{n+1}) \right\} P_{i,j,k}^{n+1} \\
&+ \frac{T_{mi,j+1/2,k}^{n+1} P_{i,j+1,k}^{n+1}}{\Delta y^2 V} + \frac{T_{mi,j,k-1/2}^{n+1} P_{i,j,k-1}^{n+1}}{\Delta z^2 V} - \left\{ \frac{1}{\Delta z^2 V} (T_{mi,j,k+1/2}^{n+1} \right. \\
&+ \left. T_{mi,j,k-1/2}^{n+1}) \right\} P_{i,j,k}^{n+1} + \frac{T_{mi,j+1/2,k}^{n+1} P_{i,j+1,k}^{n+1}}{\Delta y^2 V} + \frac{T_{mi,j,k-1/2}^{n+1} P_{i,j,k-1}^{n+1}}{\Delta z^2 V} \\
&- \left\{ \frac{1}{\Delta z^2 V} (T_{mi,j,k+1/2}^{n+1} + T_{mi,j,k-1/2}^{n+1}) \right\} P_{i,j,k}^{n+1} + \frac{T_{mi,j,k+1/2}^{n+1} P_{i,j,k+1}^{n+1}}{\Delta z^2 V} \\
&- C_{i,j,k}^{n+1} h_{i,j,k}^{n+1} - \frac{\rho_w g}{\Delta z V} (T_{mwi,j,k+1/2}^{n+1} - T_{mwi,j,k-1/2}^{n+1}) \\
&- \frac{\rho_s g}{\Delta z V} (T_{msi,j,k+1/2}^{n+1} - T_{msi,j,k-1/2}^{n+1}) + \frac{B_{i,j,k}^{n+1} P_{i,j,k}^n}{\Delta t} + \frac{C_{i,j,k}^{n+1} h_{i,j,k}^n}{\Delta t} \\
&+ q_{mi,j,k}^{n+1} = 0 \quad (A-10a)
\end{aligned}$$

$$\begin{aligned}
& \frac{T_{ei-1/2,j,k}^{n+1}}{\Delta x^2 V} P_{i-1,j,k}^{n+1} - \left\{ \frac{D_{i,j,k}^{n+1}}{\Delta t} + \frac{1}{\Delta x^2 V} (T_{ei+1/2,j,k}^{n+1} + T_{ei-1/2,j,k}^{n+1}) \right\} P_{i,j,k}^{n+1} \\
& + \frac{T_{ei+1/2,j,k}^{n+1}}{\Delta x^2 V} P_{i+1,j,k}^{n+1} + \frac{T_{ei,j-1/2,k}^{n+1}}{\Delta y^2 V} P_{i,j-1,k}^{n+1} - \left\{ \frac{1}{\Delta y^2 V} (T_{ei,j+1/2,k}^{n+1} \right. \\
& \left. + T_{ei,j-1/2,k}^{n+1}) \right\} P_{i,j,k}^{n+1} + \frac{T_{ei,j+1/2,k}^{n+1}}{\Delta y^2 V} P_{i,j+1,k}^{n+1} + \frac{T_{hi-1/2,j,k}^{n+1}}{\Delta x^2 V} h_{i-1,j,k}^{n+1} \\
& - \left\{ \frac{E_{i,j,k}^{n+1}}{\Delta t} + \frac{1}{\Delta x^2 V} (T_{hi+1/2,j,k}^{n+1} + T_{hi-1/2,j,k}^{n+1}) \right\} h_{i,j,k}^{n+1} + \frac{T_{hi+1/2,j,k}^{n+1}}{\Delta x^2} \\
& h_{i+1,j,k}^{n+1} + \frac{T_{hi,j-1/2,k}^{n+1}}{\Delta y^2 V} h_{i,j-1,k}^{n+1} - \left\{ \frac{1}{\Delta y^2 V} (T_{hi,j+1/2,k}^{n+1} \right. \\
& \left. + T_{hi,j-1/2,k}^{n+1}) \right\} h_{i,j,k}^{n+1} + \frac{T_{hi,j+1/2,k}^{n+1}}{\Delta y^2 V} h_{i,j+1,k}^{n+1} + \frac{T_{hi,j,k-1/2}^{n+1}}{\Delta z^2 V} h_{i,j,k-1}^{n+1} \\
& - \left\{ \frac{1}{\Delta z^2 V} (T_{hi,j,k+1/2}^{n+1} + T_{hi,j,k-1/2}^{n+1}) \right\} h_{i,j,k}^{n+1} + \frac{T_{hi,j,k+1/2}^{n+1}}{\Delta z^2 V} h_{i,j,k+1}^{n+1} \\
& - \frac{h_w \rho_w g}{\Delta z V} (T_{mwi,j,k+1/2}^{n+1} - T_{mwi,j,k-1/2}^{n+1}) - \frac{h_s \rho_s g}{\Delta z V} (T_{msi,j,k+1/2}^{n+1} \\
& - T_{msi,j,k-1/2}^{n+1}) + \frac{D_{i,j,k}^{n+1} P_{i,j,k}^n}{\Delta t} + \frac{E_{i,j,k}^{n+1} h_{i,j,k}^n}{\Delta t} + q_{ei,j,k}^{n+1} = 0
\end{aligned} \tag{A-10b}$$

The transmissibility at the positions $1 \pm 1/2, j \pm 1/2$ and $k \pm 1/2$ are evaluated as follows:

$$\begin{aligned}
T_{mi \pm 1/2, j, k} &= 1/2 (T_{mi, j, k} + T_{mi \pm 1, j, k}) \\
T_{mi, j \pm 1/2, k} &= 1/2 (T_{mi, j, k} + T_{mi, j \pm 1, k}) \\
T_{mi, j, k \pm 1/2} &= 1/2 (T_{mi, j, k} + T_{mi, j, k \pm 1})
\end{aligned} \tag{A-11}$$

with similar expressions written for T_e and T_h .

Define the coefficients for the variable pressures and enthalpies at each grid block. The coefficients for Equation (A-10) are: $a_i, b_i, c_i, d_i, e_i, f_i, g_i, \alpha_k, l_k, m_k, r_k$, and s_k where

$$\begin{aligned}
a_i &= \frac{T_{mi-1/2,j,k}}{\Delta x^2 V} \\
b_i &= \left\{ \frac{B_{i,j,k}}{\Delta t} + \frac{1}{\Delta x^2 V} (T_{mi+1/2,j,k} + T_{mi-1/2,j,k}) \right\} \\
c_i &= \frac{T_{mi+1/2,j,k}}{\Delta x^2 V}
\end{aligned} \tag{A-12}$$

By writing Equation (A-12) in terms of a_i and c_i , Equation (A-12) may be simplified to:

$$\begin{aligned}
 d_i &= \left\{ \frac{B_{i,j,k}}{\Delta t} + a_i + c_i \right\}, \quad d_j = \frac{T_{m,j-1/2,k}}{\Delta y^2 V} \\
 f_j &= \frac{T_{m,j+1/2,k}}{\Delta y^2 V} \\
 e_j &= f_j + d_j \\
 g_k &= \frac{T_{m,j,k-1/2}}{\Delta z^2 V} \\
 l_k &= \frac{T_{m,j,k-1/2}}{\Delta z^2 V} \\
 \alpha_k &= g_k + l_k \\
 m_i &= \frac{C_{i,j,k}}{\Delta t}, \\
 r_k &= \frac{T_{mwi,j,k+1/2} - T_{mwi}}{\Delta z V} \\
 s_k &= \frac{T_{mwi,j,k+1/2} - T_{mwi,j,k-1/2}}{\Delta z V}
 \end{aligned}$$

A simplification similar to the one carried out on Equation (A-12) is used on Equations (A-13) and (A-14). Based on the same definitions above i.e. Equations (A-12) through (A-14), the coefficients for Equation (A-10b) are:

$$\begin{aligned}
 a'_i &= \frac{T_{ei-1/2,j,k}}{\Delta x^2 V}, \quad c'_i = \frac{T_{mi+1/2,j,k}}{\Delta x^2 V}, \\
 b'_i &= \left\{ \frac{D_{i,j,k}}{\Delta t} + a'_i + c'_i \right\}, \quad d'_j = \frac{T_{ei,j-1/2,k}}{\Delta y^2 V}, \quad f'_j = \frac{T_{ei,j+1/2,k}}{\Delta y^2 V}, \\
 e'_j &= f'_j + d'_j. \tag{A-15} \\
 g'_k &= \frac{T_{ei,j,k-1/2}}{\Delta z^2 V}, \quad l'_k = \frac{T_{ei,j,k-1/2}}{\Delta z^2 V}, \quad \alpha'_k = g'_k + l'_k, \quad m'_i = \frac{T_{hi-1/2,j,k}}{\Delta^2 V}, \\
 s'_i &= \frac{T_{hi+1/2,j,k}}{\Delta^2 V}, \quad r'_i = \left\{ \frac{E_{i,j,k}}{\Delta t} + s'_i + m'_i \right\}, \quad \beta'_j = \frac{T_{hi,j-1/2,k}}{\Delta y^2 V}, \\
 v'_j &= \frac{T_{hi,j+1/2,k}}{\Delta y^2 V}, \quad u_j = \beta_j + v_j, \quad w_k = \frac{T_{hi,j,k-1/2}}{\Delta z^2 V}, \quad u'_k = \frac{T_{hi,j,k+1/2}}{\Delta z^2 V}, \\
 \beta'_k &= u'_k + w_k, \\
 v'_k &= \frac{T_{mwi,j,k+1/2} - T_{mwi,j,k-1/2}}{\Delta z V}, \quad w'_k = \frac{T_{msi,j,k+1/2} - T_{msi,j,k-1/2}}{\Delta z V}.
 \end{aligned}$$

Appendix B

Derivation of the non-linear system of equations for the sample reservoir of 8 blocks

We use our sample reservoir of 8 blocks surrounded by boundary blocks as an illustration of how to derive the system of non-linear equations. To begin with, we write Equations(5.3.1a) and (5.3.1b) for grid block labelled 1 in which $i = 1$, $j = 1$ and $k = 1$ to yield the following equations:

$$\begin{aligned}
 & a_1 P_{021} - \{b_1 + c_2 + \alpha_1\} P_{121} + C_1 P_{221} + d_1 P_{111} \\
 & + f_2 P_{131} + g_1 P_{120} + l_1 P_{122} - m_1 h_{121} - r_1 \rho_w g - s_1 \rho_s g \quad (B-1a) \\
 & + \frac{(B_{121} P_{121}^n + C_{121} h_{121}^n)}{\Delta t} + q_{m121} = 0
 \end{aligned}$$

$$\begin{aligned}
 & a'_1 P_{021} - \{b'_1 + c'_2 + \alpha'_1\} P_{121} + c'_1 P_{221} + d'_1 P_{111} \\
 & + f'_2 P_{131} + g'_1 P_{120} + l'_1 P_{122} + m'_1 h_{121} - \{r'_1 + u_2 + \beta'_1 \text{ bigr}\} \\
 & + s'_1 h_{221} + \beta_2 h_{111} + c_2 h_{131} + w_1 h_{120} + u'_1 h_{122} - v'_1 \rho_w g \quad (B-1b) \\
 & - w'_1 h_s g + \frac{(D_{121} P_{121}^n + E_{121} h_{121}^n)}{\Delta t} + q_{e121} = 0
 \end{aligned}$$

All the quantities without superscripts are assumed to be at the time level $(n + 1)$. We can rewrite Equation(B-1) with the pressure and enthalpy values at (i, j, k) in the reservoir blocks replaced with one subscript that refers to block name rather than block position relative to the origin. The rest of the pressure and enthalpy values in the boundary blocks retain the (i, j, k) positions since these are known values prescribed by the boundary conditions. This leads to the equations below:

$$\begin{aligned}
 & a_1 P_{021} - \{b_1 + c_2 + \alpha_1\} P_1 + C_1 P_2 + d_2 P_3 + f_2 P_{131} \\
 & + g_1 P_{120} + l_1 P_5 - m_1 h_1 - r_1 \rho_w g + s_1 \rho_s g \quad (B-2a) \\
 & + \frac{(B_{121} P_1^n + C_{121} h_1^n)}{\Delta t} + q_{m121} = 0
 \end{aligned}$$

$$\begin{aligned}
& a'_1 P_{021} - \{b'_1 + c'_2 + \alpha'_1\} P_1 + C'_1 P_2 + d'_2 P_3 + f'_2 P_{131} \\
& + g'_1 P_{120} + l'_1 P_5 + m'_1 h_{021} - \{r'_1 + u_2 + \beta'_1\} h_1 + s'_1 h_2 + \beta_2 h_3 \\
& + r_2 h_{131} + w_1 h_{120} + u'_1 h_5 - v'_1 \rho_w g h_w + w'_1 h_{sg} \\
& + \frac{(D_{121} P_1'' + E_{121} h_1'')}{\Delta t} + q_{c121} = 0
\end{aligned} \tag{B-2b}$$

This procedure can be continued for grid blocks 2 through 8 to yield an equation of the form:

$$\begin{aligned}
f_l(\vec{x}) = & (a_i + a'_i) P_{i-1,j,k} - \{b_i + b'_i + c_j + c'_j + \alpha_k + \alpha'_k\} P_{i,j,k} \\
& + (c_i + c'_i) P_{i+1,j,k} + (d_j + d'_j) P_{i,j-1,k} + (f_j + f'_j) P_{i,j+1,k} \\
& + (g_k + g'_k) P_{i,j,k+1} + (l_k + l'_k) P_{i,j,k+1} + m'_i h_{i-1,j,k} - (m_i + r'_i + u_j + \beta_k) h_{i,j,k} \\
& + s'_i h_{i+1,j,k} + \beta_j h_{i,j-1,k} + c_j h_{i,j+1,k} \\
& + w_k h_{i,j,k-1} + u'_k h_{i,j,k+1} - (r_k + v'_k h_w) \rho_w g \\
& - (s_k + w'_k h_s) \rho_s g + \frac{(B_{i,j,k} + D_{i,j,k})}{\Delta t} P_{i,j,k} + \frac{(C_{i,j,k} + E_{i,j,k})}{\Delta t} h_{i,j,k} \\
& + q_{mi,j,k} + q_{ci,j,k} = 0
\end{aligned} \tag{B-3}$$

where i , j and k vary from 1 to 2 and l varies from 1 through 16. Here the vector \vec{x} of the unknown variables p and h for all the 8 reservoir blocks

is:

$$\vec{x} = \begin{bmatrix} p_{121} \\ p_{221} \\ p_{111} \\ p_{211} \\ p_{122} \\ p_{222} \\ p_{112} \\ p_{212} \\ h_{121} \\ h_{221} \\ h_{111} \\ h_{211} \\ h_{122} \\ h_{222} \\ h_{112} \\ h_{212} \end{bmatrix}$$

The f_1, f_2 through f_{16} are obtained by replacing $i, j,$ and k counters by the appropriate position values as shown in Table(B-1). Expanding the form of (B-3) for $l = 1$ to $l = 16$ yields the vector equation:

$$\vec{f}(\vec{x}) = 0 \quad (B-4)$$

in which f_1 through f_{16} are as written below.

For grid block 1, $l=1$ for mass equation and $l=2$ for energy equation.

$$f_1(\vec{x}) = a_1 P_{021} - (b_1 + e_2 + \alpha_1) P_{121} + c_1 P_{221} + d_1 P_{111} +$$

$$f_2 P_{131} + g_1 P_{120}$$

$$+ l_1 P_{122} - m h_{121} - r_1 \rho_v g - s_1 \rho_s g + \frac{B_{121} P_{121}^n}{\Delta t} + \frac{C_{121} h_{121}^n}{\Delta t} +$$

$$q_{m121} = 0$$

$$f_2(\vec{x}) = a_1' P_{021} - (b_1' + e_2' + \alpha_1') P_{121} + c_1' P_{221} + d_2' P_{111} +$$

$$f_2' P_{131} + g_1' P_{120}$$

$$+ l_1' P_{122} + m_1' h_{021} - (r_1' + u_2 + \beta_1') h_{121} + s_1' h_{221} + \beta_2' h_{111} +$$

$$v_2' h_{131} + w_1' h_{120} + u_1' h_{122} - v_1' h_v \rho_v g - w_1' h_s \rho_s g +$$

$$\frac{D_{121} P_{121}^n}{\Delta t} + \frac{E_{121} h_{121}^n}{\Delta t} + q_{e121} = 0$$

For grid block 2, $l=3$ for mass equation and $l=4$ for energy equation.

$$f_3(\vec{x}) = a_2 P_{121} - (b_2 + e_2 + \alpha_1) P_{221} + c_2 P_{321} + d_2 P_{211} +$$

$$f_2 P_{231} + g_1 P_{220} + l_1 P_{222} - m h_{221} - r_1 \rho_v g - s_1 \rho_s g +$$

$$B \frac{P_{221}^n}{\Delta t} + C \frac{h_{221}^n}{\Delta t} + q_{m221} = 0$$

$$f_4(\vec{x}) = a_2' P_{2121} - (b_2' + e_2' + \alpha_1') P_{221} + c_2' P_{2321} + d_2' P_{2211} +$$

$$f_2' P_{231} + g_1' P_{1220}$$

$$+ w_1' h_{1220} + u_1' h_{1222} - v_1' h_{1v} \rho_v g - w_1' h_{1s} \rho_s g +$$

$$D \frac{P_{221}^n}{\Delta t} + E \frac{h_{221}^n}{\Delta t} + q_{e221} = 0$$

For grid block 3. $l=5$ for mass equation and $l=6$ for energy equation.

$$f_5(\vec{x}) = a_1' P_{011} - (b_1' + e_1' + \alpha_1') P_{111} + c_1' P_{1211} + d_1' P_{1101} +$$

$$f_1' P_{1121} + g_1' P_{1110}$$

$$+ t_1' P_{1112} - m h_{111} - r_1' \rho_v g - s_1' \rho_s g + \frac{B_{111} P_{111}^n}{\Delta t} +$$

$$C \frac{h_{111}^n}{\Delta t} + q_{m111} = 0$$

$$f_6(\vec{x}) = a_1' P_{011} - (b_1' + e_1' + \alpha_1') P_{111} + c_1' P_{1211} + d_1' P_{1101} +$$

$$f_1' P_{1121} + g_1' P_{1110}$$

$$+ t_1' P_{1112} + m_1' h_{011} - (r_1' + u_1' + \beta_1') h_{111} + s_1' h_{1211} +$$

$$\beta_1' h_{1101} + v_1' h_{1121}$$

$$+ w_1' h_{110} + u_1' h_{112} - v_1' h_{1v} \rho_v g - w_1' h_{1s} \rho_s g + D \frac{P_{111}^n}{\Delta t} +$$

$$E \frac{h_{111}^n}{\Delta t} + q_{e111} = 0$$

For grid block 4, $l=7$ for mass equation and $l=8$ for energy equation.

$$f_7(\vec{x}) = a_2 P_{111} - (b_2 + e_1 + \alpha_1) P_{211} + c_2 P_{311} + d_1 P_{201} +$$

$$f_1 P_{221} + g_1 P_{210}$$

$$+ l_1 P_{1212} - m h_{211} - r_1 \rho_v g - s_1 \rho_s g + B \frac{P_{211}^n}{\Delta t} +$$

$$C \frac{h_{211}^n}{\Delta t} + q_{m211} = 0$$

$$f_8(\vec{x}) = a_2 P_{111} - (b_2 + e_1 + \alpha_1) P_{211} + c_2 P_{311} + d_1 P_{201} +$$

$$f_1 P_{221} + g_1 P_{210}$$

$$+ l_1 P_{1212} + m_2 h_{111} - (r_2 + u_1 + \beta_1) h_{211} + s_1 h_{311} + \beta_1 h_{201} +$$

$$v_1 h_{1221}$$

$$+ w_1 h_{1210} + u_1 h_{1212} - v_1 h_{1v} \rho_v g - w_1 h_{1s} \rho_s g + D \frac{P_{211}^n}{\Delta t} +$$

$$E \frac{h_{211}^n}{\Delta t} + q_{e211} = 0$$

For grid block 5, $l=9$ for mass equation and $l=10$ for energy equation.

$$f_9(\vec{x}) = a_1 P_{022} - (b_1 + e_2 + \alpha_1) P_{122} + c_1 P_{222} + d_2 P_{112} +$$

$$f_2 P_{132} + g_2 P_{121}$$

$$+ t_2 P_{123} - mh_{122} - r_2 \rho_v g - s_2 \rho_s g + \frac{B_{122} P_{122}^n}{\Delta t} +$$

$$C_{122} \frac{h_{122}^n}{\Delta t} + q_{m122} = 0$$

$$f_{10}(\vec{x}) = a_1 P_{022} - (b_1 + e_2 + \alpha_1) P_{122} + c_1 P_{122} + d_2 P_{112} +$$

$$f_2 P_{132} + g_2 P_{121}$$

$$+ t_2 P_{123} + m_1 h_{022} - (r_1 + u_2 + \beta_2) h_{122} + s_1 h_{222} +$$

$$\beta_2 h_{112} + v_2 h_{132}$$

$$+ w_2 h_{121} + u_2 h_{123} - v_2 h_v \rho_v g - w_2 h_s \rho_s g + \frac{D_{122} P_{122}^n}{\Delta t} +$$

$$E_{122} \frac{h_{122}^n}{\Delta t} + q_{e122} = 0$$

For grid block 6, $l=11$ for mass equation and $l=12$ for energy equation.

$$f_{11}(\vec{x}) = a_2 P_{122} - (b_2 + e_2 + \alpha_2) P_{222} + c_2 P_{322} + d_2 P_{212} +$$

$$f_2 P_{232} + g_2 P_{221}$$

$$+ t_2 P_{223} - mh_{222} - r_2 \rho_v g - s_2 \rho_s g + \frac{B_{222} P_{222}^n}{\Delta t} +$$

$$C_{222} \frac{h_{222}^n}{\Delta t} + q_{m222} = 0$$

$$f_{12}(\vec{x}) = a_2 P_{122} - (b_2 + e_2 + \alpha_2) P_{222} + c_2 P_{322} + d_2 P_{212} +$$

$$f_2 P_{232} + g_2 P_{221}$$

$$+ l' P_{2,223} + m' h_{2,122} - (r'_2 + u'_2 + \beta'_2) h_{2,222} + s'_2 h_{2,322} +$$

$$\beta'_2 h_{2,212} + v'_2 h_{2,232}$$

$$+ w'_2 h_{2,221} + u''_2 h_{2,223} - v''_2 h_{2,v,v} \rho_v g - w''_2 h_{2,s,s} \rho_s g + D \frac{P^n_{222,222}}{\Delta t} +$$

$$E \frac{h^n_{222,222} + q_{e222}}{\Delta t} = 0$$

For grid block $\bar{7}$, $l=13$ for mass equation and $l=14$ for energy equation.

$$f_{13}(\vec{x}) = a_1 P_{1,021} - (b_1 + e_1 + \alpha_2) P_{1,112} + c_1 P_{1,212} + d_1 P_{1,102} +$$

$$f_1 P_{1,122} + g_2 P_{2,111}$$

$$+ l' P_{2,113} + m' h_{1,112} - (r'_2 + u'_2 + \beta'_2) h_{2,112} + s'_2 h_{2,112} +$$

$$C \frac{h^n_{112,112} + q_{m112}}{\Delta t} = 0$$

$$f_{14}(\vec{x}) = a_1 P_{1,021} - (b_1 + e_1 + \alpha_2) P_{1,112} + c_1 P_{1,212} + d_1 P_{1,102} +$$

$$f_1 P_{1,122} + g_2 P_{2,111}$$

$$+ l' P_{2,113} + m' h_{1,012} - (r'_1 + u'_1 + \beta'_2) h_{1,112} + s'_1 h_{1,212} +$$

$$\beta'_1 h_{1,102} + v'_1 h_{1,122}$$

$$+ w'_2 h_{2,111} + u''_2 h_{2,113} - v''_2 h_{2,v,v} \rho_v g - w''_2 h_{2,s,s} \rho_s g + D \frac{P^n_{112,112}}{\Delta t} +$$

$$E \frac{h^n_{112,112} + q_{e112}}{\Delta t} = 0$$

For grid block S. $l=15$ for mass equation and $l=16$ for energy equation.

$$f_{15}(\vec{x}) = a_2' P_{2112} - (b_2' + e_1' + \alpha_2') P_{212} + c_2' P_{312} + d_1' P_{1201} +$$

$$f_1' P_{1222} + g_2' P_{211}$$

$$+ l_2' P_{213} - m h_{212} - r_2' \rho_v g - s_2' \rho_s g + B_{212} \frac{P_{212}^n}{\Delta t} +$$

$$C_{212} \frac{h_{212}^n}{\Delta t} + q_{m212} = 0$$

$$f_{16}(\vec{x}) = a_2' P_{2112} - (b_2' + e_1' + \alpha_2') P_{212} + c_2' P_{312} + d_1' P_{1202} +$$

$$f_1' P_{1222} + g_2' P_{211}$$

$$+ l_2' P_{213} + m' h_{2112} - (r_2' + u_2' + \beta_2') h_{212} + s_2' h_{312} +$$

$$\beta_1' h_{1202} + v_1' h_{1222}$$

$$+ w_2' h_{211} + u_2' h_{213} - v_2' h_v \rho_v g - w_2' h_s \rho_s g + D_{212} \frac{P_{212}^n}{\Delta t} +$$

$$E_{212} \frac{h_{212}^n}{\Delta t} + q_{e212} = 0$$

Block Position (relat. to origin)		Pressure /enthalpy values							
f_1	(1,2,1)	1	P ₀₂₁	P ₁₂₁	P ₂₂₁	P ₁₁₁	P ₁₃₁	P ₁₂₀	P ₁₂₂
			h ₀₂₁	h ₁₂₁	h ₂₂₁	h ₁₁₁	h ₁₃₁	h ₁₂₀	h ₁₂₂
f_2	(1,2,1)		P ₁₂₁	P ₂₂₁	P ₃₂₁	P ₂₁₁	P ₂₃₁	P ₂₂₀	P ₂₂₂
f_3	(2,2,1)	2	h ₁₂₁	h ₂₂₁	h ₃₂₁	h ₂₁₁	h ₂₃₁	h ₂₂₀	h ₂₂₂
f_4	(2,2,1)		P ₀₁₁	P ₁₁₁	P ₂₁₁	P ₁₀₁	P ₁₂₁	P ₁₁₀	P ₁₁₂
f_5	(1,1,1)	3	h ₀₁₁	h ₁₁₁	h ₂₁₁	h ₁₀₁	h ₁₂₁	h ₁₁₀	h ₁₁₂
f_6	(1,1,1)		P ₁₁₁	P ₂₁₁	P ₃₁₁	P ₂₀₁	P ₂₂₁	P ₂₁₀	P ₂₁₂
f_7	(2,1,1)	4	h ₁₁₁	h ₂₁₁	h ₃₁₁	h ₂₀₁	h ₂₂₁	h ₂₁₀	h ₂₁₂
f_8	(2,1,1)		P ₀₂₂	P ₁₂₂	P ₂₂₂	P ₁₁₂	P ₁₃₂	P ₁₂₁	P ₁₂₃
f_9	(1,2,2)	5	h ₀₂₂	h ₁₂₂	h ₂₂₂	h ₁₁₂	h ₁₃₂	h ₁₂₁	h ₁₂₃
f_{10}	(1,2,2)		P ₁₂₂	P ₂₂₂	P ₃₂₂	P ₂₁₂	P ₂₃₂	P ₂₂₁	P ₂₂₃
f_{11}	(2,2,2)	6	h ₁₂₂	h ₂₂₂	h ₃₂₂	h ₂₁₂	h ₂₃₂	h ₂₂₁	h ₂₂₃
f_{12}	(2,2,2)		P ₀₁₂	P ₁₁₂	P ₂₁₂	P ₁₀₂	P ₁₂₂	P ₁₁₁	P ₁₁₃
f_{13}	(1,1,2)	7	h ₀₁₂	h ₁₁₂	h ₂₁₂	h ₁₀₂	h ₁₂₂	h ₁₁₁	h ₁₁₃
f_{14}	(1,1,2)		P ₁₁₂	P ₂₁₂	P ₃₁₂	P ₂₀₂	P ₂₂₂	P ₂₁₁	P ₂₁₃
f_{15}	(2,1,2)	8	h ₁₁₂	h ₂₁₂	h ₃₁₂	h ₂₀₂	h ₂₂₂	h ₂₁₁	h ₂₁₃
f_{16}	(2,1,2)								

Table B-1 Pressure and enthalpy values in reservoir and boundary blocks

LIST OF REFERENCES

- [1] Ambusso, W.J. and Ouma, P.A. *Thermodynamic and permeability structure of Olkaria North East Geothermal field: Olkaria fault*. Geothermal Resources Council Transactions, vol. 15, October 1991.
- [2] Bhogal, P.S. *The electrical resistivity method of geophysical prospecting and its application to geothermal exploration in the Rift Valley of Kenya*. PhD. thesis, Department of Physics, University of Nairobi, 1978.
- [3] Bhogal, P.S. *The Role of Reservoir Engineering in Geothermal Energy Development*. Discovery and Innovation vol. 1 no. 3, Sep. 1989.
- [4] Bodvarsson G.S. *Olkaria geothermal field; preliminary study of the reservoir behaviour under exploitation*. report presented to KPC, Virkir Consulting Co. Reykjavik, Iceland, 1980.
- [5] Bodvarsson, G.S. and pruess, K., *Olkaria geothermal field; Numerical studies of the generating capacity of the reservoir*. Report, Virkir Consulting Co. and KPC, Nairobi, 1981.
- [6] Bodvarsson, G.S., Pruess, K., Steffansson, V., Bjornsson, S., Ojiambo, S.B., *East Olkaria geothermal field, Kenya. History match with production and pressure decline data*, J. of Geophysical Res., vol. 92, B1, Jan. 1987.
- [7] Collins, R.E. "Flow of fluids in porous materials. Reinhold publishing Corporation", New York 1961.
- [8] Corey, A.T. *Mechanics of Heterogeneous Fluids in Porous Media*. Water Resour. pub., Fort Collins, Colorado 1972.
- [9] Faust, C.R. and Mercer, J.W., *Mathematical modeling of geothermal systems*, in proceedings of the second UN Symposium on the Development and use of Geothermal Resources, vol. 3, pp.1633-1642. UN. San Francisco, Calif., 1975.

- [10] Faust, C.R. and Mercer, J.W. *Geothermal reservoir simulation: 1. Mathematical Models for liquid-and vapour-dominated hydrothermal systems* , Water Resources Research vol.15, no. 1, February 1979.
- [11] Faust, C.R. and Mercer, J.W., *Geothermal reservoir simulation: 2. Numerical Techniques for liquid-and vapour-dominated hydrothermal systems* , Water Resources Research vol.15, no. 1, February 1979.
- [12] Freestone, D.H., "Geothermal Reservoir Engineering lecture notes ", Geothermal Institute; University of Auckland, 1992.
- [13] Garg, S.K., Pritchett, J.W. and Brownell Jr., D.H., *Transport of mass and energy in porous media* , in proceedings of second UN symposium on the Development and use of Geothermal Resources, vol. 3, pp.1651-1656, UN San Francisco, Calif., 1975.
- [14] Geothermica Italiana, Srl of Pisa, Italy. *Geothermal Reconnaissance Survey in the Menengai-Bogoria area of Kenya Rift Valley* . Report TCDCON7/85 – KEN82/002. 1985.
- [15] GENZL/KPC . Measurement Report 01 – 037 Unpublished Report, 1980.
- [16] GENZL Olkaria Scientific Review Report , November , 1986.
- [17] Glover, R.L. *Chemical characteristics of water and steam discharges in the Rift Valley* . Unpublished UN/Kenya Government Geothermal Resources Exploration Project Report, 1972.
- [18] Grant, M.A., and Whittome, A.J. *Hydrology of Olkaria geothermal field* , paper presented at New Zealand Geothermal workshop, Geothermal Institute, University of Auckland, New Zealand, 1981.
- [19] Grant, M.A., Donaldson, I.G., Bixely, P.F. "Geothermal Reservoir Engineering. Academic Press", New York, 1982.

- [20] Group 7 Incorporated. *Electrical Resistivity Survey in the Rift Valley, Kenya*. Unpublished report to the UNDP/EAPL Project, 1972.
- [21] Harlow, F.H. and Pracht, W.E., *A theoretical study of geothermal energy extraction*. J. Geophys. Res., 77(35), 7033-7048, 1972.
- [22] Hocstein, M.P., *World-wide occurrence of geothermal resources, convective and non convective systems*. Lecture notes, Geothermal Institute, University of Auckland, New Zealand, 1992.
- [23] Hochstein, M.P., Caldwell, G. and Bromley, C.J. *Reinterpretation of resistivity data of the Olkaria geothermal prospect (Gregory Rift, Kenya)*. Proceedings of 3rd NZ Geothermal workshop, 1981.
- [24] KPC. *Working document for Scientific Review Meeting*, May, 1988.
- [25] KPC. *Eburru geothermal development. Discussion papers for Scientific Review Meeting*, March, 1990.
- [26] KRTA. *Background Report for Scientific and Technical Review Meeting*, KPC Geothermal project Report, November, 1984.
- [27] Lasseter, T.J., Witherspoon, P.A., and Lippmann, M.J., *The numerical simulation of heat and mass transfer in multi-dimensional two-phase geothermal reservoirs*, in the proceedings of the second UN symposium on the Development and use of Geothermal Resources, vol. 3, pp.1715-1725, UN. San Francisco, Calif., 1975.
- [28] Mercer, J.W. and Faust, C.R., *Simulation of water- and vapour-dominated hydrothermal reservoirs*, paper presented at the 50th Annual Fall Meeting, Soc. of Petrol. Eng. AIME, Dallas, Tex., Sep. 28 to Oct. 1, 1975.
- [29] McCann, D.L. *Hydrologic Investigation of Rift Valley Catchments*, 1974.

- [30] Muna, Z.W., *Chemistry of well discharges in the Olkaria geothermal field, Kenya* . Rep. 1982-1983, 38pp. UN. Univ. Training Program, Reykjavik, Iceland, 1982.
- [31] Mwangi, M.N. and Bromley, C.J. *A review of the geophysical model of Olkaria geothermal field* . Unpublished KPC Report, 1986.
- [32] Naylor, I. *Geology of Eburru and Olkaria Prospects* , UN Geothermal Resources Exploration Project Report, 1972.
- [33] Noble, J.W. and Ojiambo, S.B. *Geothermal exploration in Kenya*, paper presented at the UN symposium on the Development and use of Geothermal Resources, UN. San Francisco, Calif., May 20-29, 1975.
- [34] O'Sullivan, M.J. and McKibbin, R., *Geothermal Reservoir Engineering* . A manual for Geothermal Reservoir Engineering courses at the Geothermal Institute, University of Auckland, 1989.
- [35] Pruess, K. *TOUGH Users Guide* L.B.L, University of California, Berkeley, 1987.
- [36] Pruess, K. and Schroeder, R.C. *SHAFT 79 User Manual* . L.B.L., University of California, Berkeley, 1980.
- [37] Smith, G.D. "Numerical solution of partial differential equations: Finite Difference methods". Third Edition, Clarendon Press, Oxford, 1987.
- [38] Wang, J.S.Y., Tsang, C.F. and Sterbentz, R.A. *State of the Art of Numerical Modelling of Thermohydrologic Flow in Fractured Rock Masses*. Environ. Geol. 4, 133-199, 1983.
- [39] Whiting, R.L. and Ramey, Jr., H.J. *Application of Material and Energy Balances to Geothermal Steam Production* , Journal of Petroleum Technology, July 1969.
- [40] Zyvoloski, G.A., ÓSullivan, M.J. and Krol, D.E. *Finite Difference*

Techniques for modelling Geothermal Resources , Num. Anal. Meth.
Geomech. 3, 355-366, 1979.